Max-Planck-Institut für Metallforschung
Stuttgart

Investigation on Diffusion Soldering in Cu/In/Cu and Cu/In-48Sn/Cu Systems

Silvana Andrea Sommadossi

Dissertation
an der
Universität Stuttgart

Bericht Nr. 125
Juli 2002

Investigation on Diffusion Soldering in Cu/In/Cu and Cu/In-48Sn/Cu Systems

Von der Fakultät Chemie der Universität Stuttgart zur
Erlangung der Würde eines Doktors der Naturwissenschaften (Dr. rer. nat.)
genehmigte Abhandlung

vorgelegt von

Silvana Andrea Sommadossi

aus Neuquén/Argentinien

Hauptberichter: Prof. E.J. Mittemeijer
Mitberichter: Prof. F. Aldinger
Mitprüfer: Prof. E. Roduner
Tag der mündlichen Prüfung: 24.07.2002

INSTITUT FÜR METALLKUNDE DER UNIVERSITÄT STUTTGART
MAX-PLANCK-INSTITUT FÜR METALLFORSCHUNG
STUTTGART, 2002

Index

1 Introduction

Joining is a metallurgical process used since the ancient times. Using the joining process as a part of the manufacturing route can offer considerable technical and economic advantages to the designer and fabricator, provided careful decisions are made about the processes to be applied, the materials to be selected, the joint configurations and the process parameters to be employed. Nowadays, an additional requirement has to be fulfilled by the joining process: the process and the resultant joints have to be environmental friendly [1]. Therefore, the material and process selection involves an additional limiting factor: the toxicity. In the electronic and microelectronic fields the joining process has to provide electrically, mechanically and thermally stable bonds at the lowest process temperature possible because the other circuit components can be very sensitive to higher temperatures.

Diffusion soldering [2] is an attractive joining method for the formation of thermally and mechanically stable Pb-free bonds in electrical and electronic devices at relatively low process temperatures, which involves interdiffusion, reaction diffusion and isothermal solidification. The fundamental requirement for the diffusion soldering process is the existence of at least one intermetallic compound between the components to be jointed.

In short, the diffusion soldering process can be described as follows. An interlayer of a low melting component is provided as a foil or a thin-film coating between the high melting joint components. The assembly is heated under moderate pressure to the bonding or process temperature and a liquid filler forms, either because the melting point of the interlayer is exceeded or due to a eutectic reaction between the low- and high-melting components. The solid phases formed through interdiffusion or reaction diffusion at the bonding temperature in the joint region exhibit a remelt temperature above the process temperature. The difference between production and service or remelt temperature can be 400 or 600°C depending on the material system.

Diffusion soldering comprises a hybrid joining process that combines some advantages of the conventional soldering or brazing with those of diffusion bonding. The favorable features of isothermal solidification are due to the transient appearance of a liquid phase, in contrast to the solid state process of diffusion bonding. Isothermal solidification in diffusion soldering allows to form strong bonds at a low temperature which remain solid at much higher temperatures. The last feature can be exploited the new high-temperature processing steps and application in electronic assemblies. Moreover, the mechanical properties of diffusion soldered joints are vastly superior to those of conventional solders and exceed the requirements in electronics industry with the additional advantage of the higher temperature stability [2,3].

The aim of this study was to characterize the diffusion soldering process applied for Cu/In/Cu and Cu/In-48Sn/Cu bonds. The investigation involved the characterization of the joint morphology, the mechanisms and kinetics for the intermetallic phase (IP) formation, and the role of the interdiffusion and the reaction diffusion process at the interfaces.

Joining of Cu substrates is the most common situation in the electronic and micro electronic field. Therefore, Cu substrates were choosen for this work. The eutectic In-48Sn solder was selected because of its relatively low melting point (120°C) in comparison to In (157°C) and Sn (232°C) [3]. Another factor involved in the material selection was the necessity of IP formation in the diffusion soldering process: In and Sn form IPs when they are combined with Cu. Cu/Sn and Cu/In couples have shown IP formation at the interface, and the Cu/Sn couples are well characterized [4]. However, the Cu/In couples are not completely investigated, so the examination of Cu/In joint was also included in the study.

The characterization of diffusion-soldered Cu/In/Cu interconnections is presented in Chapter 2. The morphology and the growth kinetics of the IPs formed in the interconnection zone in the temperature range 180-430°C were examined by scanning electron microscopy (SEM), electron probe microanalysis (EPMA), X-ray diffraction (XRD) and transmission electron diffraction analysis (TEM). The IP formation sequence was also determined. The thickness of the IP formed during the solid-solid reaction obeyed a parabolic growth law, and the growth rate constants were calculated for the IP layers which grow through solid-solid process. Using these values and the equilibrium concentrations of the IPs, the integral interdiffusion coefficients were calculated through Wagner’s approach. The interdiffusion coefficients were correlated with temperature by an Arrhenius relationship.

A similar investigation is presented in Chapter 3 for the Cu/In-48Sn/Cu diffusion-soldered joints in the temperature range of 180-400°C. By means of EPMA two binary IPs, which can dissolve a third element, were identified. Two different microstructure morphologies were observed for the IP which grows through the solid-liquid process. Thermal stability tests were performed in order to determine the maximal remelt or service temperature that the joints can withstand. The thickness of the IP layer, which grows through solid-solid process, shows a constant growth rate (linear growth) at constant temperature. The temperature dependence of the growth rate constant of that IP layer is described by an Arrhenius relationship. These joints seem to be very attractive for application because of their faster IP growth behavior in comparison with the IP growth which was found in Cu/Sn and Cu/In joints [4].

The mechanical behavior of a joint is of vital importance for any application. Therefore, Chapter 4 deals with shear strength, tensile strength and nanohardness testing, in order to describe the mechanical properties of the Cu/In-48Sn/Cu diffusion-soldered bonds. The shear, tensile and hardness values were interpreted together with fractographic analysis, using SEM in order to determine the fracture mode. Special interest was paid toward the shear testing since this kind of loading process is the most common in microelectronics due to the thermal expansion mismatch between the components. The joint consisting of a single Cu-rich IP shows excellent shear and tensile strength values.

Chapters 5 and 6 present as Appendix a similar investigation performed, in the frame of this thesis, on additional diffusion-soldered bonds, Ni/Al/Ni, where the morphology and the growth of the IP layers at 720°C is presented. The kinetic behaviour of the solid-solid IP layer growth seems to obey a parabolic growth law, i.e. it is a diffusion-controlled process. Depending of the IP present in the interconnection zone, these joints can be used under a very high service temperature, up to 1600°C!

2

Phase characterization and kinetic behaviour of diffusion-soldered Cu/In/Cu interconnections

S. Sommadossi, W. Gust, and E.J. Mittemeijer

The characterization of diffusion-soldered Cu/In/Cu interconnections is presented in this work. The main feature of this joining process is the production of a bond at a low fabrication temperature, which allows high service temperatures. The interconnection is formed entirely by intermetallic phases (IPs) which form isothermally first by a liquid-solid reaction and then by a solid-solid reaction. The morphology and the growth kinetics of the IPs formed in the interconnection zone at temperatures in the range 180-430°C were examined by electron probe microanalysis, X-ray diffraction and transmission electron diffraction analysis. In accordance with the phase diagram, the phases $Cu_{11}In_9$, Cu_2In and Cu_7In_3 (at $T < 310°C$) and Cu_2In and Cu_7In_3 (at $T > 310°C$) appeared in the interconnection zone. The thickness of the IPs formed during the solid-solid reaction obeyed a parabolic growth law. The growth rate constants were calculated for the Cu_2In and Cu_7In_3 phases. Using these values and the equilibrium concentration of the IPs, the integral interdiffusion coefficients were calculated through Wagner's approach.

2.1 Introduction

New joining methods are required to allow more flexible manufacture and to fulfil service conditions as irregular geometry, large temperature range and low pressure. Further, emerging environmental regulation worldwide, especially in Europe and Japan [1], aims at the elimination of Pb usage in electronic assemblies. As a consequence, the development of new joining techniques using Pb-free soldering alloys is required.

Diffusion soldering [2] is an attractive joining method for the formation of thermally and mechanically stable Pb-free bonds in electrical and electronic devices. The diffusion soldering process has the advantages of the conventional soldering (good joint filling and low fabrication temperature) and diffusion bonding (high service temperature, low thermal mismatch). The joints, entirely consisting of intermetallic phases (IPs), have service temperatures much higher than the low fabrication temperature. The difference between fabrication and service temperature can be around 400-600°C, depending on the materials system involved. The joints can be very thin and, in consequence, the time required for reaction is very short.

This work was focused on the characterization of the microstructure and the growth kinetics of the intermetallic phases formed in Cu/In/Cu joints during the diffusion soldering process. Cu was chosen because it is one of the most common substrate materials in many electronic applications, and indium is one of the major ingredients in many commercial solders. Until now, there are no detailed reports on the growth rates and activation energies for the formation of IPs in the Cu-In system [3]. Only some qualitative studies have been performed on the interfacial reactions between In and Cu (cf. [4],[5]).

Most of the studies on interfacial reactions during conventional soldering deal with the growth of IPs at low temperatures (especially below the melting point of the joint material). However, a deeper knowledge about the reaction at the interfaces in diffusion-soldered joints is lacking. The formation of IPs is undesired in conventionally soldered joints because they are hard and brittle and often imply a degradation of the mechanical, electrical, or even thermal properties of the soldered joints. However, attractive joints consisting entirely of IPs were already obtained in the Ag/Sn [6], Cu/Sn and Ni/Sn [7] systems.

2.2 Experimental techniques

The diffusion couples were prepared from high purity (99.999 wt.%) Cu slices with a diameter of 5-10 mm and a thickness of 2 mm and from high purity (99.999 wt.%) In foils. The surface preparation for the Cu slices consisted in grinding and polishing using 1 µm diamond paste as the last step. The foil was sandwiched between the Cu slices. A heating-load press permitted to heat up rapidly the assembly with a heating rate of 200-300 °C/s to temperatures (180, 250, 290, 360 and 430°C) above the melting point of In (156.6°C) under a slight mechanical pressure (≈ 0.5 MPa). During the subsequent annealing at the chosen temperature the isothermal reaction between In (liquid) and Cu (solid) took place and IPs formed. The heating and annealing, and the subsequent cooling took place under an Ar atmosphere in order to prevent oxidation of the sample.

After cooling down, cross-sections of the joints were prepared for metallographic analysis by embedding in epoxy, grinding and polishing, using 1 µm diamond paste as last step. A scanning electron microscope (Philips XL 30) was used to inspect the morphology of the joints. The backscattered electron micrographs showed clearly the different phases and permitted the measurement of their thickness. The thickness values of each intermetallic layer represent averages of 30 measurement points performed at regularly spaced intervals.

An electron probe microanalyser (Cameca SX100) equipped with 5 wave-length dispersive spectrometers was used to measure the chemical composition through line-scans perpendicular to the interconnection zone. Because of the limited resolution (± 2 µm) of electron probe microanalysis (EPMA), relatively large interconnection thicknesses were produced. A large thickness allowed also to acquire composition data at more locations.

A Philips X' Pert diffractometer using Cu Kα radiation at room temperature was applied to record diffraction patterns of the fracture surface of the samples broken along the central zone of the interconnection zone (i.e. parallel to the reaction fronts).

A transmission electron microscope equipped with a double tilt holder was used for electron diffraction analysis to identify the phases involved in the joint. The samples for transmission electron microscopy (TEM) analysis were prepared following a standard method [8]. For phase identification only the reflexes corresponding to a low-index zone axis were considered. For the analysis the Carinev program was applied [9]. Pearson's handbook

[10] of lattice parameters and additional publications were used as data-base for the unit cell parameters.

2.3 Results and discussion

2.3.1 *Phase development and characterization*

Several IPs have been indicated in the phase diagram of the Cu-In system [11] (see Fig. 2.1). Depending on the fabrication temperature (180, 250, 290, 360 and 430°C) two regions can be distinguished. Below 310°C, three IPs can appear: $Cu_{11}In_9$, Cu_2In (η) and Cu_7In_3 (ζ), and above 310°C two IPs can form: Cu_2In (η‘) and Cu_7In_3 (ζ). If nucleation of the phases does not pose any difficulty, all the phases which appear in the phase diagram should form and grow upon reaction initiating at the Cu/In interfaces.

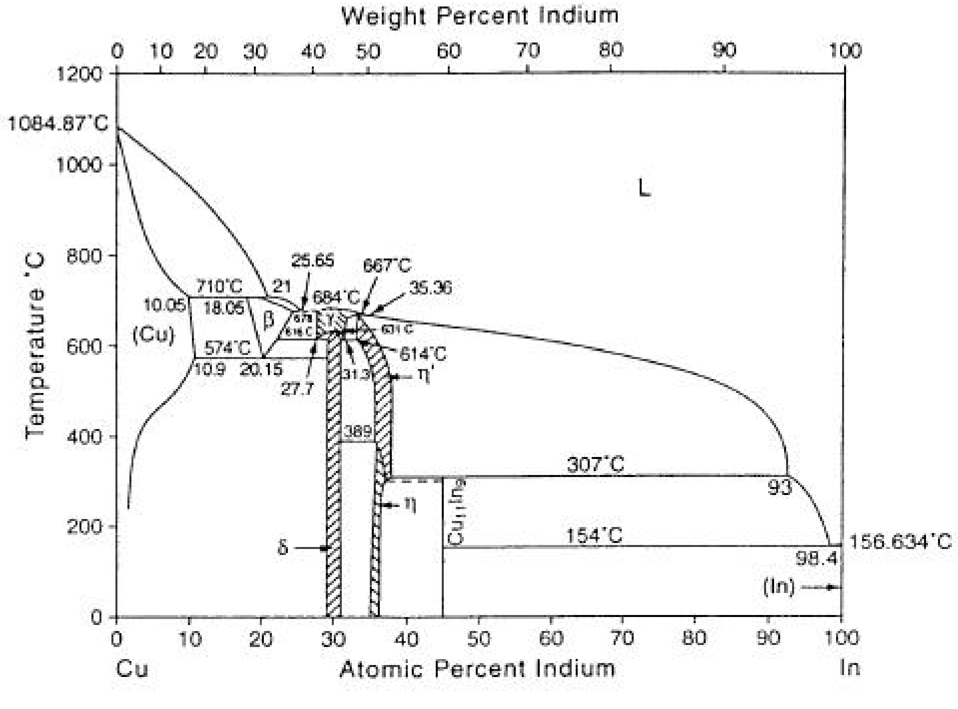

Fig. 2.1. Phase diagram of the Cu-In system [10].

The first IP formed is the IP poorest in Cu at the fabrication temperature according to the phase diagram (Fig. 2.1), which results from the reaction between the liquid (L) In and the solid (S) Cu after the dissolution of Cu and saturation with Cu of the liquid. The involved net reactions thus are:

$$9\ \mathrm{In}\,(L) + 11\ \mathrm{Cu}\,(S) \longrightarrow \mathrm{Cu_{11}In_9}\ (S) \quad ; \quad T < 310°\mathrm{C} \qquad (2.1)$$

$$\mathrm{In}\,(L) + 2\ \mathrm{Cu}\,(S) \longrightarrow \mathrm{Cu_2In}\ (S) \quad ; \quad T > 310°\mathrm{C} \qquad (2.2)$$

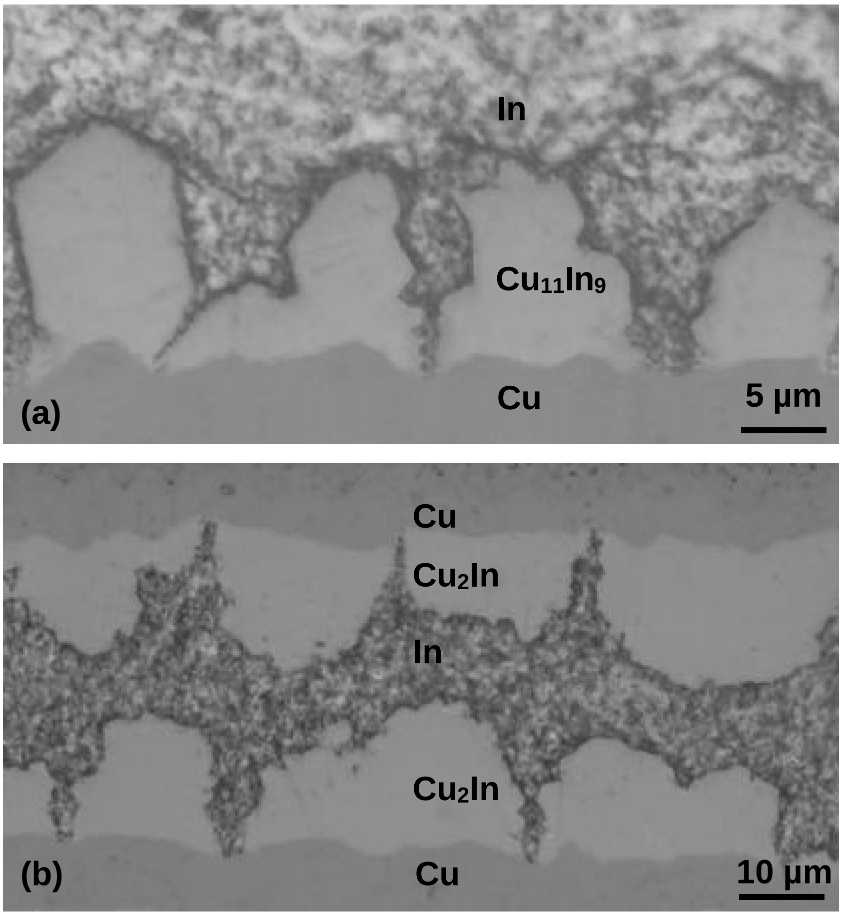

Fig. 2.2. SEM micrographs showing the morphology of the $Cu_{11}In_9$ and Cu_2In phases formed in a Cu/In/Cu sample: (a) bond after annealing at 290 °C for 30 min; (b) bond after annealing at 360 °C for 3 min.

The first stage of the diffusion soldering process, the liquid-solid reaction, led to an irregular morphology of the phases formed ($Cu_{11}In_9$ or Cu_2In). It can be seen in Fig. 2.2a and b the morphology of $Cu_{11}In_9$ in a sample annealed at 290°C for 30 min and of Cu_2In in a sample annealed at 360°C for 3 min, respectively. These results agree with results of earlier work [4] where it was found that the copper dissolution process plays an important role in the liquid-solid reaction, such that high dissolution rates appear to induce a highly non-planar morphology of the solid phase formed. As a consequence, the reaction of a solid substrate with a pre-saturated liquid will produce a solid phase with a smoother morphology than in a reaction with a pure liquid. Indeed, the $Cu_{11}In_9$ grains developing at a low temperature are more faceted, as compared to the Cu_2In grains developing at a higher temperature which exhibit relatively smoothly curved interfaces with the (originally liquid) In: it can be expected that the In-based liquid at the higher temperature more rapidly saturates with Cu.

In both cases the grains grew into the melt and deep grooves occur between the grains. These observations and the fact that the solid-liquid interdiffusion is faster than the solid-solid interdiffusion leads to the conclusion that the IP formation is supported by Cu diffusion through the melt rather than through the IP: growth takes place at the liquid/IP interface and Cu is supplied through the grain-boundary grooves. The groove density decreases with annealing time due to the lateral growth of the grains, until they have disappeared completely. Then, IP growth occurs via diffusion through the solid IP.

The microstructure of the interconnection zone of a sample annealed at 180°C for 30 days is shown in Fig. 2.3a. As can be seen in the micrograph, a single phase is present between the Cu substrate regions after the liquid In has been consumed totally. This observation is confirmed by the practically constant composition across the joint Fig. 2.3 b): the average composition value (Cu-45.1 at.% In) corresponds to the $Cu_{11}In_9$ phase (Cu-44 at.% In). The same behavior has also been observed for samples annealed at 250 and 290°C.

According to the present observations, the second IP (Cu_2In or Cu_7In_3) starts to form only after the liquid In has been totally consumed by formation of the first IP. Thereafter, the only source of In atoms is the Cu-poor IP, and thus this first IP then becomes consumed through a solid-solid reaction with Cu in order to produce the copper richer second IP. Hence, above 310°C the following reaction occurs:

$$3\,Cu_2In\,(S) + Cu\,(S) \longrightarrow Cu_7In_3\,(S) \quad ; \quad T > 310°C \qquad (2.3)$$

The second IP grows as a regular product layer as can be seen from Fig. 2.4a for a Cu/In/Cu couple annealed at 360°C for 30 days. The EPMA composition profile shown in Fig. 2.4

Fig. 2.4b for the same sample indicates constant composition values for both IPs: Cu-36.1 at.% In for Cu_2In and Cu-30.7 at.% In for Cu_7In_3 (cf. [10]).

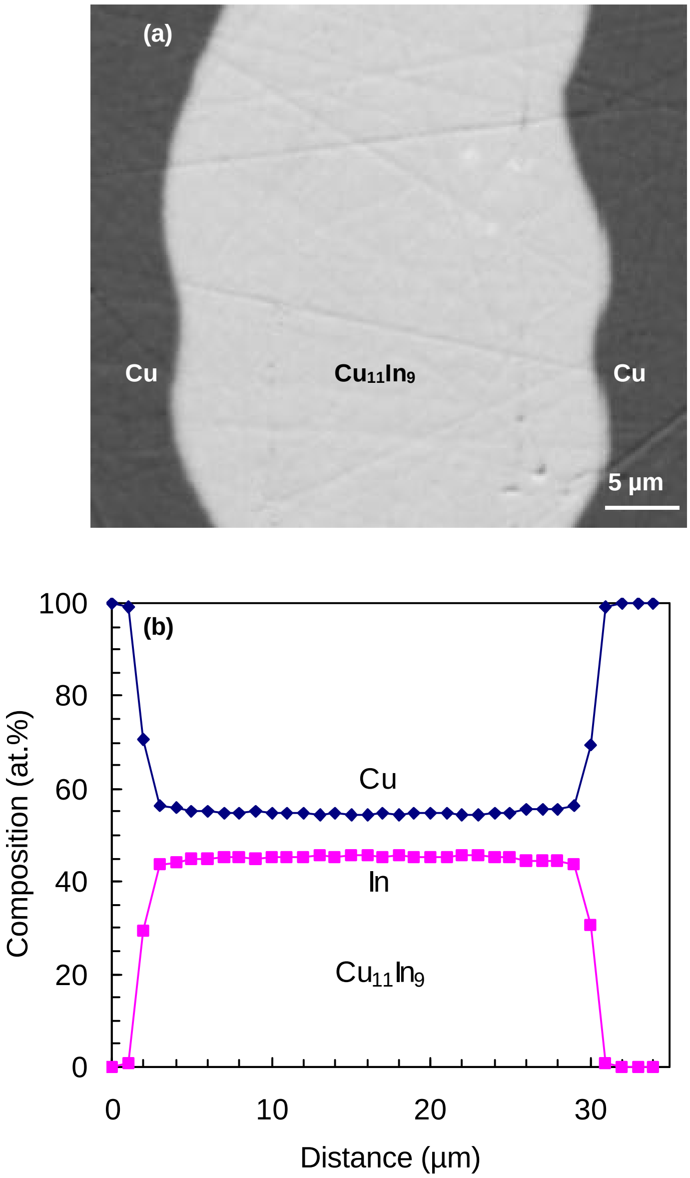

Fig. 2.3. Cu/In/Cu sample annealed at 180°C for 30 days: (a) SEM micrograph of the interconnection zone; (b) composition profile across the joint of the same sample as obtained by EPMA.

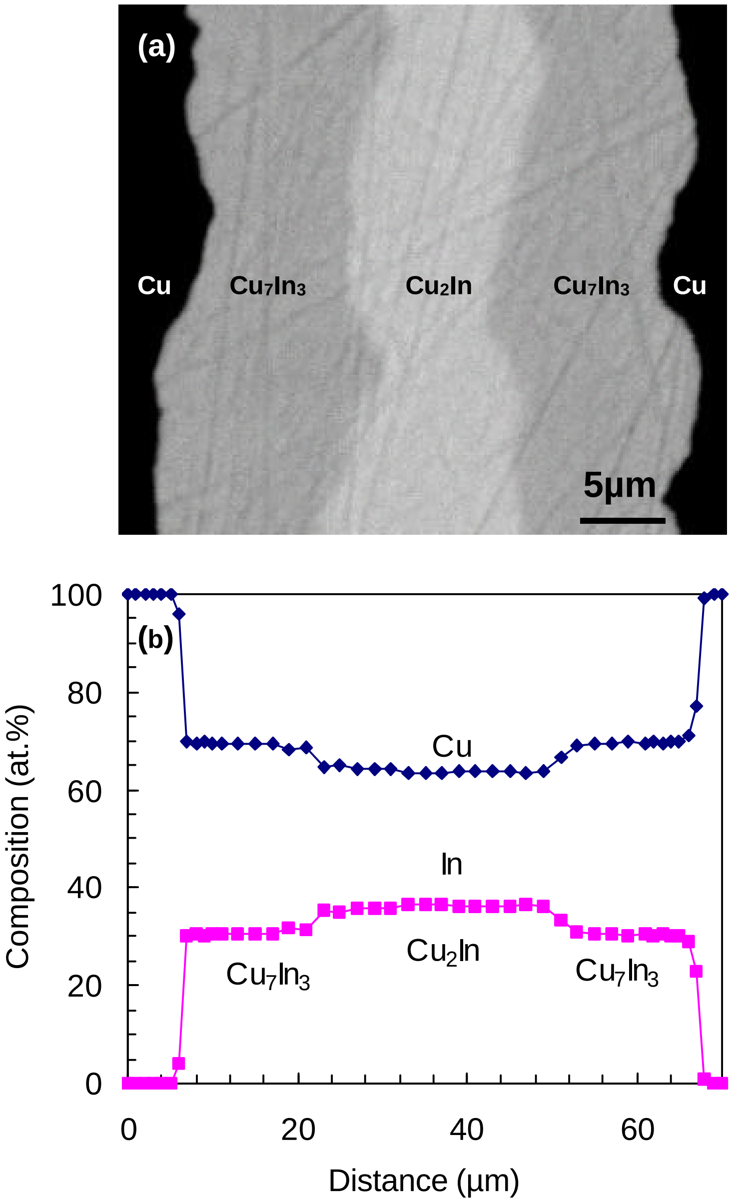

Fig. 2.4. Cu/In/Cu sample annealed at 360 °C for 30 days: (a) SEM micrograph of the interconnection zone; (b) composition profile across the joint of the same sample as obtained by EPMA.

To show the formation of IPs after the formation of the first IP at temperatures below 310°C, the microstructure of a Cu/In/Cu couple annealed at 290°C for 16 days is shown in Fig. 2.5a. The SEM micrograph suggests the presence of three IPs and the corresponding EPMA composition profile indeed shows three regions of constant composition (Fig.

2.5b): from the middle to the Cu substrate sides these IPs are $Cu_{11}In_9$ (Cu-44.8 at.% In), Cu_2In (Cu-36.6 at.% In), and Cu_7In_3 (Cu-30.6 at.% In) (cf. [10]). The formation of the Cu_2In and Cu_7In_3 phases occur by consumption of $Cu_{11}In_9$ and Cu as follows:

$$Cu_{11}In_9\,(S) + 7\,Cu\,(S) \longrightarrow 9\,Cu_2In\,(S) \quad ; \quad T < 310°C \tag{2.4}$$

$$3\,Cu_2In\,(S) + Cu\,(S) \longrightarrow Cu_7In_3\,(S) \quad ; \quad T < 310°C \tag{2.5}$$

The traditional diffusional kinetics theory for the formation of IPs at the interfaces of diffusion couples (cf. [12],[13]) supposes for multiple phase growth that all phases start to grow simultaneously, ignoring possible incubation times. However, IPs do not necessarily form simultaneously, but may develop sequentially (cf. [14],[15]). Also, the rate of growth of a particular phase may be extremely small in comparison with the other phases, and the occurrence of such a phase may not be detected experimentally using techniques, such as EPMA, of limited spatial resolution. In the last case the apparent absence of the phase can be interpreting wrongly as a problem of nucleation [16].

Against this background the apparent absences of the phases with a high Cu content (Cu_2In and Cu_7In_3 below 310°C and Cu_7In_3 above 310°C) may be understood during the stage where only formation and growth of the Cu-poor phase ($Cu_{11}In_9$ below 310°C and Cu_2In above 310°C) was detected.

According to the experimental observations reported above, the first IP that had formed (significantly) contained the maximum concentration of the metal with the lowest melting point (In). Then, the next IPs containing increasing amounts of the metal with the high melting point (Cu) were detected. Hence, the phase sequence observed as a function of the annealing time and as function of the distance to the Cu substrates followed the order given by the equilibrium phase diagram. The appearance sequence of the IPs is shown schematically in a summarizing way in Fig. 2.6.

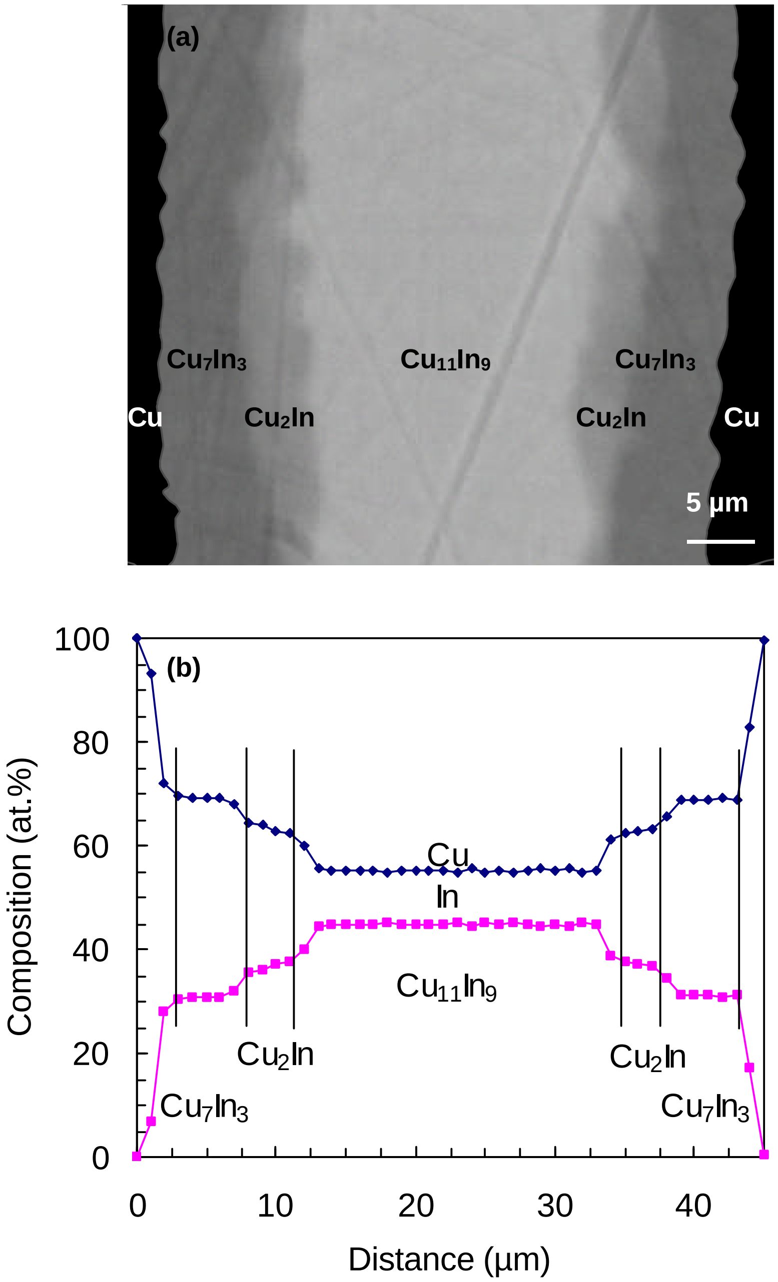

Fig. 2.5. Cu/In/Cu sample annealed at 290 °C for 16 days: (a) SEM micrograph of the interconnection zone; (b) composition profile across the joint of the same sample as obtained by EPMA.

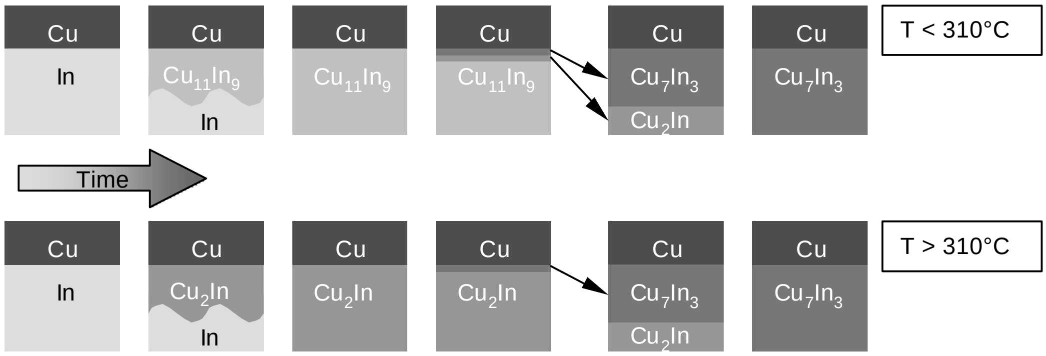

Fig. 2.6. Schematic representation of the appearance sequence of IPs in Cu/In/Cu diffusion soldered joints.

In order to complete the phase identification, X-ray diffraction analyses were performed on the fractured surfaces of the interconnections. Only the $Cu_{11}In_9$ phase (for crystallographic parameters see [17]) could be identified in samples annealed at 180 and 290°C (see Fig. 2.3 and Fig. 2.5); the other IPs could not be detected convincingly by this means (see also [4],[5]). Therefore, transmission electron microscopy (TEM) diffraction analyses were performed here as well, in order to performed phase analysis on a highly localized scale. The position of the electron diffraction analyses on a foil prepared from a Cu/In/Cu sample aged at 290°C for 16 days have been indicated in Fig. 2.7. The reflexes observed could be ascribed to $Cu_{11}In_9$, Cu_2In and Cu_7In_3 for the positions 1, 2, and 3, respectively. A similar analysis was applied to samples fabricated above 310°C, and the electron diffraction analyses then indicated the presence of the Cu_2In and Cu_7In_3 phases.

Finally, it is remarked that according to the phase diagram, Cu_2In and Cu_7In_3 possess a high melting point which makes possible a high service temperature for the joints. Further, it can be seen from Fig. 2.3-Fig. 2.5 that the interconnection zone shows no defects as pores or voids, indicating that drastic volume changes do not occur during the formation of the IPs.

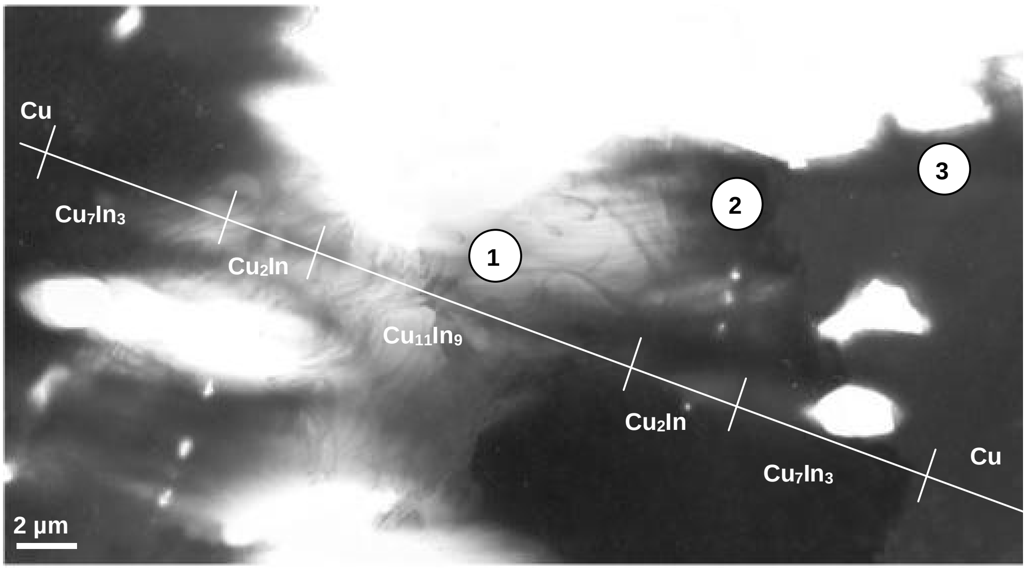

Fig. 2.7. TEM bright field micrograph of a Cu/In/Cu sample aged at 290 °C for 16 days. The position of the electron diffraction analyses on the electron transparent foil prepared from a joint.

2.3.2 Reaction kinetics

Here the growth kinetics for the IPs formed by solid-solid reaction diffusion processes is considered. For determination of the kinetics of the intermetallic layer growth measurements of the layer thicknesses were performed (cf. Section 2.2). The growth of an IP is often presented by a general power law [13] :

$$\Delta x = k_0\, t^n \qquad \text{or} \qquad \log \Delta x = \log k_0 + n \log t \tag{2.6}$$

If *n* equals ½ the IPs obey a parabolic growth law, which is compatible with diffusion as rate controlling process for the formation of the layers. If *n* equals 1 the layers grow linearly, suggesting that an interface reaction is rate limiting for the formation of the IPs [18].

The present experimental results show that the average *n* values are very close to 0.5, considering the experimental errors (Fig. 2.7 and Table 2.1). Therefore, it can be concluded that the intermetallic layers obey the parabolic growth law indicating rate control by volume diffusion. The square of the thickness of the intermetallic compound layers has been plotted as a function of the reaction time for the growth of the Cu_2In and Cu_7In_3 layers at 180, 250 and 290°C in Fig. 2.8a-c, respectively. The growth of the Cu_7In_3 layer at the additional temperatures 360 and 430°C is shown in Fig. 2.8d. Table 2.1 summarizes the results obtained by systems fitting of straight lines to the experimental data plotted in Fig. 2.8.

Obviously, the growth rates for the IPs increase with increasing temperature. The growth of the Cu_7In_3 layer is faster than that of the Cu_2In layer below 310°C. This may be understood as a consequence of the formation of the Cu_2In layer according to Eq. (2.4) and its decomposition according to Eq. (2.5). Because of the experimental errors, only approximate incubation times for both phases have been given in Table 2.1. It can be seen from Fig. 2.8 that the incubation times (t_0) for the IPs increase with decreasing temperature. Note that the incubation times for the IPs of the samples annealed at the lowest temperature, 180°C, are 1000 h approximately!

Table 2.1. Exponential value (*n*), growth rate constant (*k*), fit quality (r^2), and the approximate incubation time (t_0) for the formation of the Cu_2In and Cu_7In_3 phases.

T (°C)	δ (Cu_7In_3)			η (Cu_2In)			t_0 (h)
	n	*k* (µm²/h)	r^2	*n*	*k* (µm²/h)	r^2	
180	0.58	$3x10^{-4}$	0.97	0.53	$8x10^{-5}$	0.83	1000
250	0.51	0.017	0.99	0.43	0.003	0.99	20
290	0.42	0.073	0.98	0.40	0.024	0.97	5
360	0.40	0.62	0.99	-	-	-	1
430	0.53	3.47	0.99	-	-	-	0

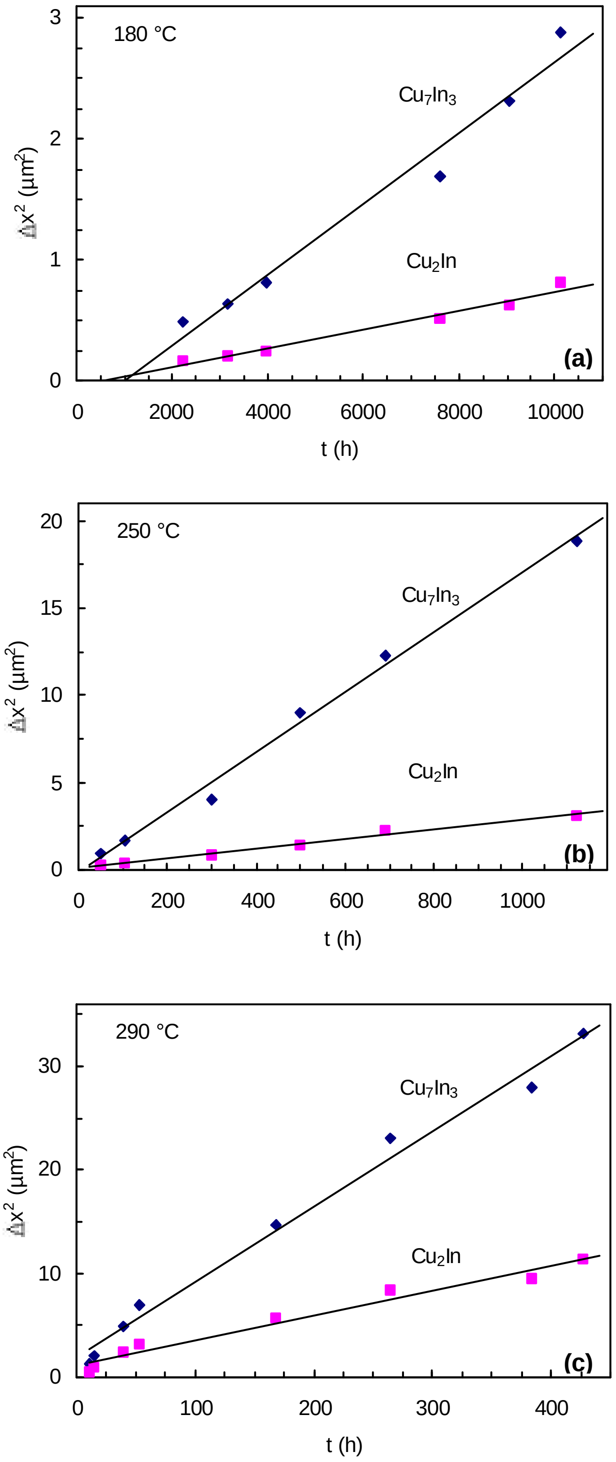

Fig. 2.8. The squared thickness of the Cu_2In and Cu_7In_3 layers as a function of the reaction time: (a) joint at 180°C; (b) at 250°C; (c) at 290°C; (d) at 360 and 430°C.

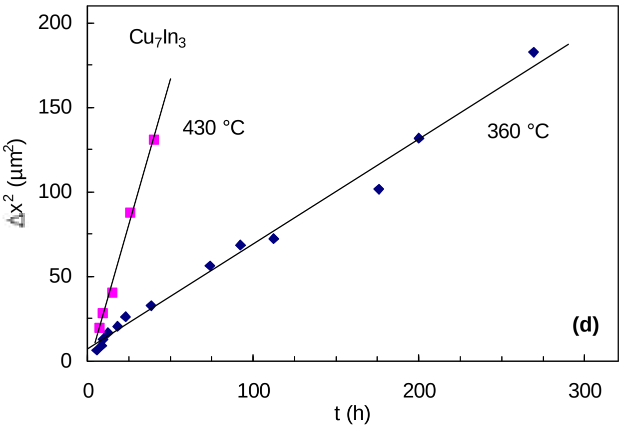

Fig. 2.8. Continued.

2.3.3 Interdiffusion coefficients

Treatments of single phase and multiphase diffusion in binary systems were presented by Kidson [12] and later by Wagner [13]. By modifying the Sauer-Freise generalization [19] of the Boltzmann-Matano analysis (cf. [20],[21]), Wagner developed a relationship between the interdiffusion coefficient, the parabolic growth rate constant and the concentrations at the interfaces, thought to be constant and equal to their equilibrium values. This approach is very convenient because the concentration profile determined for each of the intermetallic layers formed in the reaction zone of Cu/In/Cu interconnections is practically a horizontal line (see Fig. 2.2-Fig. 2.4 and what follows). As a consequence, the application of the Boltzmann-Matano analysis is associated with a very large error since the concentration gradient approaches zero and thus ∂x/∂C goes to infinity (x = distance coordinate, C = concentration). To handle this problem, an integral interdiffusion coefficient, $\tilde{D}_{\text{int}}$, is introduced [13] by integrating the interdiffusion coefficient, $\tilde{D}$, in phase i over the distance coordinate and thereby avoiding determination of the concentration gradient. Thus in the case where formation of phase i occurs, from phases (i-1) and (i+1) coexisting with phase i, the following expression holds:

$$\tilde{D}^{i}_{\text{int}} = \Delta N^{i}\tilde{D}^{i}_{av} = \frac{\left(N^{i} - N^{(i-1)''}\right)\left(N^{(i+1)'} - N^{i}\right)}{N^{(i+1)'} - N^{(i-1)''}}k^{i} \qquad (2.7)$$

$$k^i = \frac{\left(\Delta x^i\right)^2}{2t} \tag{2.8}$$

where i is the serial number of a particular phase considered for the evaluation of $\widetilde{D}_{\text{int}}$, i.e. corresponding to the integral interdiffusion coefficient $\widetilde{D}^i_{\text{int}}$, $\Delta N^i = N^{i\,'} - N^{i\,''}$ is the difference in the composition of component B (B = indium) in phase i at the interfaces between the phases (i-1) and i and between the phases i and (i+1), N^i (= ½ ($N^{i\,'} + N^{i\,''}$) is the average mole fraction of component B in phase i, $N^{(i-1)''}$ is the mole fraction of component B in phase (i-1) coexisting with phase i, $N^{(i+1)'}$ is the mole fraction of component B in phase (i+1) coexisting with phase i and k^i is the parabolic constant for the growth of phase i between phases (i-1) and (i+1) coexisting with phase i. Equation (2.7) was obtained under the following conditions:

- The interface concentrations do not change with time.
- The layer growth is proportional to the square root of the elapsed time.
- The differences between the molar volumes of the various phases are negligible.

Applying Eq. (2.7) for the calculation of the integral interdiffusion coefficients of the η (Cu_2In) and δ (Cu_7In_3) phases, it follows:

$$\widetilde{D}^d_{\text{int}} = \Delta N^d \widetilde{D}^d_{av} = \frac{\left(N^d - N^{Cu'}\right)\left(N^{h''} - N^d\right)}{N^{h''} - N^{Cu'}} k^d \tag{2.9}$$

$$\widetilde{D}^h_{\text{int}} = \Delta N^h \widetilde{D}^h_{av} = \frac{\left(N^h - N^{d'}\right)\left(N^{\mathrm{Cu_{11}In_9}''} - N^h\right)}{N^{d\,'} - N^{Cu_{11}In_9''}} k^h \tag{2.10}$$

The equilibrium concentration values were taken from the equilibrium phase diagram [10]. The $N^{Cu'}$ value is considered to be zero since the composition profiles (see Fig. 2.3-Fig. 2.5) show no presence of In atoms in Cu at the Cu/IP interface. Now the integral interdiffusion coefficients can be calculated from the parabolic growth constants listed in Table 2.1.

The Arrhenius relation for $\widetilde{D}_{\text{int}}$

$$\tilde{\mathrm{D}}_{\mathrm{int}} = \tilde{\mathrm{D}}_{\mathrm{int}}^{0} \exp(-\tilde{Q}_{\mathrm{int}} / RT), \qquad (2.11)$$

where $\tilde{\mathrm{D}}_{\mathrm{int}}^{0}$ is the pre-exponential factor and $\tilde{Q}_{\mathrm{int}}$ is the activation energy at a temperature T, can be fitted very well to the data (see Fig. 2.8). The results for $\tilde{\mathrm{D}}_{\mathrm{int}}^{0}$ and $\tilde{Q}_{\mathrm{int}}$ have been given in Table 2.2. The pre-exponential values differ about a factor of 2 for Cu_2In and Cu_7In_3; the activation energies are about equal.

The low values of the activation energies for the interdiffusion in the Cu_2In and Cu_7In_3 phases (100-110 kJ/mol) may be ascribed to the presence of fast diffusion paths (short-circuit diffusion). It has also been suggested that a growing IP may contain a relatively large amount of vacancies [18], which enhances substitutional diffusion. It is noted that the growth (diffusion) mechanism for the Cu_7In_3 phase was found to be independent of the reaction temperature being above or below 310°C (cf. Fig. 2.9); i.e. independent of the presence or absence of $Cu_{11}In_9$.

Table 2.2. The integral interdiffusion coefficient values of the Cu_2In and Cu_7In_3 phases and the Arrhenius parameters.

T (°C)	$\tilde{\mathrm{D}}_{\mathrm{int}}^{d}$ (m^2/s)	$\tilde{\mathrm{D}}_{\mathrm{int}}^{h}$ (m^2/s)
180	1.8×10^{-21}	4.2×10^{-22}
250	1.0×10^{-19}	1.6×10^{-20}
290	4.5×10^{-19}	1.3×10^{-19}
360	4.1×10^{-18}	-
430	2.3×10^{-17}	-
$\tilde{Q}_{\mathrm{int}}$ (kJ/mol)	99.1	108.7
$\tilde{\mathrm{D}}_{\mathrm{int}}^{d}$ (m^2/s)	6.1×10^{-10}	1.3×10^{-9}

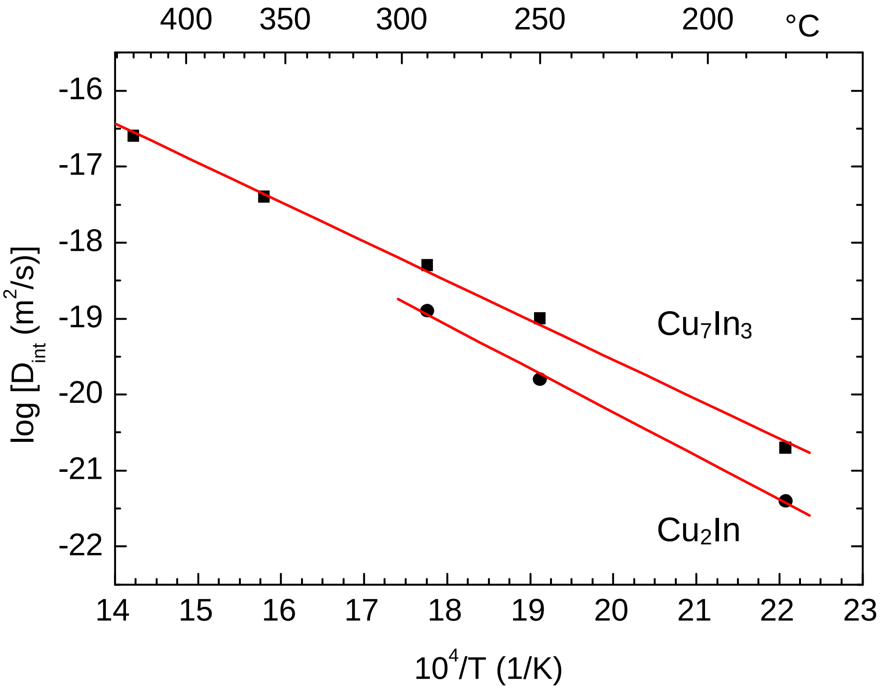

Fig. 2.9. Arrhenius plot of the integral interdiffusion coefficients for the Cu_2In and Cu_7In_3 phases (cf. Table 2.2).

2.4 Conclusions

- The first IP to be formed upon diffusion soldering Cu/In/Cu is the IP most rich in In at the reaction temperature: $Cu_{11}In_9$ at T < 310 °C and Cu_2In at T > 310°C. This In-rich IP grows into the liquid with a non-layered shape. The Cu for this IP formation is supplied by dissolution from the substrate and diffusion in the liquid.
- After all liquid In has been converted into the first solid IP, the other IPs form by a solid-solid reaction, in the order of increasing Cu amount: $Cu_{11}In_9 \rightarrow Cu_2In \rightarrow Cu_7In_3$ at T < 310°C and $Cu_2In \rightarrow Cu_7In_3$ at T > 310°C.
- The IPs formed by a solid-solid reaction grow in planar (layered) fashion. Their growth obeys a parabolic rate law, indicating that volume diffusion is the rate-controlling step.

- The growth of Cu_2In and Cu_7In_3 at 180°C, between Cu and $Cu_{11}In_9$, exhibits a large incubation time, suggesting difficult nucleation.
- The relatively small values for the activation energies for the intergral interdiffusion in the Cu_2In and Cu_7In_3 phases can be due to large defect concentrations as large vacancy concentrations in growing IPs.
- No change in the activation energy for the growth of Cu_7In_3 around 310°C was found, indicating that the rate-limiting mechanism of formation of Cu_7In_3 is not affected by the simultaneous growth of the Cu_2In phase above 310°C.
- The diffusion soldering process investigated leads to almost defect-free interconnections (free of large pores or voids), and with potential service temperatures much higher than the fabrication temperature.

3 Characterization of the reaction process in diffusion-soldered Cu/In-48Sn/Cu joints

S. Sommadossi, W. Gust, E.J. Mittemeijer

This work describes a Pb-free solder alternative for the interconnection technology and its implementation in a diffusion soldering technique: In-48at.%Sn solder (eutectic alloy) , with a melting point of 120°C. The system proposed has the advantages of both traditional soldering and diffusion bonding, i.e., good joint filling, high service temperature, and good mechanical properties. The diffusion reaction processes in Cu/In-48at.%Sn/Cu joints were investigated between 180 and 400°C. Electron microprobe analysis revealed the presence of one or two intermetallic layers in the interconnection zone: a layer of the η phase below 200°C, and layers of the η and ζ phases above 200°C. The η and ζ phases form through a solid-liquid and a solid-solid diffusion reaction, respectively. Below 200°C the η phase exhibits two different morphologies: large coarse grains at the η/(originally liquid)In-48at.%Sn interface and a fine-grained region at the Cu/η interface. The thickness of the ζ layer shows a constant growth rate (linear growth) at constant temperature. The temperature dependence of the growth rate constant of the ζ layer is described by an Arrhenius relationship with an activation energy equal to 121 kJ/mol and a pre-exponential factor of about 57 m/s.

3.1 Introduction

Due to the emerging environmental regulation worldwide impelling the elimination of Pb usage in electronic assemblies, the search of suitable Pb-free alloys has become one of the key research activities in microelectronics (cf. [1],[3],[22],[23]). Popular substitutes of Pb-based solders are Sn-based solders. Among the alloy families Sn-Ag, Sn-Au, Sn-Bi and Sn-In, the In-48at.%Sn eutectic alloy (further denoted by In-48Sn) is the one with the lowest melting point (120°C).

Several studies dealing with the reaction process of Cu and In-Sn alloys were performed (cf. [23]-[27]). Most of these works concerned relatively low reaction temperatures: especially temperatures below the melting point of the eutectic alloy were applied in order to simulate the service conditions of soldered joints. It was reported [27] that the reaction products developing between the Cu side and the In-48Sn eutectic alloy side were two layers of two intermetallic phases (IPs): $Cu_2(In,Sn)$ at the Cu side and Cu_2In_3Sn at the solder side. These IP layers appeared after dipping the Cu specimen in the In-48Sn melt for 3-40 s. The kinetic behaviour of the formation of the IPs was studied in the temperature range 70-110°C. The growth of the whole IP layer, consisting of $Cu_2(In,Sn)$ and Cu_2In_3Sn layers, was due mainly to the growth of the Cu_2In_3Sn layer. The thickness of the whole IP layer depended approximately parabolically on time at high temperatures and linearly at low temperatures. However, no detailed proof for the phase identification was presented in the earlier work. Since the diffusion soldering process takes place at process temperatures above the melting point of the solder, the results reported in [27] cannot be extrapolated without more ado. Therefore, a detailed study on the microstructure, the phase identification, and the kinetics of growth of the IPs formed during the diffusion soldering process for Cu/In-48Sn is presented. The temperature range used in the present study was 180-400°C.

This work presents the characterization of the Cu/In-Sn reaction resulting from a diffusion soldering process (cf. [2],[6],[28]). In short, this bonding technique consists in joining components with high melting point using a thin interlayer of solder material with low melting point. The assembly is held at a temperature above the melting point of the interlayer of solder material under a certain pressure, until all the low melting point interlayer has transformed into solid IPs. The resulting joint allows application at service temperatures much higher than the low manufacture temperature. Further advantages of this technique are a small joint area and a good joint filling. Multicomponent diffusion concepts as presented here can provide design strategies to improve the performance of alloys and coatings that must resist degradation and aging at elevated service temperatures.

3.2 Experimental techniques

The diffusion couples were prepared from high purity (99.999 wt.%) Cu slices with a diameter of 5-10 mm and a thickness of 2 mm. In-Sn eutectic composition alloys were prepared from high purity (99.999 wt.%) In and Sn obtaining foils with 100-200 µm thickness by cold rolling. The surface preparation for the Cu slices (≈ 2 mm) consisted in grinding and polishing using 1 µm diamond paste in the last step. The In-48Sn foil was sandwiched between the two Cu slices. A laboratory built heating-load press permitted to heat up rapidly the assembly with a heating rate of 200-300 °C/s to temperatures (180, 220, 290, 360 and 400°C) above the melting point of In-48Sn (120°C) under a slight mechanical pressure (≈ 0.5 MPa). During the subsequent annealing the isothermal reaction between In-48Sn (liquid) and Cu (solid) took place and the IPs formed. The treatment was carried out in Ar atmosphere in order to prevent oxidation.

After annealing, cross-sections of the joints were prepared for the metallographic analysis by embedding in epoxy, grinding and polishing, using 1 µm diamond paste in the last step. Optical microscopy was used to inspect the morphology of the joints. The optical micrographs showed clearly the different IP layers and permitted the measurement of the reaction-layer thicknesses. Each thickness value determined represents the average value of 30 measurements performed at regular intervals.

An electron probe microanalyser (Cameca SX100) equipped with 5 wave-length dispersive spectrometers was used to measure the chemical composition along line-scans perpendicular to the interconnection zone. Because of the limited spatial resolution (± 2 µm) of electron probe microanalysis (EPMA) reaction layers of thickness much larger than 2 µm were investigated.

3.3 Results and discussion

3.3.1 Phase Identification

The reactions between solder alloy and substrate material depend upon the thermodynamics and kinetics of a multicomponent system. Since most solder alloys consist of more than two elemental components, as also in this study, a ternary (or higher order) system has to be considered for understanding the occurrence of possible reaction products, even when the substrate is a pure metal. As a first approach to predict appearance of certain phases, the equilibrium phase diagram for the system concerned, if available, may be used. The solder–substrate reaction in a diffusion soldering process involves an initial solid-liquid reaction and a subsequent solid-solid diffusion reaction, possibly occurring at different temperatures. Very few (even only) ternary phase diagrams have been determined accurately in a wide range of temperature. For the Cu-In-Sn system, phase-diagram data have been provided by [29]. The data reported in Ref. [29] concern Cu-In-Sn alloys with a Cu content larger than 50 at.% at temperatures above 400°C: the isothermal section at 400 °C, i.e., at the lowest temperature for which data are available, is shown in Fig. 3.1.

The composition profiles across the reaction layers as determined by EPMA are shown for various samples in Fig. 3.2-Fig. 3.4. The observed abrupt composition changes indicate the occurrence of two IP layers of the following average compositions (numbers refer to at.%): Cu-16In-27Sn and Cu-10In-13Sn. According to the Cu-In-Sn phase diagram shown in Fig. 3.1 these average composition values are located in the η and ζ phase regions. The η and ζ phase symbols refer to the binary IPs Cu_2In and $Cu_{10}Sn_3$, which can dissolve a third element (Sn and In, respectively). The η phase represents a continuous solid solution between the Cu-Sn and Cu-In systems. The high-temperature phase ζ ($Cu_{10}Sn_3$) is stabilized at room temperature by the addition of In [29]. Because the melting points of the ternary η and ζ phases are about 500 and 600°C, respectively, the joint is stable at service temperatures much higher than the fabrication temperature. A temperature stability test, which consists of heating quickly the joint under a slight tensile stress and determining the temperature of rupture, showed that the joints can withstand temperatures up to 750°C. The EPMA analyses performed on the fracture surfaces of broken joints show that η and ζ layers transform rapidly during the heating process into the solid solution of Cu (a) which has a higher melting point than the η and ζ phases [29]. Thus the first objective of the diffusion soldering process was achieved.

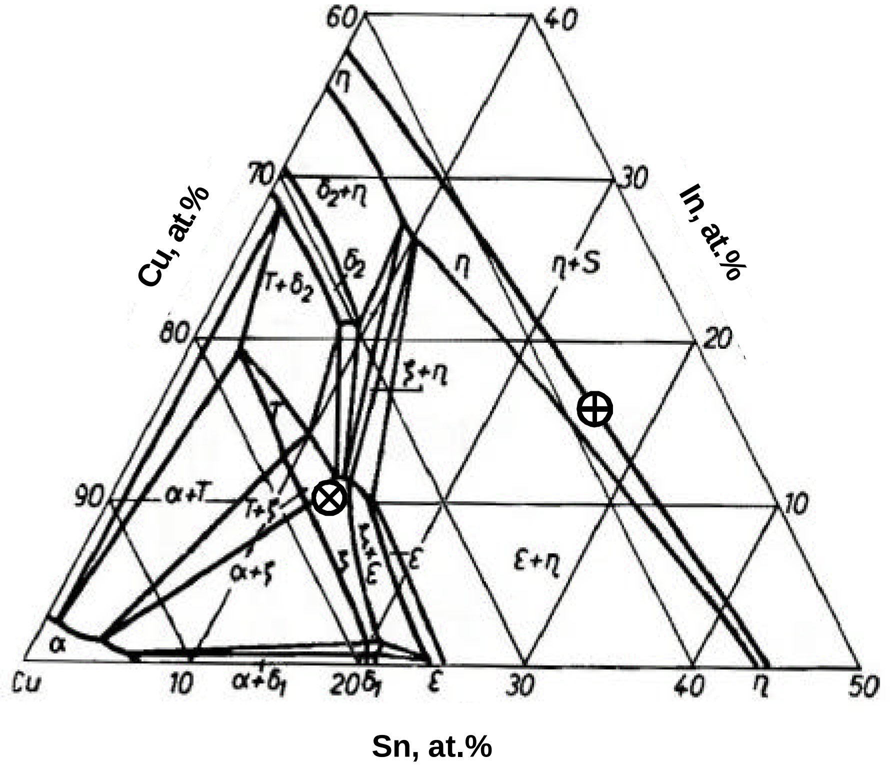

Fig. 3.1. Isothermal section of the ternary Cu-In-Sn phase diagram at 400°C [29], showing the average composition values of the ζ ⊗ and η ⊕ IPs.

The first IP formed is the η phase which develops as an irregular layer in the interconnection zone (see Fig. 3.2) through a liquid-solid diffusion reaction between Cu and the In-48Sn solder. The second IP that appears is the ζ phase which develops as a planar layer between Cu and the η phase through a solid-solid diffusion reaction process. The ζ phase does not appear below 200 °C; only the η phase forms below 200°C (see Fig. 3.2). The reaction layer grows until the liquid In-48Sn has been consumed. During this stage both layers thicken (at $T > 200$°C). After the solder material has been consumed, the η phase is used for further growth of the ζ phase, since the η phase is the only source of both In and Sn atoms. After longer annealing times at high temperatures, the ζ phase starts to decompose in term and In and Sn atoms diffuse into the Cu substrates to form the solid solution α shown in Fig. 3.1. This solid solution formation is reflected by the gradual concentration change within the Cu substrate close to the interface with the joint, as observed in the composition profile of a sample annealed at 400°C for 30 days (see Fig. 3.4). It indicates that after prolonged service times at high temperatures the interconnection zone will consist of a solid solution α, thereby increasing the temperature stability of the joint.

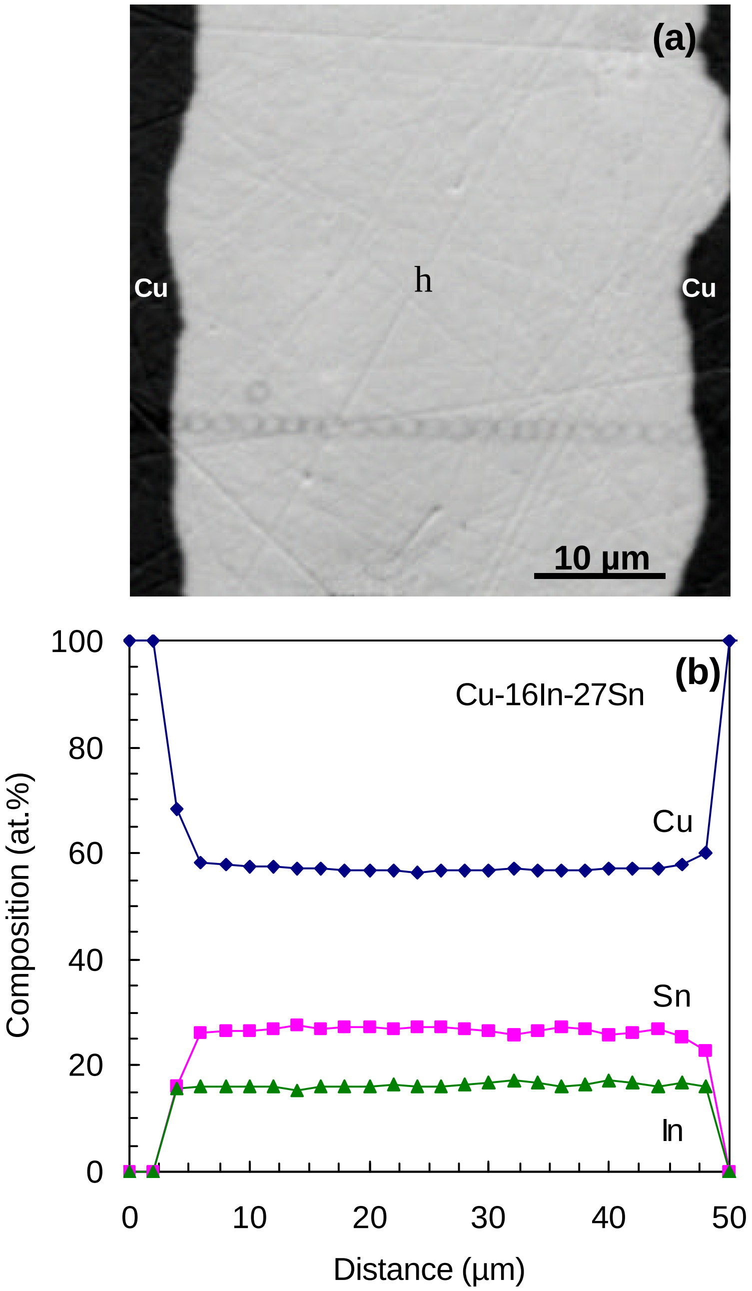

Fig. 3.2. Backscattered electron micrograph of a Cu/In-48Sn/Cu sample annealed at 180°C for 30 days (a) and the composition profiles across the reaction layer, as obtained by EPMA (b).

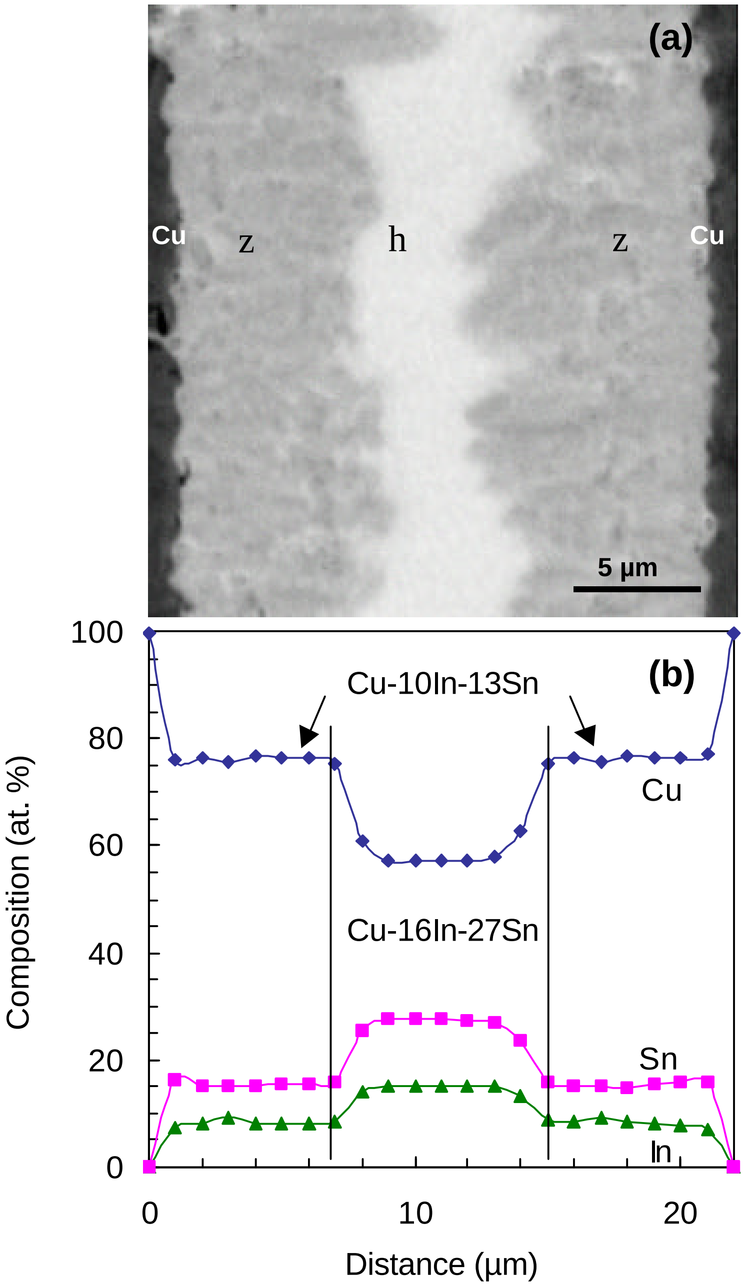

Fig. 3.3. Backscattered electron micrograph of a Cu/In-48Sn/Cu sample annealed at 290°C for 30 min (a) and the composition profiles across the reaction layer, as obtained by EPMA (b).

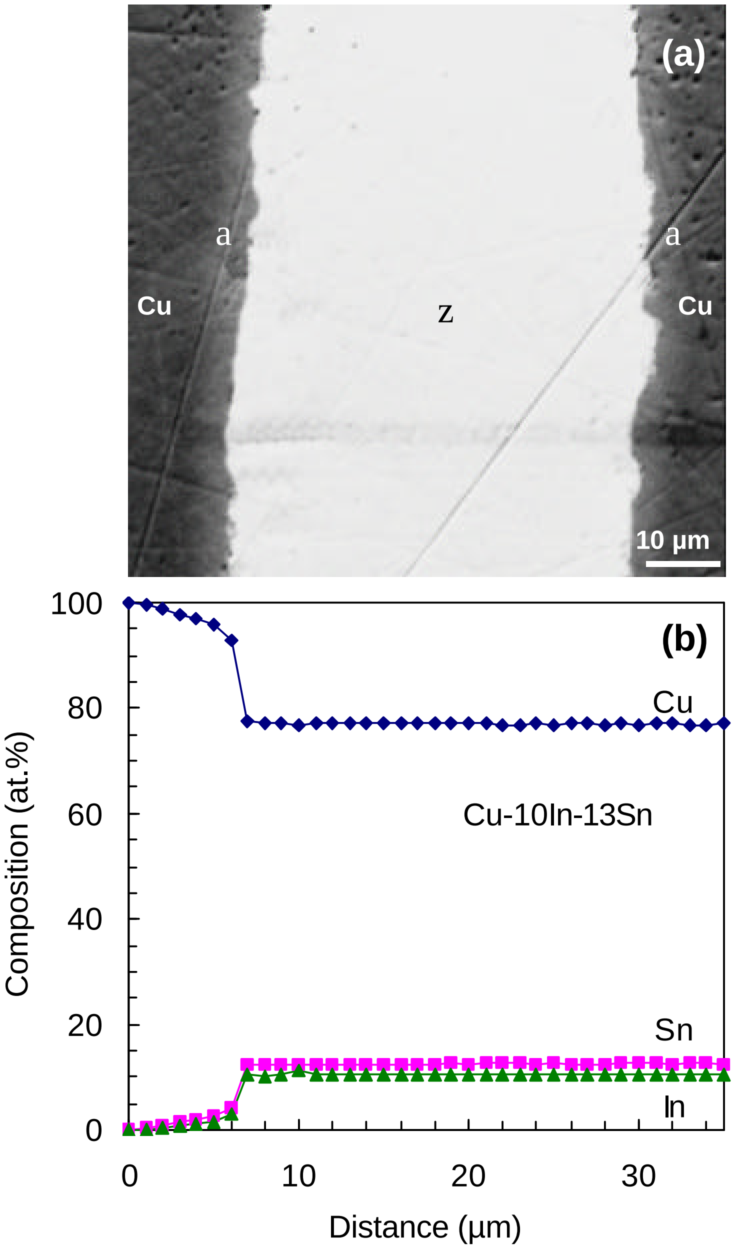

Fig. 3.4. Backscattered electron micrograph of a Cu/In-48Sn/Cu sample annealed at 400°C for 30 days (a) and a portion of the composition profiles across the reaction layer, as obtained by EPMA (b).

Optical micrographs showed that, possibly, a third discontinuous phase appeared as suggested by thin stripes (≈ 0.2 µm thickness) observed at the η/ζ interface (see Fig. 3.5). The composition of that phase could not be determined by EPMA because its particle extent was smaller than 2 µm (i.e., of the order of EPMA spatial resolution). According to the observations, this phase does not grow significantly during the annealing and it has disappeared after the η consumption. Without knowledge of the composition of this phase and sufficient ternary phase-diagram data it is currently impossible to trace the diffusion path in the phase diagram [30].

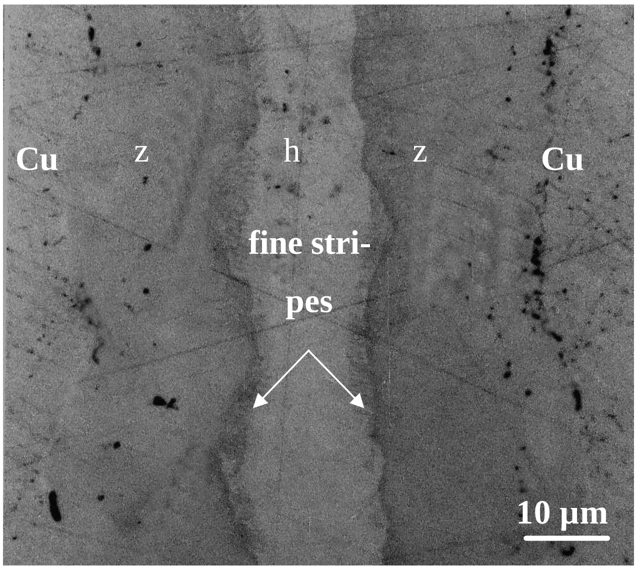

Fig. 3.5. Optical micrograph showing the morphology of the discontinuous stripes at the η/ζ interface.

When only the growth of the η phase takes place, i.e., below 200°C, two different morphologies for the η phase can be discerned. As shown in Fig. 3.6, the first η grains developing at the solid/liquid interface are large and their shape suggests their growth into the liquid In-48Sn. At a later stage, a fine-grained morphology develops that seems to pertain to growth into the solid Cu. The boundary between the two microstructures of the η phase corresponds to the original Cu/In-48Sn interface (see also [31]). A similar observation was made for the growth of Ni_3Sn_4 at the solid Ni/liquid Sn interface [32]. Hence, the η phase apparently forms by two mechanisms: (i) Cu atoms diffuse through the solid η, and react with the liquid at the liquid/grain interface, and (ii) In and Sn atoms diffuse through the solid η phase to the Cu/η interface and react there with Cu atoms. Upon continued reaction the initially coarse η grains at the solid/liquid interface grow laterally and the grooves disappear. The relative thicknesses of the region of coarse grains due to Cu diffusion and of fine grains due to In and Sn diffusion is 2:1 approximately (see Fig. 3.6). It may suggest that the mobility of the Cu atoms in the η phase is higher than the mobility of the In and Sn atoms through the η phase. Such a phenomenon is described in [33] as leading to a duplex microstructure, where both sublayers can differ in shape, size and/or orientation of their grains.

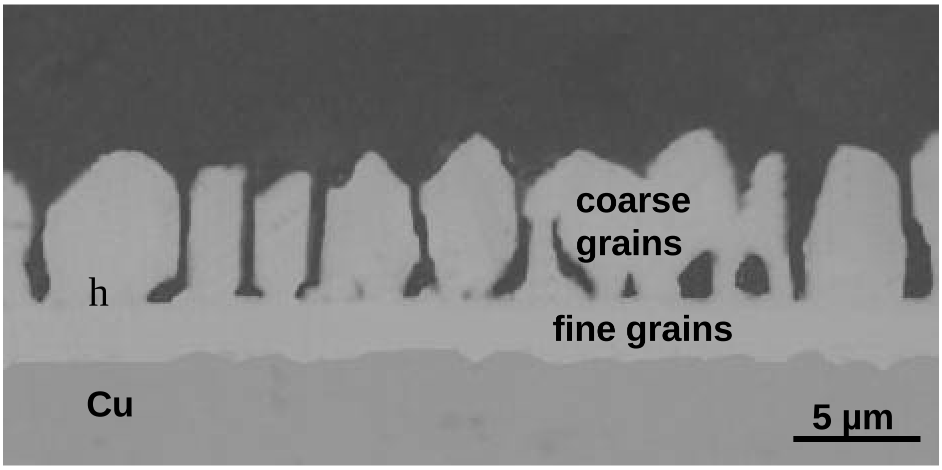

Fig. 3.6. Etched cross-section of a sample diffusion soldered at 200°C for 30 min, showing the two different microstructures of the phase η: fine and coarse grains.

3.3.2 Kinetics

Since the ζ phase is the IP with the highest melting point in the joint, i.e., the most attractive IP in view of application (see Section 3.1), its growth behaviour was investigated here at 220, 290, 360 and 400°C. The growth of an intermetallic layer may generally be described by a power law:

$$\Delta x = k\, t^n \qquad \text{or} \qquad \log \Delta x = \log k + n \log t \tag{3.1}$$

where Δx is the layer thickness, k is the growth rate constant, t is the reaction time, and n is an exponent which contains information about the rate controlling mechanism (cf. [34]-[36]). One can distinguish between IP layer growth governed by volume diffusion across the growing product phase ($n = ½$) and IP layer growth by reaction at the interface ($n = 1$).

The results shown in Fig. 3.7 for the growth of the ζ layer indicate that the n values are very close to 1 at all temperatures applied. Hence, it is concluded that the rate controlling step in the ζ layer growth is the reaction at the interface whit a growth rate-constant independent from reaction time. The results for the n values and the growth rate constants, and the statistical errors corresponding to the straight line fits in Fig. 3.7 are presented in Table 3.1. Extrapolation of the straight lines in Fig. 3.7 indicates that negligible values occur for the possible incubation time for ζ layer growth, except for the sample annealed at 220°C which shows an incubation time of about 13 h.

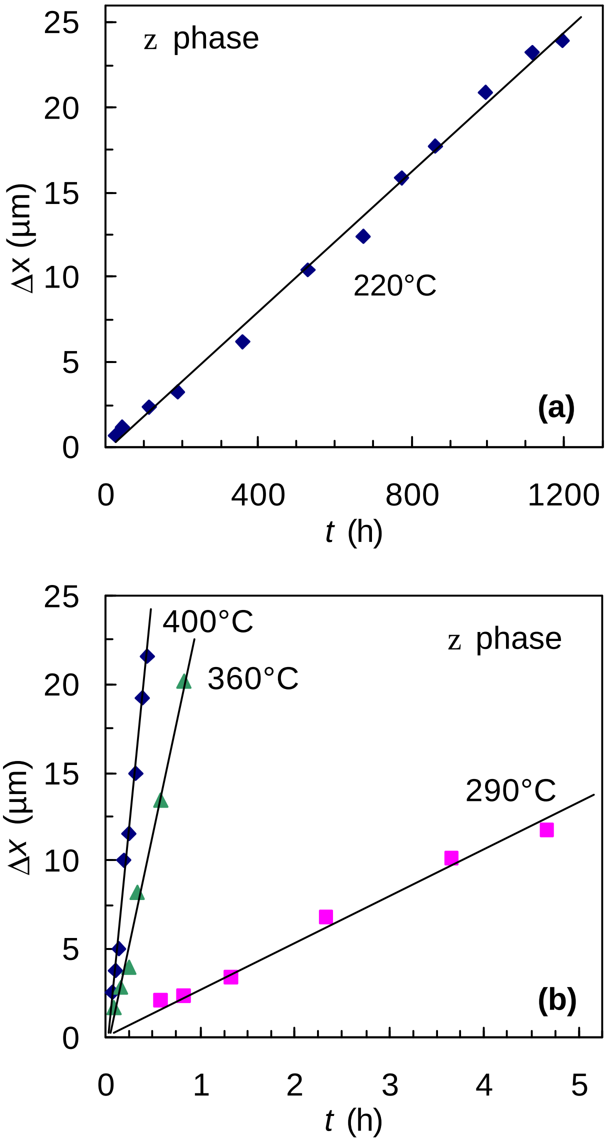

Fig. 3.7. The thickness of the ζ phase layer as a function of the reaction time for joints annealed at 220°C (a) and 290, 360 and 400°C (b).

Table 3.1. Growth rate exponent n obtained from Eq. (3.1) and growth rate constant k (r^2 = goodness-of-fit parameters of linear regression in Fig. 3.7)

	$\log \Delta x = A + n \log t$		$\Delta x = k\,t$, when $n = 1$	
T (°C)	n	r^2	k (m/s)	r^2
220	0.92	0.991	$5.8\text{x}10^{-12}$	0.995
290	0.90	0.986	$6.9\text{x}10^{-10}$	0.991
360	1.12	0.974	$7.0\text{x}10^{-9}$	0.989
400	1.17	0.993	$1.5\text{x}10^{-8}$	0.995

In the literature evidence of linear growth was obtained at lower temperatures (T < 100°C) for the Cu_6Sn_5 phase in Cu/Sn couples (cf. [37],[38]). At higher temperatures (T > 100°C) the growth of this phase obeys a parabolic (i.e., $n = ½$) or a sub-parabolic relationship (i.e., $n < ½$) (cf. [4],[7],[39]). The growth of the IPs in Cu/In couples was reported to be of parabolic nature (see section 2.3.2 and [5]). Further, considering the reaction between the In-Sn solder and Au, another noble metal like Cu, a parabolic relationship for $AuIn_2$ layer growth has been observed [40]; here the Sn atoms appear not to operate in the reaction. However, the growth of the $AuIn_2$ layer, resulting from the reaction between the Pb-In solder and Au, seems to be very different from the growth of the $AuIn_2$ layer observed for the Au/In-Sn system, since the $AuIn_2$ layer growth observed for the Au/Pb-In system obeys a linear relationship with the Pb atoms not operating in the reaction [41].

From the point of view of the diffusion soldering process, the linear growth behaviour observed for ζ layer growth in Cu/In-48Sn is advantageous: linear growth allows more rapid IP formation and reduces manufacturing process time. The growth rate constant of reaction layer formation (at constant pressure) may be described by an Arrhenius relationship according to,

$$k = k_0 \exp(-Q / \mathrm{R}T) \qquad (3.2)$$

where Q denotes the activation energy for growth process, R is the gas constant, and k_0 is the pre-exponential coefficient. The Arrhenius plot for the growth rate constant of the ζ layer is shown in Fig. 3.8 (values for k from Table 3.1). The activation energy for the growth process appears to be 121 kJ/mol and the pre-exponential coefficient is 57 m/s.

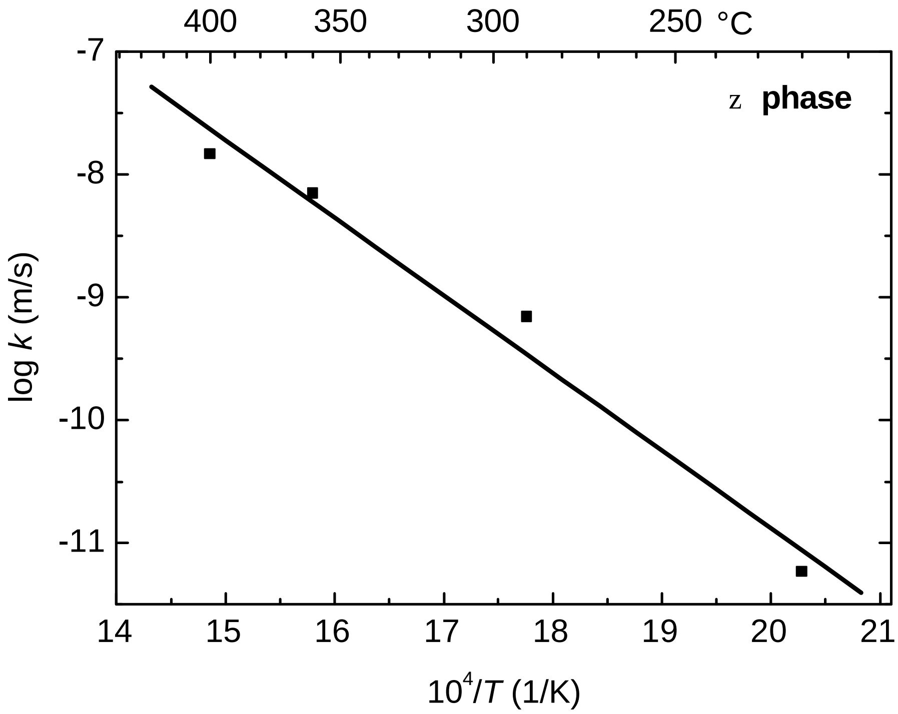

Fig. 3.8. Arrhenius plot for the growth rate constant of the ζ layer (see Table 3.1).

The IP growth behaviour and the IP crystal structure may be related as follows: the $Cu_{10}(Sn,In)_3$ or ζ phase is hexagonal (a = 0.7330 nm, c = 0.7864 nm) and exhibits a superstructure symmetry based on the ζ (AgZn) prototype [42]. The $Cu_{10}Sn_3$ original structure can be visualized as a stacking of six main layers of atoms perpendicular to c with all the Sn atoms in two of these layers separated by $c/2$ and such that no first neighbour Sn–Sn contacts occur [28]. Therefore, it is likely that the majority component, Cu, can diffuse in the ζ phase on its own sublattice by a vacancy mechanism, whereas the minority atoms (In and Sn) have to move via Cu positions in the lattice involving disturbance of the ordered structure. Therefore, the Cu atoms may diffuse faster through the ζ phase than the In and Sn atoms. This suggests that the main growth of the ζ layer takes place at the ζ/η interface.

Indeed, additional experiments performed in the temperature range 220-400°C in this work, using Cu and In-48Sn sputtered layers on Si, support this suggestion: the Si/Cu interface was used as a marker and it was observed that the ζ/η interface moved faster in the direction of the η phase than the Cu/ζ interface in the direction of the Cu substrate, indicating that the ζ formation occurs mainly at the ζ/η interface.

3.4 Conclusions

- Two intermetallic phase (IP) layers develop in Cu/In-48Sn couples with the following average composition in at.%: Cu-16In-27Sn and Cu-10In-13Sn, which correspond to the η and ζ regions according to the Cu-In-Sn phase diagram. The η phase develops through a solid-liquid reaction; the ζ phase develops through a solid-solid reaction.
- Below 200°C, only the η phase forms, the ζ phase did not appear up to at least 30 days annealing. Above 200°C, both the η and ζ phases grow simultaneously.
- When the η phase grows alone, i.e., below 200°C, it shows two different morphologies: large coarse η grains which grow into the liquid In-48Sn due to diffusion of Cu from the substrate and a fine-grained region which grows into the solid Cu due to In and Sn diffusion through the η layer .
- The thickness of the ζ phase layer, which forms through a solid-solid reaction, shows a linear dependence of thickness on reaction time for annealing temperatures between 220 and 400°C: the reaction is controlled by reaction at the interface.
- The activation energy for growth of the ζ phase is 121 kJ/mol and the pre-exponential coefficient is 57 m/s.
- The observed linear dependence on reaction time for the thickness of the ζ layer and the high melting points of the η and ζ phases (600 and 500°C, respectively) are favourable for application of this system in diffusion soldering: resulting joints can withstand *high* service temperatures after fabrication at a *low* temperature.

4 Mechanical properties of Cu/In-48Sn/Cu diffusion-soldered joints

S. Sommadossi[1]*, J. Huici*[1,2]*, P.K. Khanna*[3]*, W. Gust*[1]*, E.J. Mittemeijer*[1]

[1]Max Planck Institute for Metals Research and Institute of Physical Metallurgy, Stuttgart University, Germany
[2]Engineering Faculty, Comahue National University, Neuquén, Argentina
[3]Central Electronics Engineering Research Institute, Pilani, Rajasthan, India

Cu/Cu joints were produced in the temperature range 200-360°C by the diffusion soldering process, using the In-Sn eutectic alloy as solder material. Two intermetallic phases (IPs) appeared in the interconnection zone, η (Cu-poor IP) and ζ (Cu-rich IP) layers, but below 200°C only η grew. Three mechanical tests were performed to characterize the mechanical behaviour of diffusion-soldered Cu/In-48Sn/Cu joints: the tensile and shear strengths and the (nanoindentation) hardness were measured. The results show that the ζ phase has better mechanical properties than the η phase. The hardness measurements indicate that the most brittle IP layer is the η layer. The η phase has two crystallization morphologies: a duplex microstructure, involving a weak interface between sublayers composed of relatively small grains and relatively large grains, respectively. The ultimate shear and tensile strengths show similar tendencies for all joints. The ultimate shear strength of the joints improves almost 3 times when the η phase is converted into the ζ phase by a solid-solid diffusion reaction process. The surface of the In-48Sn films was etched before the diffusion soldering to improve the mechanical properties. The resulting joints, if composed of a single ζ layer, can withstand stresses above 155 MPa.

4.1 Introduction

The diffusion soldering process is a combination of the conventional soldering and diffusion bonding process and thereby presents several advantages in comparison with these traditional joining methods [2]. Diffusion soldering is attractive because it requires a low fabrication temperature whereas the joint can withstand a high service temperature, of about 400°C above the fabrication temperature. The eutectic In-48at.%Sn alloy is a promising candidate for diffusion soldering because of its low melting point (120°C), its good wetting behaviour [2] and the possibility to form intermetallic phases (IPs) with Cu components according to the phase diagram. The microstructural and kinetical characterization of diffusion soldered Cu/In-48Sn/Cu joints was performed earlier in this project (see Section 3).

The mechanical behaviour of a joint determines largely its practical importance (cf. [3],[22],[23],[43]) since joints must form both an electrical and a mechanical connection. In general, the mechanical properties of a material are characterized by its response to externally imposed stresses or strains.

A large number of investigations on the mechanical behaviour of solder alloys were focused on conventionally soldered joints (cf. [3],[23],[43],[44]). In a soldered joint the interconnection zone consists mainly of solder alloy and relatively thin layers of IPs close to the original components to be joined. Only a few studies were devoted to the mechanical properties of interconnections formed entirely of IPs, as resulting from diffusion soldering (cf. [2],[28],[45],[46]). In the present work tensile, shear and nanohardness testing was performed for diffusion soldered Cu/In-Sn/Cu joints. The ultimate tensile strength (UTS) and ultimate shear strength (USS) and the hardness values are discussed, also on the basis of performed fractographic analyses. The ultimate shear and tensile strength values are given by the maximum engineering stress values (the engineering stress is the stress calculated from the applied load with respect to de original specimen cross-section). Special attention has to be paid to the shear strength tests since this is the type of loading most common under normal service conditions; the differences in the thermal expansion experienced between the components in the joint upon application at high service temperature are the principal origin for the shear loading.

4.2 Experimental techniques

Diffusion-soldered joints were made by coating cold-worked Cu substrates (99.999 wt.%) with a In-48Sn layer by sputtering and subsequent annealing under stress, as follows. The Cu surfaces were polished by ultramilling to get a mirror-like surface finishing. A 5 µm thick In-48Sn film was deposited on the Cu substrate by sputtering from a In-48Sn target (99.999 wt.%) in a plasma beam apparatus. After this procedure the samples (each composed of two Cu substrates covered with an In-48Sn film) were diffusion soldered at the process temperatures (200, 290 and 360°C) under a slight compressive stress of 0.5-5 MPa. The compressive pressure was used to control the joint thickness and geometry. A bond thickness of 10 ± 1 µm was achieved. Additional joints were prepared using a 100 µm thick In-48Sn foil (99.999 wt.%), thereby achieving a joint thickness of 20 ± 2µm.

The relatively high oxidation affinity of Sn and In can lead to a thin oxide layer of about 5 nm thickness on the In-48Sn sputtered layer at room temperature, which acts as a diffusion barrier in the subsequent diffusion soldering [47]. Therefore, to improve the quality of the surface of the sputtered In-48Sn layer, the surface was etched using an etching agent consisting of a solution of 6 M HCl + 2 M $FeCl_3$ [48]. The samples were immersed about 1 min in the solution, followed by ultrasonic cleaning in alcohol. A group of samples was prepared under a vacuum of 10^{-5} mbar in a furnace, and a group of samples was prepared in air.

Inspection of the joint cross-section was performed by means of light microscopy (LM), scanning electron microscopy (SEM) and electron probe microanalysis (EPMA; wavelength dispersive analysis), see Section 3. The fracture surfaces after shear and tensile testing were analyzed by SEM. The fractography investigation also included analyses of the composition of the fractured surfaces in the SEM (EDX; energy dispersive analyses). This information was combined with cross-sectional observation of the fractured interconnection zone by LM in order to determine where the fracture took place.

To perform the nanohardness measurements, a cross-section of the Cu/In-48Sn/Cu joints had to be prepared carefully, since nanohardness measurements are very sensitive to the roughness. The samples were embedded in resin, ground and polished using 6, 3 and 1 µm diamond paste and 0.25 µm SiO_2 colloidal suspension. The hardness measurements were performed by scanning force microscopy (SFM) with a contact mode indentation as described in detail in [49]. The hardness measurements were made using a scanning nanoindenter [50] consisting of a depth-sensing force transducer (Hystron TriboScope) combined with a commercial scanning probe microscope (NanoScope III MultiMode, Digital Instruments) equipped with a three-sided pyramidal Berkovich diamond tip [51]. With this combination, the indenter tip can also be used as a probe for contact-mode SFM imaging. This makes it possible to select the area of interest, and to position the tip before indentation with an accuracy of 10 nm [49]. By this means the image of the residual imprint of the indentation can be obtained. The indentations were carried out by applying a constant load of 100 nN and a relatively short load-time cycle: 5 s for loading and 5 s for unloading, obtaining a depth resolution of 0.2 nm.

An INSTRON tensile testing machine was used to carry out the tensile and shear strength tests to obtain the UTS and USS values. The tests were performed at room temperature under a displacement rate of 0.5 mm/min. The geometry of the samples applied for shear and tensile testing is shown in Fig. 4.1: a single lap joint was used for the shear testing, and a disc joint was used in the tensile testing. In both cases the external Cu surfaces of the Cu/In-48Sn/Cu assembly were fixed to steel sample holders with an epoxy glue (Duralco 4525 by Polytec). These Cu surfaces were polished by ultramilling and the steel surfaces were polished with 4000 grinding paper. The sample dimensions were designed such that glue failures, *before* fracturing of the joint occurs, was avoided (see Fig. 4.1). A set of 5-6 samples was tested for each combination of process parameters.

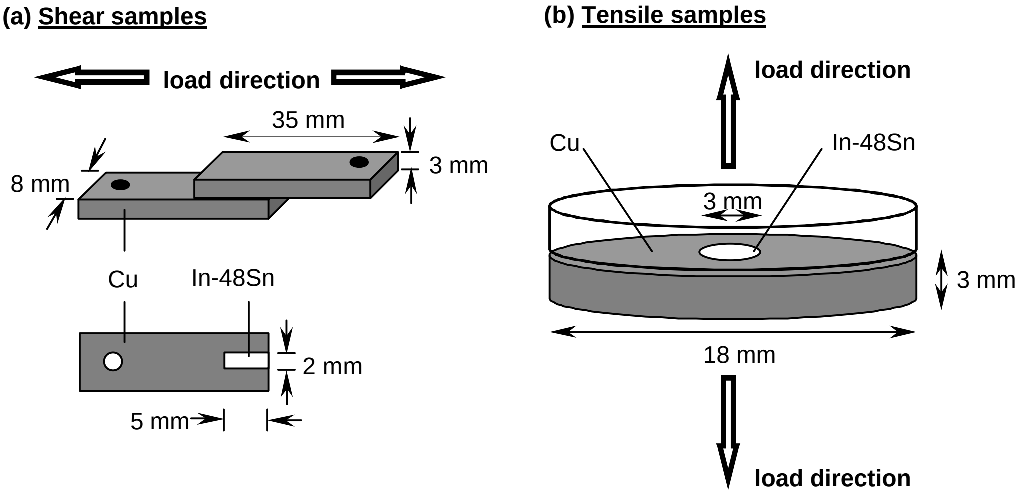

Fig. 4.1. Sample geometry used for shear testing (a) and tensile testing (b).

4.3 Results and discussion

Two IPs are formed in the interconnection zone at the annealing temperatures: η–$Cu_2(In,Sn)$ and ζ–$Cu_{10}(Sn,In)_3$. The η phase forms first in a solid-liquid diffusion reaction process and the ζ phase forms subsequently in a solid-solid diffusion reaction processes. Only the η phase forms below 200°C, i.e. the ζ phase does not appear even up to 30 days annealing time. Above 200°C the η phase and the ζ phase grow simultaneously, forming a Cu/ζ/η/In-48Sn couple (see Section 3).

In order to analyse the influence of the IPs on the mechanical behaviour of the joints, all possible combinations of the occurring IPs were tested. On the basis of the earlier kinetic study (see Section 3), it was possible to produce joints consisting of: Cu/η/Cu, Cu/ζ/η/ζ/Cu and, Cu/ζ/Cu. Several joint cross-sections are shown in Fig. 4.2.

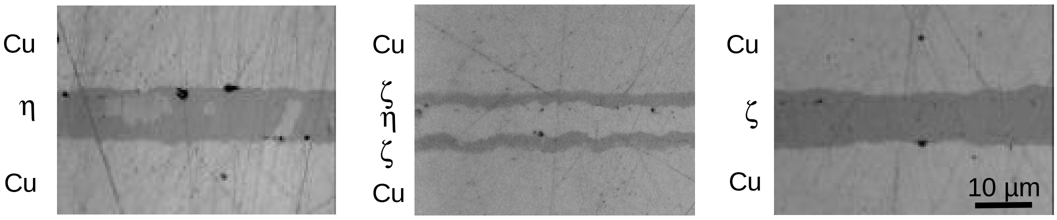

(a) 200°C, 120 min (b) 290°C, 20 min (c) 290°C, 80 min
360°C, 50 min

Fig. 4.2. Light optical micrographs showing the microstructure of Cu/In-48Sn/Cu diffusion-soldered joints under several conditions.

4.3.1 Shear strength measurements

The samples used for the shear test, with the geometry sketched in Fig. 4.1, were annealed in a furnace under vacuum of 10^{-5} mbar. The values measured for the USS (see Section 4.2) have been gathered in Table 4.1.

Evidently, the joints containing an η phase layer show very low USS values, in comparison with the joints consisting exclusively of ζ phase. The SEM observations indicate that the fracture occurred always through the η phase layer (if present). It is concluded that the η phase is the weakest phase in the interconnection zone. The weakness of the η phase layer may be ascribed to ist overall relatively large grain size due to the liquid-solid reaction and ist microstructural inhomogenity (see Section 4.3.3); the ζ phase, grown by a solid-solid reaction, has a relatively small grain size and has a homogeneous microstructure (see Section 3). A smaller grain size generally, corresponds with better mechanical properties [52].

Table 4.1. Ultimate shear strength (USS) values for Cu/In-48Sn/Cu joints.

Joint production			USS	IPs in	Rupture
T (°C)	t (min)	Remarks	(MPa)	Joint	through
200	80		4 ± 2	η	η
	80	etched	6 ± 2	η	η
290	20		8 ± 3	η, ζ	η
	20	etched	>30 ± 3*	η, ζ	-
	80		22 ± 2	ζ	ζ
	80	etched	>146 ± 8*	ζ	-
360	20		20 ± 3	ζ	ζ
	50		23 ± 2	ζ	ζ
	50	etched	>155 ± 15*	ζ	-

* The joint did not fracture. At that stress value the test was stopped because the Cu sheets started to deform plastically.

To determine the influence of the thin oxide film on the sputter deposited In-48Sn surfaces, an etching procedure was employed (see Section 4.2). The use of the etching agent on the In-48Sn sputtered surfaces improves very much the mechanical performance of the joints: see results listed in Table 4.1. The USS values of the etched samples produced at 290 and 360°C could not be determined accurately because the Cu sheets deformed plastically before the joint fractured! (The USS* values shown in Table 4.1 were calculated by taking the load values just before the Cu plates started to deform plastically). In any case it can be concluded that the USS increases more than 6.7 times when the etching procedure is employed, i.e. it reaches values higher than 155 MPa of joints consisting of a single layer of ζ phase.

Further evidence for the detrimental effect of the oxidation of the In-48Sn layer was obtained from the shear strength testing of two groups of samples fabricated at 290°C: (a) under a vacuum of 10^{-5} mbar and (b) in air. The results are shown in Table 4.2. The USS values appear to be more sensitive to the atmosphere quality in samples where the η phase is present too. The USS increases distinctly when the atmosphere quality improves (i.e. when the amount of oxygen in the atmosphere is reduced).

Table 4.2. Influence of the atmosphere quality on USS.

Joint production at 290°C		USS (MPa)	IPs in joint	Rupture through
t (min)	Remarks			
15	air	4 ± 1	η, ζ	η
20	vacuum	8 ± 3	η, ζ	η
60	air	19 ± 1	ζ	ζ
80	vacuum	22 ± 2	ζ	ζ

Several experiments were also performed in order to determine the influence of the type of In-48Sn joint material and of the joint material thickness on the mechanical properties of the joints. USS values of samples produced using an In-48Sn sputtered layer and of samples produced using an In-48Sn foil are shown in Table 4.3. The USS is practically insensitive to the use of either In-48Sn foil or sputtered In-48Sn layer, for all temperatures and times investigated: for the same joint thickness, the joints prepared at 290°C for 80 min using the sputtered In-48Sn layer and those prepared at 290°C for 90 min using the In-48Sn foil gave USS values of 22 and 21 MPa, respectively. The joint thickness has an effect on the USS, especially for the samples where the η phase was present: the USS increased from 8 to 20 MPa when the joint thickness increased from 10 to 20 µm for joints manufactured at 290°C for 20 and 30 min of reaction time, respectively; a similar observation holds for samples annealed at 360°C.

Table 4.3. Effect of the joint material type (In-48Sn foil or sputtered layer) and the joint thickness on the USS values.

Joint production				USS	IPs in	Rupture
T (°C)	t (min)	Interlayer	Thickness (µm)	(MPa)	joint	through
290	20	sputter	10	8 ± 3	η, ζ	η
	30	foil	20	20 ± 3	η, ζ	η
	60	foil	20	23 ± 3	η, ζ	η
	80	sputter	10	22 ± 2	ζ	ζ
	90	sputter + foil	10	21 ± 1	ζ	ζ
360	5	foil	20	24 ± 4	ζ	ζ
	15	foil	20	27 ± 5	ζ	ζ
	20	sputter	10	20 ± 3	ζ	ζ

4.3.2 Tensile strength measurements

The samples used for the tensile testing, with the geometry sketched in Fig. 4.1, were annealed in a furnace under a vacuum of 10^{-5} mbar. The values measured for the UTS (see Section 4.2) have been gathered in Table 4.4. The trends observed for the UTS are similar to those for the USS. Fracture always takes place trough the η layer. The samples which have only the ζ phase are stronger than the samples with (also) a η layer. When the In-48Sn sputtered layer was etched in advance of joining the UTS increased dramatically: for a joint consisting entirely of a ζ layer an UTS of 160 MPa was achieved. These relatively high UTS values are comparable to those reported for bonds used in structural applications [53].

Table 4.4. Ultimate tensile strength (UTS) values for the Cu/In-48Sn/Cu joints.

Joint production			UTS	IPs in	Rupture
T (°C)	t (min)	Remarks	(MPa)	joint	through
200	80	-	13 ± 3	η, ζ	η
290	20	-	25 ± 2	η, ζ	η
360	50	-	56 ± 3	ζ	ζ
	50	etched	160 ± 5	ζ	ζ

4.3.3 Fracture morphology

A representative example of the fractured surface morphology after shear testing is shown in the SEM micrograph of Fig. 4.3. Three parts of the fracture surface can be observed on the micrograph showing a step-shaped geometry where part A is on the top and part C is on the bottom of the step-shaped fracture surface. Part A, B and C are roughly parallel to the intercace with the Cu substrate. The EPMA measurements on the joint cross-section of the same sample indicated that the η and ζ IPs are present in the interconnection zone. EPMA performed on the fractured surface indicated that the three parts (A, B and C) correspond to the same IP layer, i.e. the η phase layer. Hence the fracture takes place through the η layer. The same type of fracture morphology was observed for samples consisting of only a single ζ layer; see the cross-sectional view in Fig. 4.4.

The part B, either within η or within ζ IPs shows a transgranular fracture mode. The sharp changes of the fracture direction at the transitions A-B and B-C indicate intergranular fracture behaviour when the fracture moves from one fracture plane to another one. The straight lines visible on the surface part C (Fig. 4.3) are remnants of the ultramilling process on the Cu surface (see Section 4.2): the flat surface parts A and C are located near to the original Cu/solder interfaces, but within the IP layer, see the schematic illustration in Fig. 4.5. The surface part B is approximatelly in the middle of the joint, which suggests that it practically coincides with the original interface between both In-48Sn layers (cf. joint production description in Section 4.2).

The fracture takes place mainly at the A and C parts of the fracture surface as is illustrated in Fig. 4.6. The extension of part B is very small in Fig. 4.6, which is typical for fracture through ζ (see also Fig. 4.3 and Fig. 4.4). The ripples on surface part A shown in Fig. 4.6 are oriented more or less perpendicular to the direction of shear loading. This morphology appear only when fracture occurred through ζ phase, which may be related to the higher strength of ζ as compared to η, indicating a higher capacity of ζ to accommodate plastic deformation before fracture may occurs.

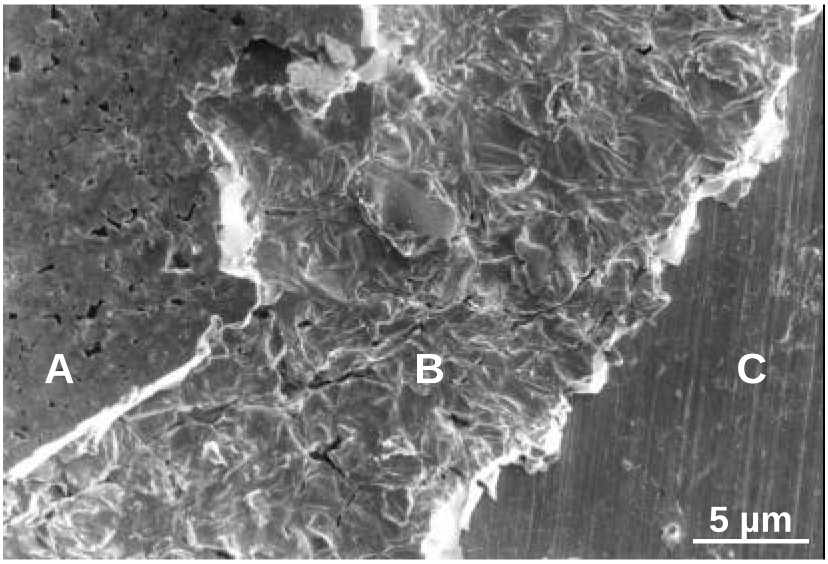

Fig. 4.3. SEM micrograph of the fracture surface after shear testing of a diffusion-soldered joint at 290 °C for 15 min. A, B and C correspond to fracture surfaces within the η layer (see also Figs 4.4 and 5).

For discussing fracture through the η layer, it should be recognized that η layer exhibits two different crystallization morphologies: the η layer is composed of two sublayers of small and large grains, respectively (See Section 3). The grains of the sublayer, that developed by growing into the liquid, are relatively large, the grains of the second sublayer, that developed by growing into the solid, are relatively small (see also [32],[33]). The interface between the sublayers of large and small grains is likely the mechanically weakest place in the interconnection zone and, indeed, the C and A parts of the fracture surface are the largest parts of the fracture surface.

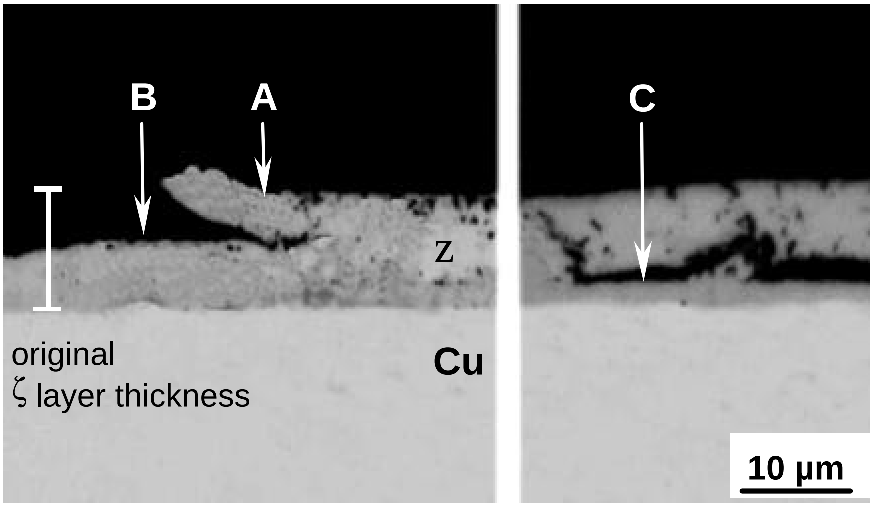

Fig. 4.4. Optical micrograph of the cross-section of the joint diffusion-soldered at 290°C for 90 min after shear testing. A, B and C show where the fracture takes place.

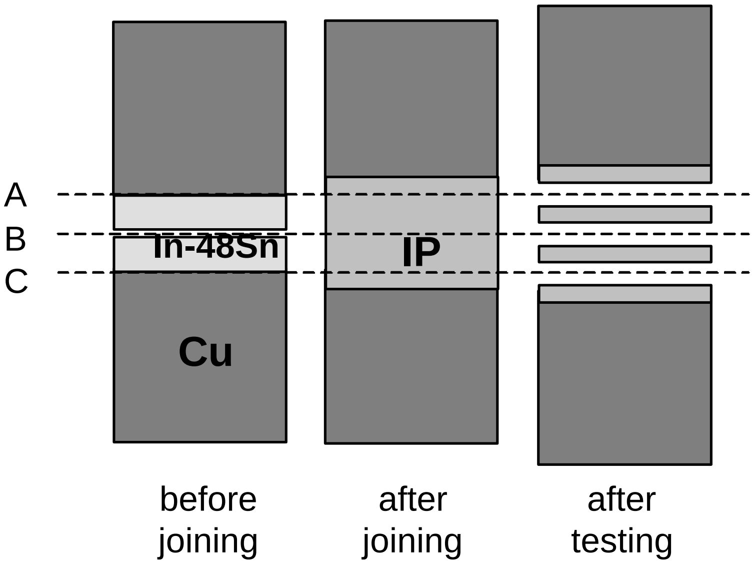

Fig. 4.5. Schematic cross-section of a fractured joint after the mechanical testing.

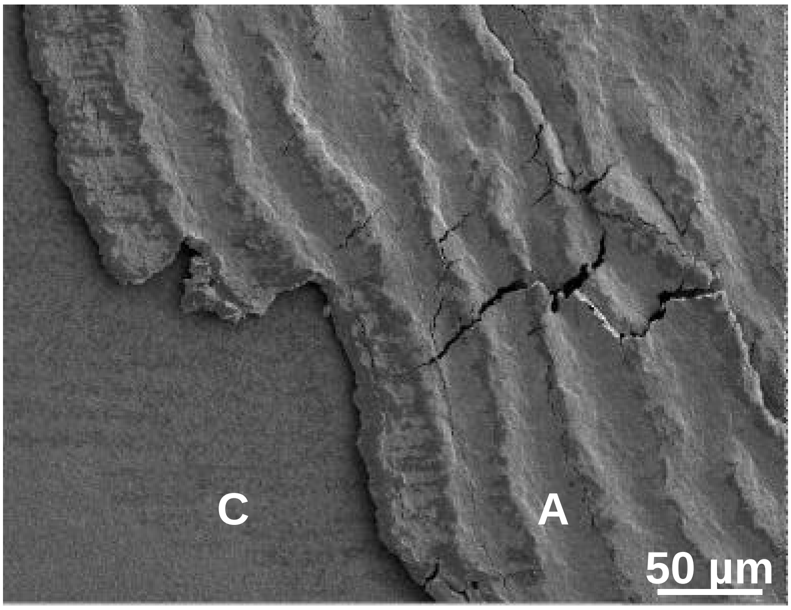

Fig. 4.6. SEM micrograph of the fracture surface of a diffusion-soldered joint at 290°C for 80 min as a result of the shear test. A and C correspond to fracture surface within ζ layer (cf. Fig. 4.5).

4.3.4 Nanohardness measurements

Because of the thin cross-sectional area of the intermetallic layers, a nanoindentation test system was used for measuring hardness values. Preliminary topographic inspection was performed by SFM to select a cross-sectional area of suitable (= moderate) constant roughness.

Typical triangular indentation marks can be seen in Fig. 4.7 for a joint annealed at 290°C for 40 min consisting of η and ζ layers. The indentation area decreases from Cu (left in Fig. 4.7) to the middle of the joint, indicating qualitatively that Cu is the softest material and that the η layer is the hardest IP. A careful observation of the area around the indentation marks revealed no cracking, indicating that the IPs can plastically deform without fracturing.

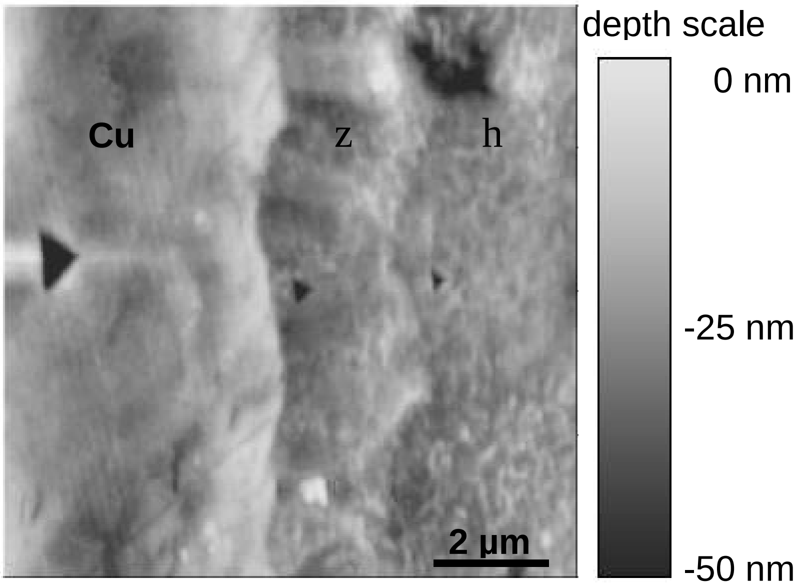

Fig. 4.7. SFM micrograph of hardness indentations on the joint cross-section of a sample diffusion-soldered at 290 °C for 40 min.

The average hardness values for each IP layer in the joint have been summarized in Table 4.5. The Cu, ζ and η phases show hardness values of 2.3, 6.7 and 9.5 GPa, respectively. The temperature and the annealing time do not influence significantly the hardness values for the IPs. The hardness values of the ζ layers are comparable with those reported for the total intermetallic layer present in conventionally soldered Cu/In-Sn/Cu joints [44].

The nanohardness measurement performed on joints prepared at 200°C consisting of a single η layer indicate that the η layer is slightly harder in the middle than at the sides close to Cu (Fig. 4.8). The hardness difference is about 1.3 GPa. This may be ascribed to the duplex microstructure of the η layer: the large grained part in the middle of the layer appears to be harder than the fine grained part near to Cu. Note that in both cases, the size of the nanoindentation was smaller than the grain size; so the grain size difference is not expected to influence the hardness difference observed. It may be suggested that the difference in hardness is due to a difference in preferred orientation. When the interconnection zone consists of a single ζ layer no hardness differences across the layer were found, presumably because ζ layer has a homogeneous microstructure (see Section 3).

Table 4.5. Average hardness values for the IPs in diffusion soldered Cu/In-48Sn/Cu joints. The Cu hardness value is 2.3 ± 0.2 GPa for all samples.

Joint production		Hardness	IPs in the joint
T (°C)	t (min)	(GPa)	and indentation position
200	120	9.4 ± 0.4	η, in the middle of the joint
		8.1 ± 0.5	η, close to Cu
290	10	9.6 ± 0.4	η
		-	ζ, too thin to be measured
	40	9.5 ± 0.2	η
		6.7 ± 0.3	ζ
360	30	6.7 ± 0.3	ζ

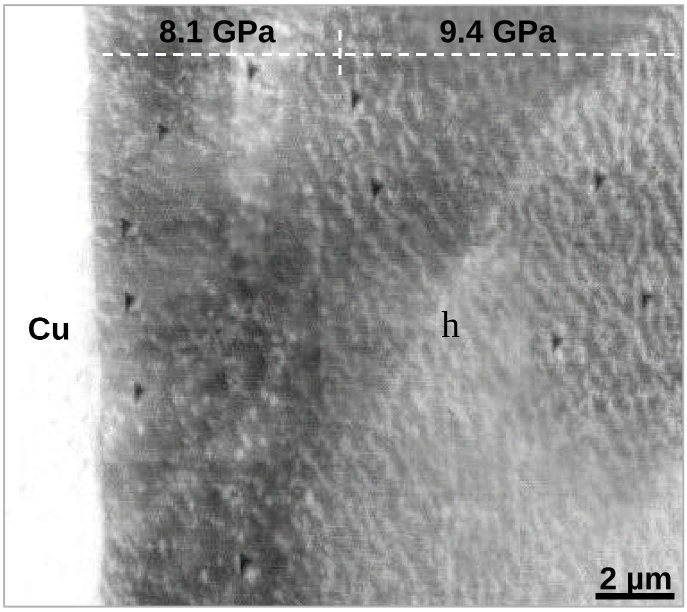

Fig. 4.8. SFM micrograph of nanohardness indentations on the joint cross-section diffusion-soldered at 200 C for 40 min.

These results are consistent with the shear and tensile testing: the η layer is the most brittle (hardest) IP and the weakest part in the joint; the critical location for the fracture development in joint containing an ? phase layer is the interface between the η sublayers of large and small grains.

4.4 Conclusions

- When, in Cu/In-48Sn/Cu joints, the η phase is present as a single layer or accompanied by ζ layers, upon shear and tensile testing fracture occurs through the η phase layer. The resulting USS and UTS values are low. When only the ζ phase is present, much better mechanical properties occur: the USS values increase at least 3 times when η converts completely into ζ phase.
- The etching of the surface of the In-48Sn layer (either as a foil or produced by sputtering) to remove the unavoidable oxide layer improves drastically the USS and UTS values.
- The fracture surfaces have a stepped shape: three fracture surface parts are observed. Two parts are very flat and appear to be near to the original interfaces between the Cu substrates and the In-48Sn solder; the third part, of minor extent, is approximately in the middle of the joint, where the original In-48Sn layers met upon joint production. This third part shows a transgranular fracture mode.
- The η layer, which formed through liquid-solid reaction, has a duplex microstructure (due to two different crystalization structures) exhibiting a weak interface between the corresponding sublayers of large and small grains. The ζ layer, which formed through solid-solid reaction, has a homogeneous microstructure.
- The hardness values of the ζ and η layers are about 3 and 4 times higher, respectively, than that of Cu. The duplex microstructure of the η layer corresponds with two different hardness values within the same η layer.
- The shear and tensile strength values and the hardness values can be consistently interpreted as that the weakest part is the η layer, with fracture initiation at the transition from a large-grained microstructure to a fine-grained microstructure in the η layer.
- Several applications can be suggested for Cu/In-48Sn/Cu joints using in essence the diffusion soldering process as described here. The USS and UTS obtained for the joints allow application in the field of microelectronics. Since the joints consisting only in ζ phase can resist shear and tensile strength values of about 150 MPa without fracturing, a

structural application can be suggested as well. Because the joints produced show a thermal stability up to 750°C (see Section 3), applications where high service temperatures are needed are feasible too.

5 Zusammenfassung

Neue Umweltgesetze, besonders in Europa und Japan [1], erfordern die Beseitigung des Pb-Einsatzes in der Elektronik. Die Entwicklung neuer Verbindungsverfahren, wie Pb-freies Weichlöten, ist deshalb dringend erforderlich. Das Diffusionslöten (*diffusion soldering*) [2] ist ein neues und attraktives Verbindungsverfahren für die Herstellung Pb-freier Verbindungen, die thermisch und mechanisch stabil sind.

In der vorliegenden Arbeit wurden die Wachstumskinetik und morphologie der intermetallischen Phasen (**IP**) untersucht, die in der Reaktionszone von Cu/In/Cu- und Cu/In-48Sn/Cu-Verbindungen entstehen. Die Phasen Cu_2In und Cu_7In_3, die in Cu/In/Cu-Verbindungen durch Fest-fest-Reaktion wachsen, zeigen ein parabolisches Wachstumsgesetz, d.h., das Wachstum ist volumendiffusionskontrolliert. Das Wachstum der ζ-Phase, die sich auch durch eine Fest-fest-Reaktion zwischen Cu und der η-Phase in der Cu/In-48Sn/Cu-Verbindungszone bildet, zeigt eine lineare Abhängigkeit der Schichtdickenzunahme mit der Reaktionszeit, d.h., das Wachstum ist durch eine Reaktion an der Grenzfläche gesteuert. Die ζ-Phase wächst viel schneller als die Phasen Cu_2In und Cu_7In_3 in den binären Cu/In/Cu-Diffusionspaaren. Der Diffusionsprozess, der das IP-Wachstum bestimmt, wurde durch Berechnung der betreffenden Diffusionskoeffizienten gekennzeichnet. Die kleinen Werte für die Aktivierungsenergie (100-120 kJ/mol) der Interdiffusion in den Phasen Cu_2In, Cu_7In_3 und ζ können durch eine große Leerstellen-konzentration bedingt sein. Diese Konzentration kann sehr hoch sein, besonders in Materialien, die sich noch im Wachstum befinden und sich folglich noch nicht im thermodynamischen Gleichgewicht befinden.

Da elektrische Verbindungen mechanisch stabil sein müssen, sind auch die mechanischen Eigenschaften wesentlich. Um eine komplette Kennzeichnung der Verbindungen zu geben, wurden Zug- und Scherversuche sowie Nano-Härtetests an diffusionsgelöteten Cu/In-48Sn/Cu-Verbindungen durchgeführt. Diese Verbindungen wurden mechanisch untersucht, weil sie schneller entstehen als die Cu/In/Cu-Verbindungen. Die Härte-Ergebnisse sind im Einklang mit den Zug- und Scherversuchen. Sie zeigen, daß die η-Phase die schwächste IP in den Verbindungen ist. Die Zug- und Scherversuche am Verbindungen, die nur eine einzelne ζ-Schicht haben, weisen Bruchfestigkeitswerte von ≈ 150 MPa auf. Wärmebeständigkeitsversuche haben gezeigt, daß die Cu/In-48Sn/Cu-Verbindungen hohen Temperaturen bis zu 750°C ohne Bruch widerstehen können.

5.1 Einleitung

Beim Diffusionslöten werden zwei Substrate, die verbunden werden sollen, mit einer dünnen Zwischenlage eines Weichlotes versehen [2]. Die zu lötenden Teile werden bei einer Temperatur oberhalb des Schmelzpunktes der Zwischenlage eine bestimmte Zeit lang gehalten und leicht gegeneinander gedrückt, bis sich das Lot vollkommen in IP umgewandelt hat. Die resultierenden Verbindungen bestehen dann völlig aus IP und halten deshalb Betriebstemperaturen stand, die höher sind als die Herstellungstemperatur! Der Unterschied zwischen Herstellungs- und Betriebstemperatur kann –je nach Materialsystem– bis zu 400 und 600°C betragen. Das Diffusionslöten hat die Vorteile des herkömmlichen Weichlötens (*soldering*), d.h., gute Füllung der Verbindung und niedrige Herstellungstemperatur, und aber gleichzeitig den großen Vorteil der hohen Betriebstemperatur.

Kupfer wurde gewählt, weil es ein übliches Substratmaterial in vielen elektronischen Anwendungen ist, und Indium ist ein Hauptbestandteil in vielen kommerziellen Lötmitteln. Ein bekannter Ersatz der Pb-reichen Weichlote sind die Sn-haltigen Weichlote. Die eutektische In-48Sn-Legierung hat einen sehr niedrig Schmelzpunkt (120°C). Die Praxis verlangt eine möglichst niedrige Herstellungstemperatur, um eine thermische Schädigung der anderen Stromkreisbestandteile zu vermeiden.

Die Diffusionslötungen der Cu/In/Cu- und Cu/In-48Sn/Cu- Verbindungen wurden zwischen 180 und 430°C bzw. 180 und 400°C untersucht. Mittels Rasterelektronenmikroskopie (**SEM**), Elektronenstrahlmikroanalyse (**EPMA**), Röntgenstrahlbeugung (**XRD**) und Elektronbeugunganalyse (**TEM**) wurden die Phasen charakterisiert und die Morphologie und Wachstumskinetik der IP in der Verbindungszone untersucht. Die meisten Untersuchungen von Grenzflächenreaktionen während des konventionellen Weichlötens beruhen auf dem Wachstum von IP bei niedrigen Temperaturen (besonders unterhalb des Schmelzpunktes des Zwischenlagenmaterials). Jedoch fehlt ein tieferes Verständnis der Grenzflächenreaktionen in Diffusionslötverbindungen, z.B. die Kenntnis der betreffenden Diffusionskoeffizienten und anderer kinetischer Parameter. In dieser Arbeit werden Konzepte über die Mehrkomponenten-diffusion vorgestellt, die als Designstrategie zur Verbesserung von Lötverbindungen dienen können.

Das mechanische Verhalten einer Verbindung ist ein wichtiger Aspekt seiner Zuverlässigkeit (cf. [3],[22],[23],[43]). Es gibt viele Arbeiten über das mechanische Verhalten von konventionell weichgelöteten Verbindungen (cf. [3],[23]). In einer weichgelöteten Verbindung besteht die Verbindungszone hauptsächlich aus Lötmittellegierung und verhältnismäßig dünnen Schichten von IP nahe am Substrat. Jedoch gibt es nur wenige Arbeiten, in denen die mechanischen Eigenschaften von Verbindungen untersucht werden, die völlig aus IP verstehen (cf. [3],[28],[45],[46]). Deshalb wurden die Zug- und Scherfestigkeit und die Härte bestimmt und zusammen mit fraktographischen Analysen (SEM) interpretiert, um das mechanische Verhalten der diffusionsgelöteten Verbindungen zu beschreiben. Besonderes Interesse wurde auf den Schertest gerichtet, weil dieser in der Praxis am meisten eingesetzt wird. Die Unterschiede in den Werten der Wärmeausdehnungkoeffizienten zwischen den einzelnen Materialien sind der Hauptgrund für die Erzeugung von Scherspannungen im Verbindungssystem.

5.2 Experimentelle Hinweise

5.2.1 Proben Herstellung

Die Diffusionspaarungen wurden aus Cu-Scheiben hoher Reinheit (99,999 Gew.%) mit einem Durchmesser von 5-10 mm und einer Dicke von 2 mm hergestellt. Als Weichlot wurde die eutektische Legierung In-48Sn verwendet, deren Ausgangsmaterialien eine Reinheit von 99,999 Gew.% hatten. Diese Legierung wurde zu 100-200 µm dicken Folien verarbeitet. Das Vorbereiten der Oberfläche der Cu-Scheiben wurde mittels mechanischer Politur erzielt. Die Folien aus In oder In-48Sn wurden dann zwischen zwei Cu-Scheiben unter einen geringfügigen mechanischen Druck von ≈ 0,5 MPa gesetzt. Eine Lötpresse ermöglichte, den Verbundaufbau von Cu-Scheiben und Folie mit einer Heizrate von 200-300 °C/s zu den gewünschten Temperaturen (180 - 430°C) oberhalb des Schmelzpunktes von In (156°C) bzw. In-48Sn (120°C) aufzuheizen. Während der nachfolgenden Auslagerung fand die Reaktion zwischen der flüssigen Zwischenlage (In oder In-48Sn) und dem festen Cu statt, was die Bildung der IP ermöglichte. Die thermische Behandlung wurde unter Ar-Atmosphäre durchgeführt, um Oxidation zu verhindern.

Die Verbindungen für die mechanischen Versuche wurden aus zwei sich überlappenden Cu-Streifen gebildet, die in der Überlappungszone mit einer gesputterten In-48Sn-Schicht versehen waren. Die In-48Sn-Schicht betrug 5 µm. So hatte die Verbindungszone eine Dicke von 10 ± 1 µm. Eine andere Gruppe von Proben wurde mit einer 100 µm dicken In-

48Sn-Folie vorbereitet (Verbindungsdicke 20 ± 2 µm; das restliche Lotmaterial wurde beim Löten seitlich herausgepreßt). Um die Qualität der gesputterten In-48Sn-Oberfläche zu verbessern, wurde ein Ätzmittel (6 M HCl + 2 M $FeCl_3$) zur chemischen Politur verwendet [48].

5.2.2 Kinetische Untersuchungen

Nach der thermischen Behandlung wurden Querschliffe der Verbindungen für die metallographische Analyse vorbereitet. Die Proben wurden in Epoxi-Harz eingebettet und poliert, mit 1 µm Diamantpaste im letzten Politurschritt. Die optischen Aufnahmen zeigten die unterschiedlichen IP in den Cu/In-48Sn/Cu-Verbindungen und ermöglichten das Messen der Schichtdicke. Ein Rasterelektronenmikroskop (Philips XL 30) wurde benutzt, um die Morphologie der Cu/In/Cu-Verbindungen zu kennzeichnen. Rückstreuaufnahmen wurden verwendet, um die Dicke der IP-Schicht zu messen. Es wurde jeweils der Mittelwert aus 30 Einzelmessungen, die in regelmäßigen Abständen durchgeführt wurden, bestimmt.

5.2.3 Phasenidentifikation

Es wurde eine Elektronenstrahlmikrosonde (Cameca SX100) mit einem dispersiven Spektrometer für die Bestimmung der chemischen Zusammensetzung der Verbindungszone eingesetzt. Wegen der begrenzten Genauigkeit (± 2 µm) wurden die Verbindungszonen viel dicker als 2 µm hergestellt. Ein Röntgenstrahldiffractometer (Philips X' Pert, Cu-Kα-Strahlung) wurde verwendet, um an der Bruchoberfläche der Verbindungen bei Raumtemperatur Beugungsaufnahmen zu machen. Ein Transmissionselektronenmikroskop mit einem doppelten Neigungshalter wurde für die Elektronenbeugungsanalyse benutzt. Die Proben für die Elektronenbeugung wurden nach einer Standardmethode vorbereitet [8].

5.2.4 Mechanische Eigenschaften

Um die Nano-Härtemessungen durchzuführen, muß der Querschnitt der Cu/In-48Sn/Cu-Verbindungen sehr sorgfältig vorbereitet werden, weil Nano-Härtemessungen stark von der Oberflächenrauhigkeit abhängen. Die Proben wurden in Epoxi-Harz eingebettet, mit 0,25 µm Diamantpaste und OP-S-Suspension (Mastermet) in der letzten Stufe poliert. Die Härtemessungen wurden mit Hilfe eines Rasterkraftmikroskops (NanoScope III MultiMode, Digitalinstruments) durchgeführt, dass mit einem Nanoindenter (Hystron TriboScope) gekoppelt war [49]. Die Kombination dieser Geräte erlaubt die Nutzung der Indenterspitze zur Vermessung der Härte als auch zur Aufnahme der rasterkraftmikroskopischen Bilder. Die Eindrücke wurden mit einer dreiseitigen Pyramidenspitze (Berkovich [51]) gemacht. Der Belastungs- und Entlastungszeit betrug für alle Eindrücke 5 s. Die Härtemessungen wurden mit einer Maximallast von 100 nN durchgeführt.

Eine Zugfestigkeitsprüfmaschine (Instron) wurde benutzt, um die Zug- und Schertests durchzuführen. Die Ergebnisse dieses Versuches sind die Bruchfestigkeit vor dem Bruch, wenn die Verbindungen unter Zug- bzw. Scherspannung belastet werden. Die Versuche wurden bei Raumtemperatur und unter einer Zuggeschwindigkeit von 0,5 mm/min durchgeführt. Beide externe Cu-Oberflächen der Cu/In-48Sn/Cu-Proben wurden an Stahlprobenhaltern mit einem Epoxid-Kleber (Duralco 4525, Polytec) befestigt. Die Cu-Oberflächen wurden mittels einer Ultrafräse und Politurpapier 4000 poliert. Für jeden Versuchsparameter (Zeit, Druck, Verbindungstemperatur) wurden 5-6 Proben geprüft.

5.3 Ergebnisse und Diskussion

5.3.1 Kennzeichnung der diffusionsgelöteten Cu/In/Cu-Verbindungen

Die erste IP, die sich in der Cu/In/Cu-Verbindung nach dem Diffusionslöten bildet, ist die IP mit dem höchsten In-Gehalt, die bei der Reaktionstemperatur gemäß Zustandsdiagramm stabil ist: $Cu_{11}In_9$ bei Temperaturen T < 310°C und Cu_2In bei T > 310°C. Diese In-reichen IP wachsen in der Flüssigkeit mit einer unregelmäßige Schichtform. Die Cu-Atome zur Bildung dieser IP werden durch Auflösung vom Substrat und dann durch Diffusion in der Flüssigkeit geliefert. Bild 5.1 zeigt die erste Stufe der IP-Bildung.

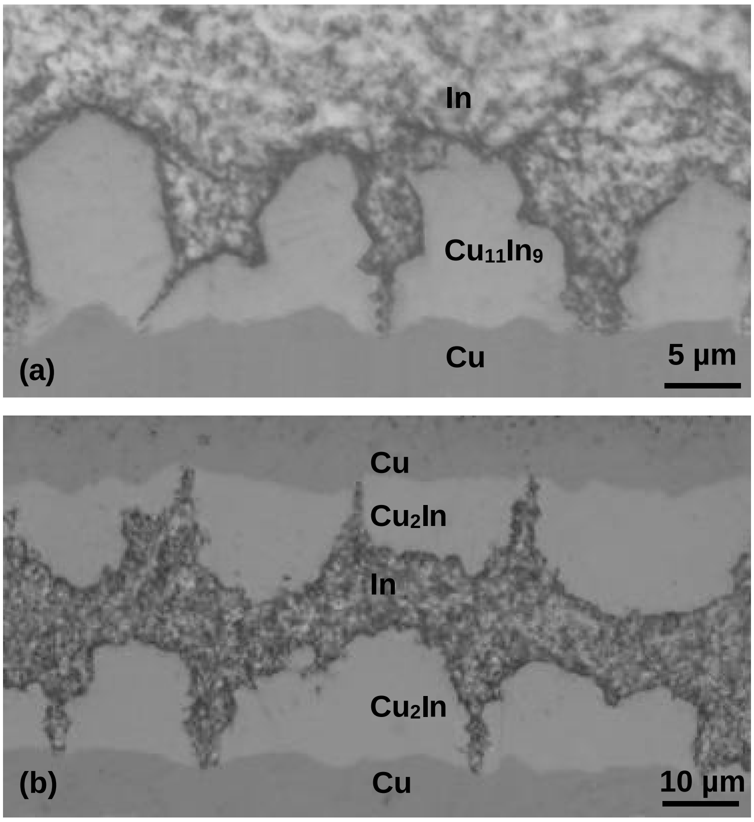

Bild 5.1. SEM-Aufnahme einer Cu/In/Cu-Verbindung, die (a) 30 min bei 290°C und (b) 3 min bei 360°C ausgelagert war.

Nachdem das ganze flüssige In in die erste feste IP umgewandelt worden ist, bilden sich die anderen IP durch eine Fest-fest-Reaktion. Die Reihenfolge der IP zeigt einen zunehmenden Cu-Gehalt:

$Cu_{11}In_9 \rightarrow Cu_2In \rightarrow Cu_7In_3$ bei $T < 310$ °C und

$Cu_2In \rightarrow Cu_7In_3$ bei $T > 310$ °C.

Eine Darstellung dieser Umwandlungsreihenfolge zeigt Bild 5.2 (s. Abschnitt 2.3.1).

Die IP wachsen durch die Fest-fest-Reaktion als planare Schicht. Die Zeitabhängigkeit der Schichtdickenzunahme folgt einem parabolischen Wachstumsgesetz: $\Delta x^2 = k_2.t$, d.h., das Wachstum dieser IP ist volumendiffusionskontrolliert. Die Wachstumsgeraden von Cu_2In und Cu_7In_3 bei 180°C weisen eine große Inkubationszeit auf, was auf eine schwierige Keimbildung hindeutet. Cu_2In wächst langsamer als Cu_7In_3 bei allen Auslagerungstemperaturen. Bild 5.3 zeigt dies für 290°C. Die Wachstumskonstanten k_2 wurden für Cu_2In und Cu_7In_3 bei 180, 250, 290, 360 und 430°C ermittelt (s. Abschnitt 2.3.2).

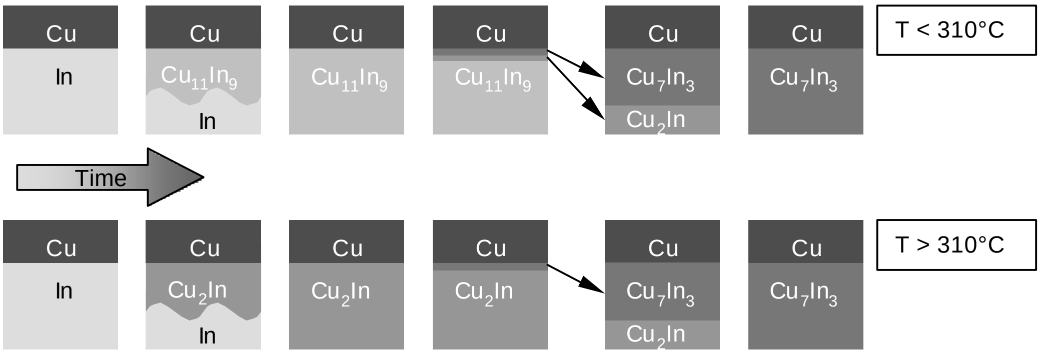

Bild 5.2. Schematische Darstellung der Umwandlungsreihenfolge von IP in diffusionsgelöteten Cu/In/Cu-Verbindungen.

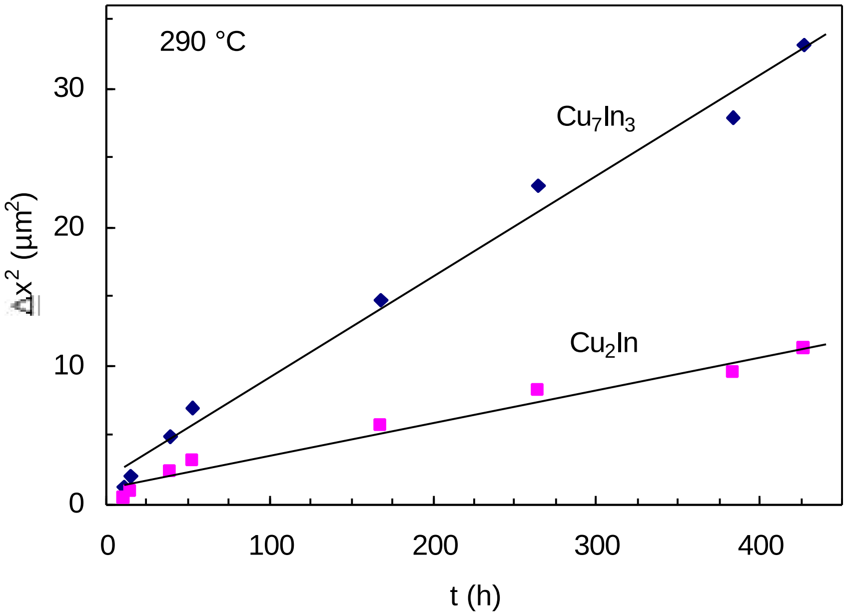

Bild 5.3. Parabolisches Wachstum von Cu_2In und Cu_7In_3 bei 290°C.

Mit den Wachstumskonstanten und den Gleichgewichtkonzentrationen der IP wurden die integralen Interdiffusionskoeffizienten nach der Wagner-Methode berechnet. Die ermittelten Diffusionskoeffizienten wurden als Funktion der reziproken Auslagerungstemperatur gemäß der Arrhenius-Beziehung aufgetragen (Bild 5.4). Die kleinen Werte für die Aktivierungsenergie (≈ 100 kJ/mol) der Interdiffusion in Cu_2In und Cu_7In_3 können durch eine große Leerstellen-Konzentration bedingt sein. Diese Konzentration kann sehr hoch sein, besonders in Materialien, die sich noch im Wachstum befinden. Wie Bild 5.4 zeigt, wurde keine Änderung der Aktivierungsenergie für das Wachstum von Cu_7In_3 ober- und unterhalb von 310 °C gefunden. Somit wird das Wachstum von Cu_7In_3 nicht durch das simultane Wachstum von Cu_2In unterhalb von 310°C beeinflusst (s. Abschnitt 2.3.4).

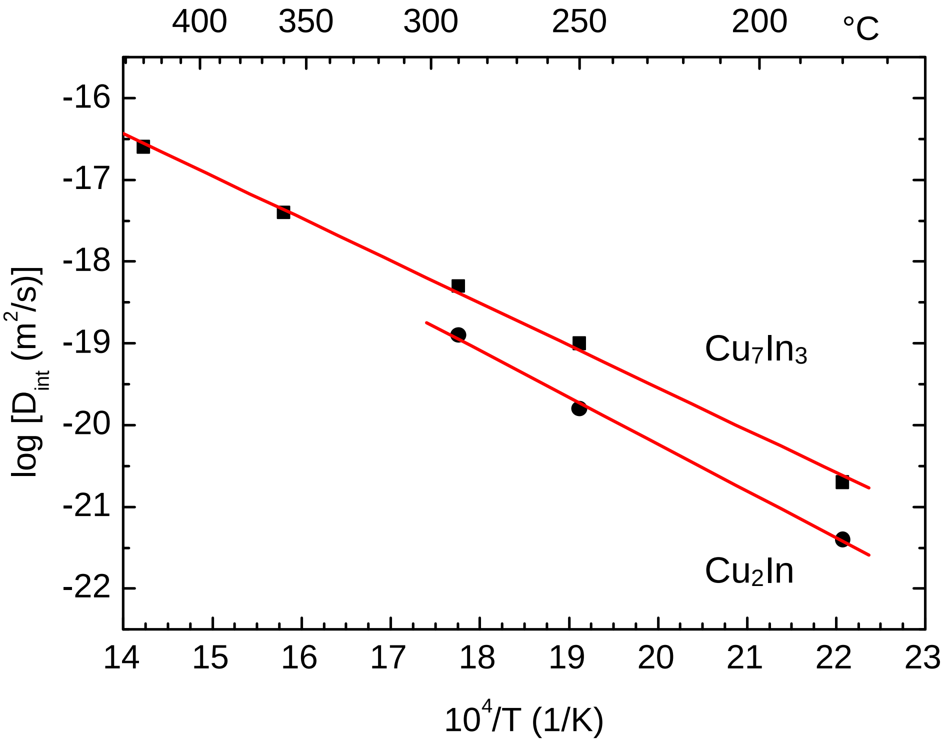

Bild 5.4. Arrhenius-Auftragung der ermittelten Interdiffusionskoeffizienten für die Phasen Cu_2In und Cu_7In_3.

Die Untersuchung zeigt, daß die Verbindungen fast frei sind von großen Poren oder Löchern. Die möglichen Betriebstemperaturen der hergestellten Verbindungen sind viel höher als die Herstellungstemperatur. Aber die Untersuchungen zeigen auch, daß man eine relativ lange Reaktionszeit für das Wachstum der IP mit hohem Schmelzpunkt braucht.

5.3.2 Grenzflächereaktionsprozess in diffusionsgelöteten Cu/In-48Sn/Cu-Verbindungen

In den Cu/In-48Sn/Cu-Paaren entwickeln sich zwei Schichten von IP mit folgenden Durchschnittsgehalten (At.%): Cu-16In-27Sn und Cu-10In-13Sn, die den η- und ζ-Regionen im Zustandsdiagramm Cu-In-Sn [29] entsprechen. Unterhalb von 200 °C wird nur die η-Phase in der Verbindungszone gebildet. Die ζ-Phase entwickelt sich nicht innerhalb von 30 Tagen bei 200°C Auslagerungstemperatur. Oberhalb von 200°C, wachsen die η- und ζ-Phasen gleichzeitig. Bild 5.5 zeigt dies für eine Probe, die 30 min bei 290°C ausgelagert wurde. Wenn die η-Phase alleine wächst (T < 200°C), hat sie zwei unterschiedliche Kristallmorphologien: große η-Körner, die in Richtung des flüssigen In-48Sn wachsen, und eine feinkörnige Region, die in Richtung festes Cu wächst (s. Abschnitt 3.3.1).

Das Wachstum der ζ-Phase, die sich durch eine Fest-fest-Reaktion zwischen Cu and η-Phase bildet, zeigt eine lineare Abhängigkeit der Schichtdickenzunahme mit der Reaktionszeit, d.h. $\Delta x = k_{1\,?}\, t$. Folglich wird das Wachstum der ζ-Phase zwischen 220 und 400°C durch eine Reaktion an der Grenzfläche gesteuert. Bild 5.6 zeigt das kinetische Verhalten der ζ-Schicht bei 290, 360 und 400°C. Sie wächst viel schneller als die Schichten in den binären Cu/In/Cu-Diffusionspaaren. Die Aktivierungsenergie für das Wachstum der ζ-Phase beträgt 121 kJ/mol und die Präexponentialgröße hat den Wert 57 m/s (s. Abschnitt 3.3.2).

Wärmebeständigkeitsversuche haben gezeigt, daß die Verbindungen hohen Temperaturen bis zu 750 °C ohne Bruch widerstehen können. Die EPMA-Analysen nach den Wärmebeständigkeitsversuchen zeigten, daß sich die η- und ζ-Phasen während der Hochtemperaturbehandlung in den Cu-reichen Mischkristall umwandeln, der eine noch viel höhere Festigkeit aufweist. Die hohen Schmelzpunkte der gebildeten Phasen (500-750°C) ermöglichen die Anwendung der diffusionsgelöteten Verbindungen bei hohen Betriebstemperaturen (s. Abschnitt 3.3.1).

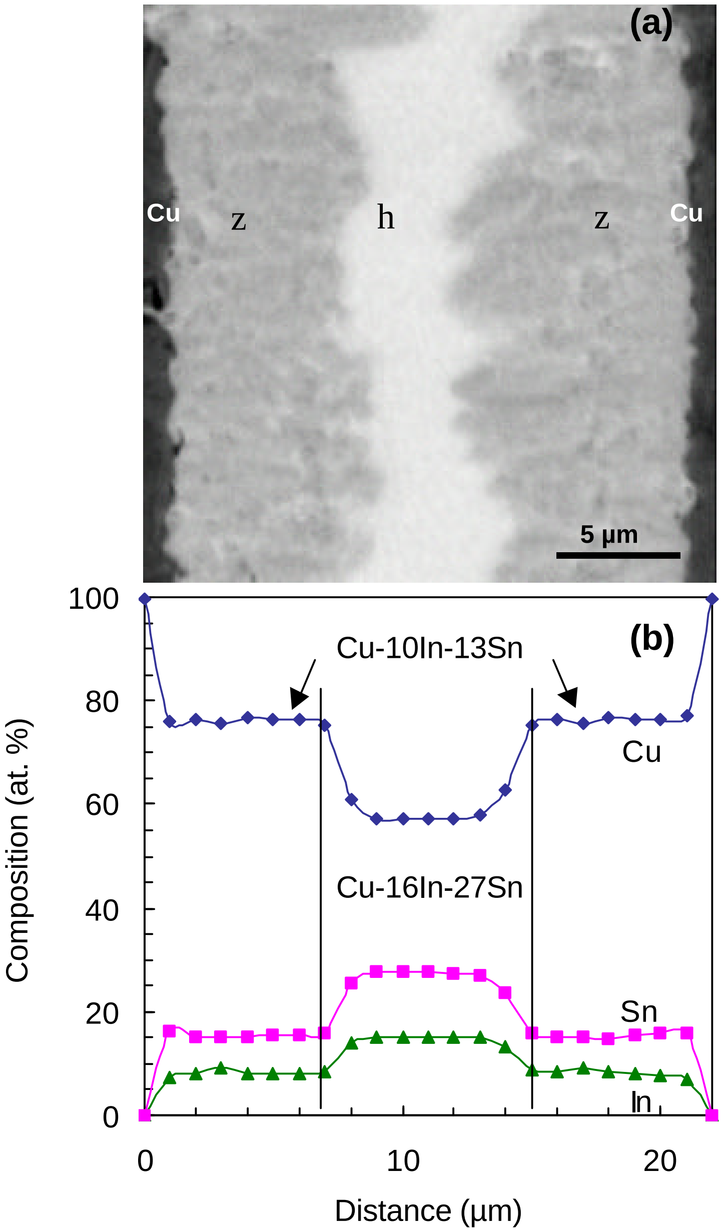

Bild 5.5. SEM-Aufnahme einer Cu/In-48Sn/Cu-Verbindung nach Auslagerung von 30 min bei 290°C (a) und die Konzentrationsprofile der Verbindungszone (b).

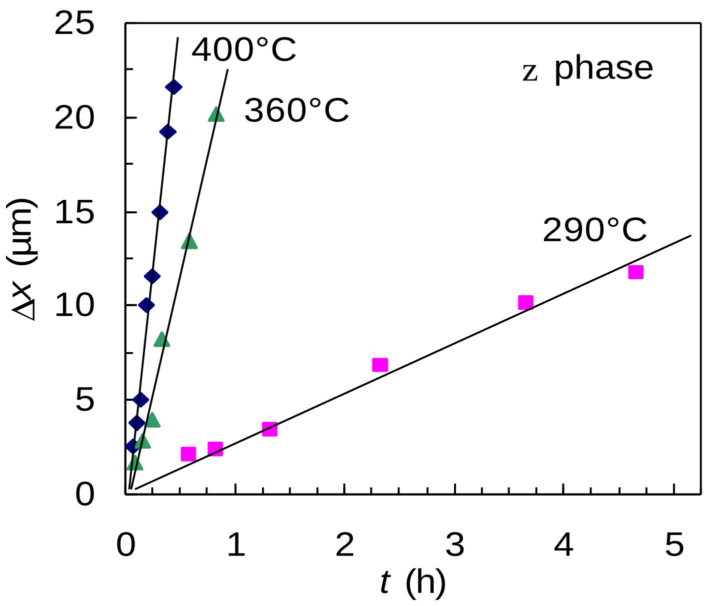

Bild 5.6. Lineares Wachstum der ζ-Phase bei verschiedenen Auslagerungstemperaturen.

5.3.3 Mechanische Eigenschaften der Cu/In-48Sn/Cu-Verbindungen

Wenn die Verbindungszone eine η-Schicht enthält (alleine oder zusammen mit einer ζ-Schicht), tritt der Bruch in der η-Schicht auf. Die Bruchfestigkeitswerte in den Zug- und Scherversuchen waren in diesen Fällen sehr niedrig. Wenn nur die ζ-Phase anwesend ist, werden bessere mechanische Eigenschaften beobachtet. Die Bruchfestigkeitswerte in den Scherversuchen erhöhen sich fast auf das Dreifache, wenn die η-Phase vollständig in die ζ-Phase umwandelt ist (s. Abschnitt 4.3.1-2).

Die η-Schicht, die durch eine Flüssig-fest-Reaktion wächst, weist ein grob- und ein feinkörniges Gefüge auf (s. Abschnitt 3.3.1). Die ζ-Schicht hat dagegen eine homogene feinkörnige Struktur, da sie durch eine Fest-fest-Reaktion wächst. Die Bruchoberflächen stellen eine Stufenform dar, bei der drei Bruchflächen beobachtet wurden. Zwei Bruchflächen (A und C, Bild 5.7) sind sehr flach und scheinen an der ursprünglichen Grenzfläche zwischen Cu und dem In-48Sn-Lot aufzutreten, ungefähr dort, wo das grob- und in das feinkörnige Gefüge übergeht. Diese A- und C-Bruchflächen dominieren. Die dritte Fläche (B, Bild 5.7) liegt ungefähr in der Mitte der Verbindungszone. Wie Bild 5.7 zeigt, entsteht die

B-Bruchfläche durch transgranulen Bruch. Der Bruch wird durch die Region mit den großen Körnen begrenzt. Bild 5.8 zeigt Bruchverhalteb als der Querschnittansicht.

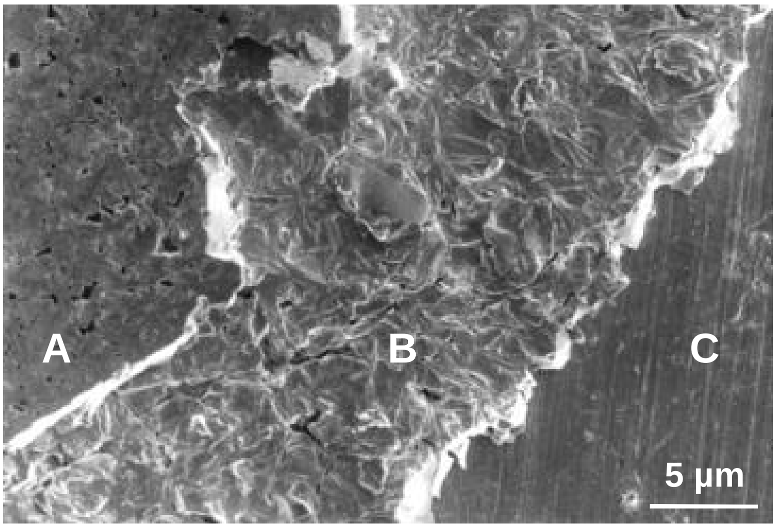

Bild 5.7. SEM-Aufnahme der Bruchoberfläche einer 15 min bei 290°C ausgelagerten Probe.

Das Ätzmittel verbessert die Scherbruchfestigkeitswerte um einen Faktor 1,5 in den Proben, die eine einzelne η-Schicht aufweisen, um fast einen Faktor 4 in den Proben, die aus η- und ζ-Schichten bestehen, und um einen Faktor 6,7 in den Proben, die nur eine einzelne ζ-Schicht haben. Die Scherversuche zeigten Bruchfestigkeitswerte von ≈ 150 MPa. Ein ähnliches Verhalten wurde in den Zugversuchen beobachtet.

Bild 5.9 zeigt schematisch die Härtewerte der einzelnen IP. Die Härtewerte der η- und ζ-Schichten sind ungefähr 4- bzw. 3mal höher als die von Cu. Folglich ist die η-Schicht spröder als die ζ-Schicht. Außerdem wurde die doppelte Kristallisationsmorphologie der η-Phase durch zwei unterschiedliche Härtewerte hervorgehoben. Diese Härte-Ergebnisse sind im Einklang mit den Zug- und Scherversuchen, die zeigten, daß die η-Phase die schwächste IP in den Verbindungen ist (s. Abschnitt 4.3.4).

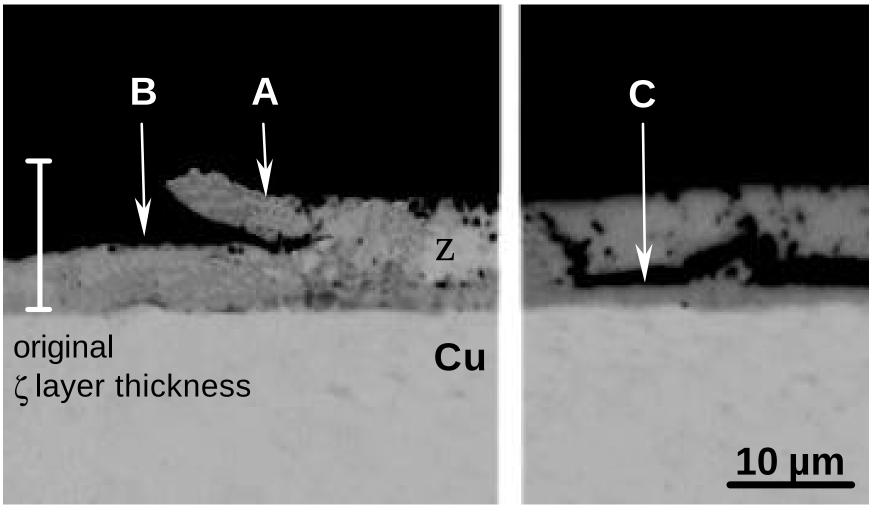

Bild 5.8. Rißverlauf in einer 90 min bei 290°C ausgelagerten Probe.

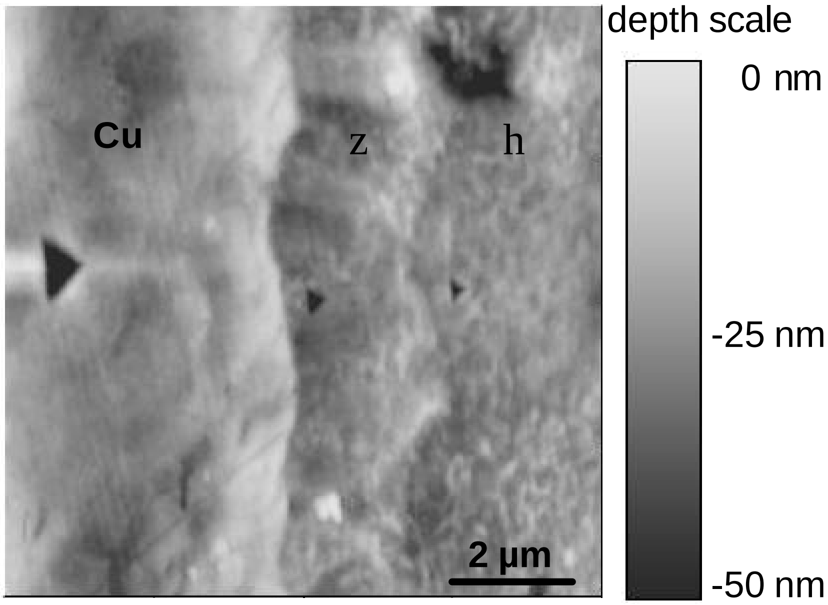

Bild 5.9. Rasterkraft-Aufnahme der Härteeindrücken auf dem Verbindungszone einer 40 min bei 290°C ausgelagerten Probe.

5.4 Ausblick

Einige Anwendungen können für diffusionsgelötete Cu/In-48Sn/Cu-Verbindungen vorgeschlagen werden. Die niedrigen Prozeßtemperaturen und die kurzen Prozeßzeiten sind innerhalb des traditionellen Weichlötenverfahrens (siehe [3],[22]). Folglich ist der traditionelle mikroelektronische Bereich, wo das Weichlötenverfahren benutzt wird, ein gutes Anwendungsfeld, da die Zug- und Scherbruchfestigkeitswerte, die unsere Verbindungen erreicht haben, für solche Anwendung hoch genug sind. Da die Verbindungen, die nur eine einzelne ζ-Schicht haben, Scher- und Zugbruchfestigkeitswerte bis etwa 150 MPa aufweisen, können sie auch dort eingesetzt werden, wo es auf hohe mechanische Festigkeit ankommt. Da eine Wärmebeständigkeit bis etwa 750°C vorliegt, werden sich garantiert neue Anwendungsgebiete ergeben.

6 Appendix A: Phase characterization of diffusion-soldered Ni/Al/Ni interconnections

G.A. López, S. Sommadossi, P. Zieba, W. Gust, E.J. Mittemeijer*

*Institute of Metallurgy and Materials Science, Polish Academy of Sciences, Reymonta St. 25, 30-059 Cracow, Poland

The formation and growth of intermetallic phases in the Ni-Al system during a novel joining process for Ni/Ni interconnections based on diffusion soldering has been studied. The Ni/Al/Ni bonds were accomplished by isothermal solidification and subsequent interdiffusion of Ni and Al in the Ni/Al/Ni joints held at a temperature of 720°C. Optical and scanning electron microscopy, electron probe microanalysis and X-ray diffraction analysis were used to characterize the microstructural changes as a function of reaction time. The following phases appeared sequentially: liquid Al $\rightarrow$ Al_3Ni $\rightarrow$ Al_3Ni_2 $\rightarrow$ AlNi (stoichiometric) $\rightarrow$ AlNi (Ni-rich) $\rightarrow$ $AlNi_3$. At intermediate stages two to four phases coexisted. The NiAl phase occurred in two variants, namely a Ni-rich AlNi (60 at.% Ni) and stoichiometric AlNi. The joining process was completed after 30 h of reaction. Then only $AlNi_3$ was present in the Ni/Al/Ni interconnection zone. The quality of the resultant bond and the high melting point of the $AlNi_3$ phase (1360°C) indicate a great potential of the diffusion soldering for the joining of heat dissipating devices used in electronics and electrotechnics.

6.1 Introduction

The Al-Ni system [54] is of great interest due to the high melting intermetallic phases (see phase diagram shown in Fig. 6.1), which are of considerable practical importance. For example, the $AlNi_3$ compound is the principal strengthening phase in nickel-base superalloys [55]. Further, the AlNi phase is utilized for a protective coating which distinctly increases the resistance of nickel-base superalloys to oxidation and sulfidation at high temperatures [56].

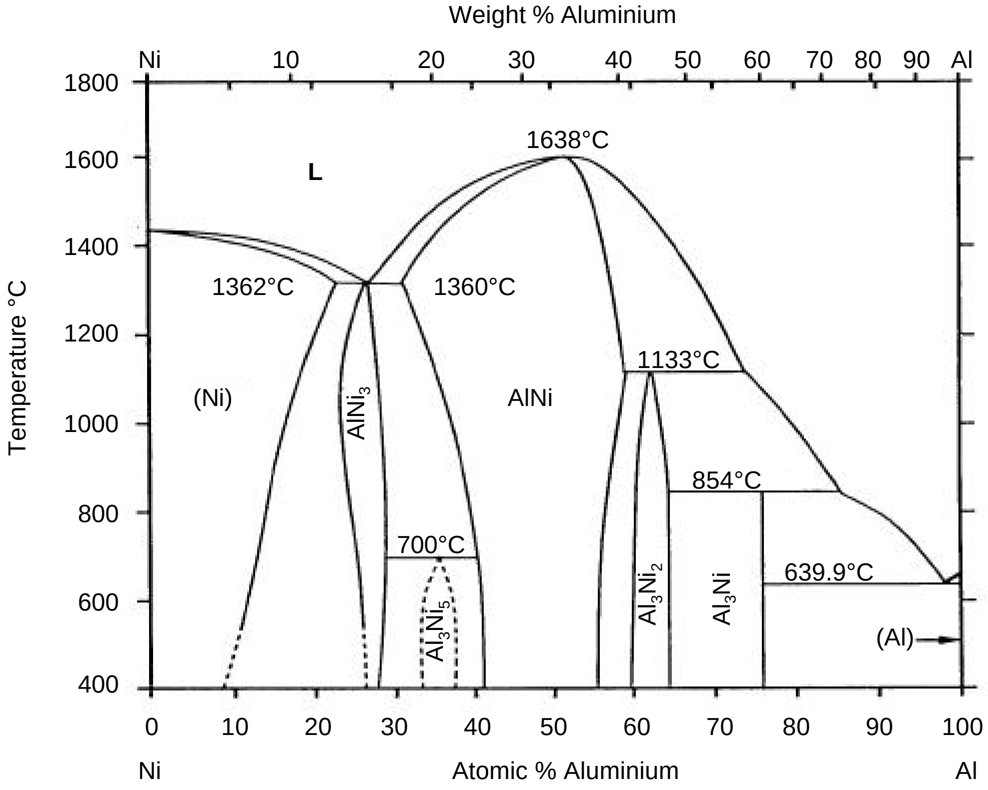

Fig. 6.1. The Ni-Al phase diagram [54].

Therefore, a strong interest exists to understand the diffusion processes and the formation of the intermetallic compounds in the Al-Ni system. Most of the research until now has been focused on the solid -solid reaction between Ni and Al (see cf. [57],[58]), as diffusion in the solid state plays an important role in the formation and degradation of aluminide coatings on heat resistant alloys. Other studies have demonstrated the role of the AlNi phase in the outer zone of coatings as inhibitor of carbides [56]. Less attention was paid to the interaction between liquid Al and solid Ni. Recently, it was investigated the latter reaction and found only the Al_3Ni and Al_3Ni_2 phases after isothermal reaction at 600, 700 and 800^{o}C (see cf. [58],[59]).

In the present paper, it is shown that intermetallic compounds can be successfully used to establish Ni/Al/Ni bonds during diffusion soldering. This process uses the principle of diffusion brazing but it is performed at a lower temperature. The bond formed entirely consists of intermetallic phases, having melting temperatures much higher than the temperature used for the fabrication of the joint. A preliminary investigation [60] showed convincingly that annealing at 700°C for 30 min produced strong Ni/Al/Ni joints composed of Al_3Ni_2, AlNi and $AlNi_3$. Due to the high melting points of these phases (1133-1638°C) the joints are expected to have a good thermal stability. This makes the Ni/Al/Ni diffusion soldering process very attractive for joining of heating elements and thick-film hot plates. It can also be successfully applied for the mounting of electronic devices (power resistors or transistors), showing an enormous heat dissipation which prevents the use of conventional soft soldering.

This work particularly focuses on the identification and characterization of the phases appearing at subsequent stages of the diffusion soldering of Ni/Ni interonnections using an Al interlayer.

6.2 Experimental

High purity Ni (99. 999 wt.%) was used for the preparation of substrates with a diameter of 10 mm and a thickness of 1 mm, by rolling and cutting using a diamond wheel. Then, the substrate was polished (using 1 µm diamond paste in the last step). Subsequently, a commercial Al foil (15 µm thick) was sandwiched between two such Ni substrates. The assembly was then heated up with a heating rate of 200-300 K/s to 720°C. Such a temperature enables the reaction between liquid Al and solid Ni, leading to the formation of intermetallic phases. The joint was fabricated under a slight mechanical pressure (≈ 0.5 MPa) in a specially prepared thermal load press kept under vacuum (10 Pa) in an Ar box to limit oxidation of the sample. The temperature of the sample was continuously measured by a thermocouple.

6.2.1 Metallography and Composition Analysis

Cross-sections were prepared for the metallographic analysis by embedding of the joints in epoxy, and subsequent grinding and polishing, using 1 µm diamond paste in the last polishing step. Then the unetched samples were inspected by optical and scanning electron microscopy (LM, SEM). The measurements of the chemical composition in the interconnection zone were carried out using an electron probe microanalyser (EPMA; Cameca SX100) equipped with 5 wave-length dispersive spectrometers. The analysis was carried out on the samples at an accelerating voltage of 15 kV, a beam current of 20 nA, and a take-off angle of 40 degrees. The time per single measurement was 60 s and the working distance was 10 mm. The intensities of the Ka X-ray lines were taken as the difference of the peak maxima and the background intensities at the left and right of the peaks using TAP (for Al) and LLIF (for Ni) crystals. The measured Al Ka and Ni Ka intensities were divided by those of the pure Ni and Al standards, respectively. The concentration values were then calculated from the intensity ratios applying the approach of Puchou and Pichoir [61]. The composition was measured along a line perpendicular to the interfaces in steps of 1 µm. In the case of very thin layers (as thin as 2 µm) the analysis was performed along a line parallel to the interfaces within the intermetallic layers.

Some of the chemical analyses were also performed using a Link ISIS energy-dispersive X-ray (EDX) spectrometer attached to the scanning electron microscope Philips XL 30. In this case the samples to be analysed were polished only with 1 µm diamond paste and inspected using back-scattered electrons. The analyses were carried out at an accelerating voltage of 20 kV, at a take-off angle of the X-ray radiation of 45 degrees, and at a working distance of 9.9 mm. The generated Ni Kα and Al Kα radiations were acquired for at least 100 s per single measurement. The chemical composition was calculated by applying the ZAF (atomic number, adsorption, fluorescence) correction procedure included in the Link ISIS software and by using pure Ni and Al standards.

6.2.2 X-Ray Diffraction Analysis

The X-ray diffraction technique was used for phase identification. Diffraction patterns were collected using a Philips X’ Pert diffractometer employing Cu Ka radiation at room temperature. The data were acquired in the diffraction angle range $10^{o} \leq 2\theta \leq 120^{o}$, with a step width of 0.05^{o} and a step time of 25 s. The measurements were performed on the fracture surface of the samples broken along the central zone of the interconnection.

6.3 Results and Discussion

A cross-sectional view of the Ni/Al/Ni interconnection after 2 min reaction time at 720°C is shown in Fig. 6.2. The continuous layer adjacent to the Ni substrates consists of the Al_3Ni_2 compound. The EPMA analysis across the joint revealed (Fig. 6.2) two distinct plateaus corresponding to the intermetallic compounds Al_3Ni and Al_3Ni_2. As the analysis was performed across the Al_3Ni bridge shown in Fig. 6.2 unreacted Al was not detected. The X-ray diffraction pattern from a fracture surface of the joint (see Fig. 6.3) could be indexed, assuming the presence of a hexagonal Al_3Ni_2 phase(with lattice parameters a = 4.036 Å and c = 4.90 Å) and an orthorhombic Al_3Ni phase (with a = 6.598 Å, b = 7.352 Å and c = 4.802 Å [62]). The X-ray diffraction pattern contained also peaks corresponding to pure unreacted Al and Ni substrate. On this basis it can be concluded that the central region consists of unreacted Al and crystals of the Al_3Ni phase which forms bridges with the layers of Al_3Ni_2.

Apparently, at the early stage of the isothermal solidification process, the Al_3Ni phase is formed very fast by the dissolution of Ni into the liquid Al and crystallization from the liquid phase. Thereafter, the Al_3Ni_2 phase develops by diffusion of Ni into the Al_3Ni phase in association with the reaction:

$$Ni + Al_3Ni \rightarrow Al_3Ni_2 \tag{6.1}$$

The irregular shape of the Al_3Ni_2/Al_3Ni interface (Fig. 6.2) indicates that this reaction does not occur equally fast. The liquid Al is trapped within the Al_3Ni phase, which is surrounded by layers of Al_3Ni_2, is shown in Fig. 6.2. Further formation of Al_3Ni requires a continuous supply of Ni atoms from the substrate through the Al_3Ni_2 layer. As a large part of diffusing atoms is used up for the formation and growth of Al_3Ni_2 this might result in a deficiency of Ni atoms in the central part of the joint and in the formation of fissures and pores.

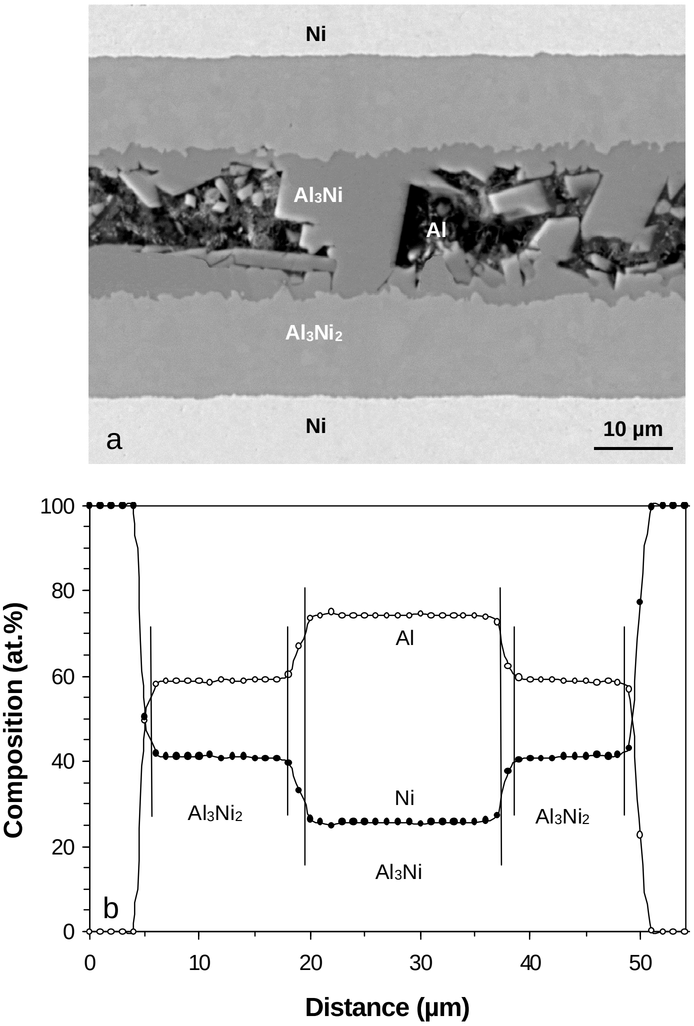

Fig. 6.2. SEM micrograph of the cross-sectional view of a Ni/Al/Ni interconnection after 2 min of reaction time at 720°C (a) and corresponding EPMA line-scans for Al and Ni (b).

The metallographic analysis has revealed that beyond 5 min of reaction time at 720°C the entire quantity of Al has been converted into three different intermetallic compounds (see Fig. 6.4). On the basis of EPMA (Fig. 6.4) and X-ray diffraction analysis it could be concluded that the central dark gray broad band consists of the Al_3Ni_2 phase and is surrounded by adjacent AlNi layers of black colour and an $AlNi_3$ adjacent to the Ni substrates.

With reference to the above discussion of Fig. 6.2 it is concluded that all the earlier formed Al_3Ni phase has been consumed by the growing Al_3Ni_2 phase. The widths of AlNi and $AlNi_3$ layers are at the limit of the spatial resolution offered by the EPMA analysis. Therefore, only one plateau (from the Al_3Ni_2 phase) is revealed by the EPMA across the Ni/Al/Ni interconnection (Fig. 6.4). All the phases form continuous layers and it is suggested that they grow due to solid state diffusion and transformation according to the schemes:

$$Ni + Al_3Ni_2 \rightarrow 3\ AlNi \quad \text{and} \quad 2\ Ni + AlNi \rightarrow AlNi_3 \qquad (6.2)$$

After 20 min of annealing, four different layers are present in the joint (Fig. 5a). The central Al_3Ni_2 phase with irregular interfaces is consumed by the growing AlNi phase. The phase adjacent to the Ni substrate is $AlNi_3$ as previously. A fourth “layer” is clearly visible between the AlNi and $AlNi_3$ layers. It can be seen that this phase develops in a very irregular manner.

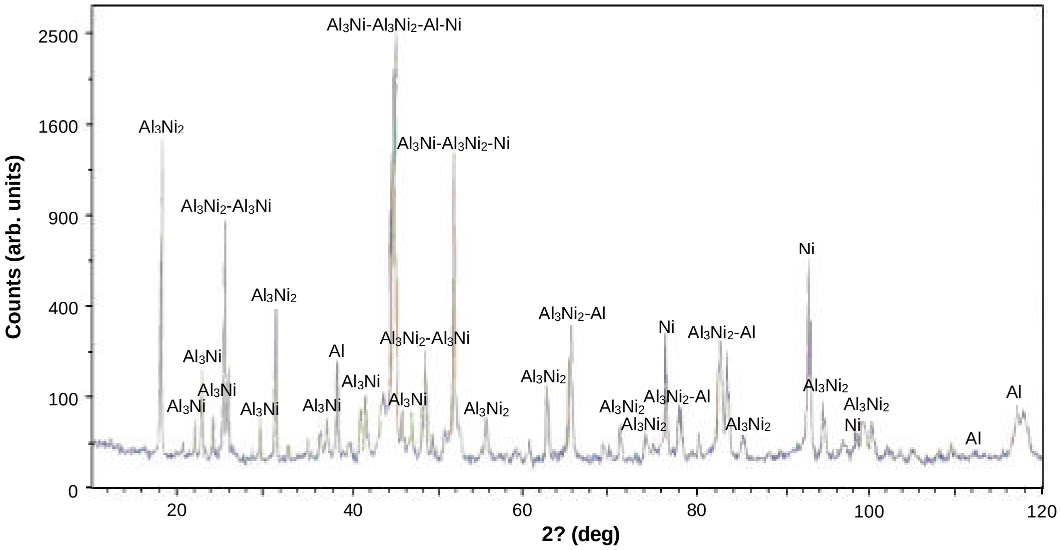

Fig. 6.3. X-ray diffraction pattern of the Ni/Al/Ni interconnection after 2 min of reaction time at 720°C.

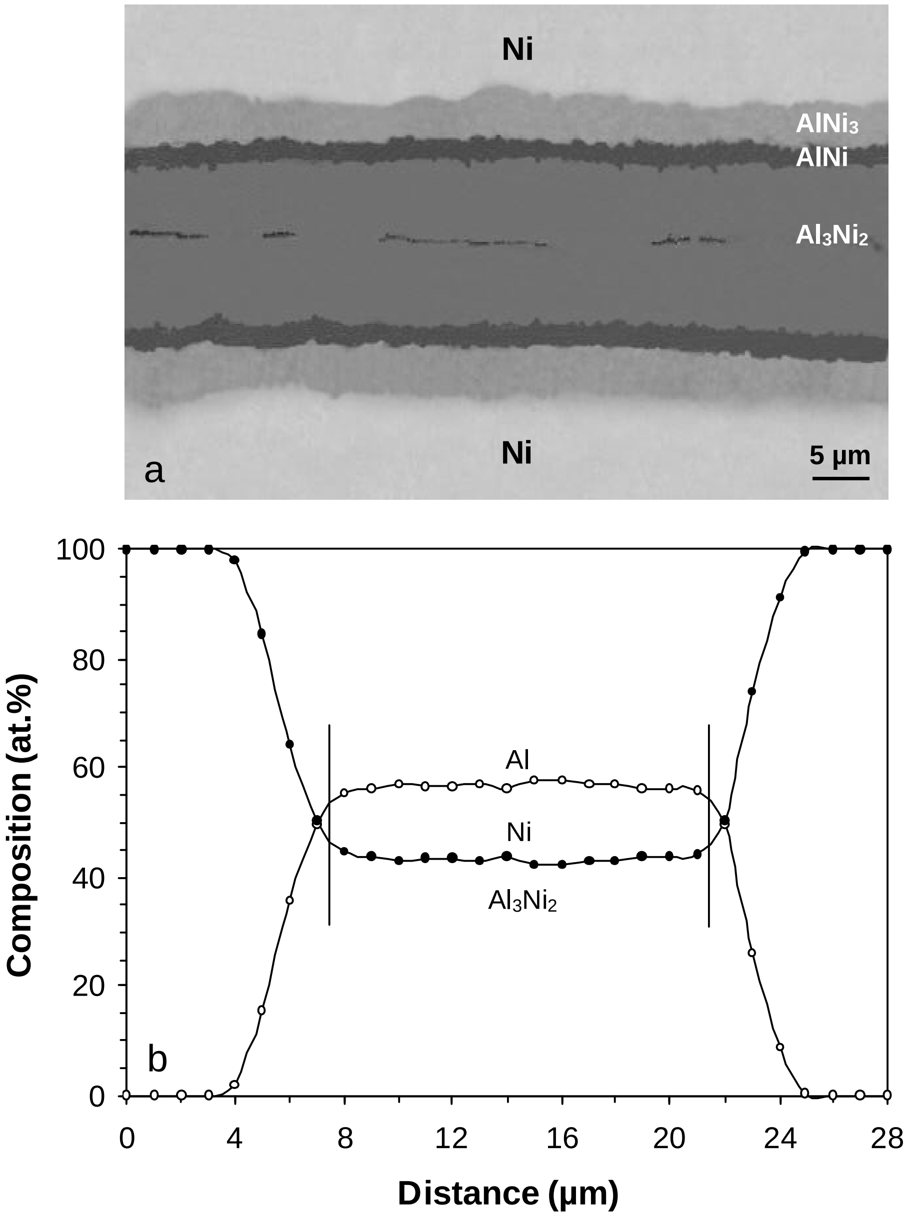

Fig. 6.4. Optical micrograph of the cross-sectional view of a Ni/Al/Ni interconnection after 10 min of reaction time at 720°C (a) and corresponding EPMA line-scans for Al and Ni (b).

The results obtained by the EDX technique are shown in Fig. 5b. The composition of the central zone corresponds to the Al_3Ni_2 compound. The zone adjacent to Al_3Ni_2 is likely to be AlNi, close to its stochiometric composition. The layer adjacent to the Ni substrate contains approximately 75 at.% Ni and 25 at.% Al which corresponds to the $AlNi_3$ phase. Due to the irregular morphology of the fourth “layer”, EDX point analysis was performed in those areas where the thickness of the “layer” was the largest. The average result from 10 such measurements using a special weak beam condition (5 kV to improve the spatial resolution) was found to be 58.5 at.% Ni. This is close the maximum Ni content in AlNi possible at the fabrication temperature (see Fig. 6.1). It is suggested that the fourth layer consists of a Ni-rich AlNi phase, what will be discussed later. X-ray diffraction analysis performed on the fracture surface of a joint after 20 min reaction time revealed the presence of the Al_3Ni_2 phase. The peaks corresponding to AlNi and $AlNi_3$ were not detected, although the thickness of the Al_3Ni_2 layer is not sufficient to avoid the penetration of the X-ray beam.

Further annealing leads to the presence of three zones in the joint (see Fig. 6.6 recorded after 3 h at 720°C). From the composition profiles measured along the layers (Fig. 6.6), the phases were identified as $AlNi_3$ (layer adjacent to Ni), Ni-rich AlNi (58.9 at.% Ni) and AlNi (central zone). Note that in this case the Ni-rich AlNi phase forms a continuous layer with irregular outer interfaces. X-ray diffraction analysis, conducted as described above, indicated the presence of the AlNi phase. The peaks corresponding to Al_3Ni_2 and $AlNi_3$ were not present. The first absence can be explained as a result of a consumption of this phase to form the AlNi. No explanation for the absence of the $AlNi_3$ peaks can be offered presently.

The EPMA line-scan along the central NiAl zone revealed that the composition of this phase is close to the stoichiometric value (50-52 at.% Ni). It could be expected that rather Al-rich or Ni-rich AlNi should appear because intrinsic diffusion coefficients of Ni and Al decrease as a function of composition in the direction of the stoichiometric composition starting at both sides of the composition range for the AlNi phase. The minimum intrinsic diffusion coefficient occurs for both diffusing species at approximately 49 at.% Al (see cf. [57],[63]).

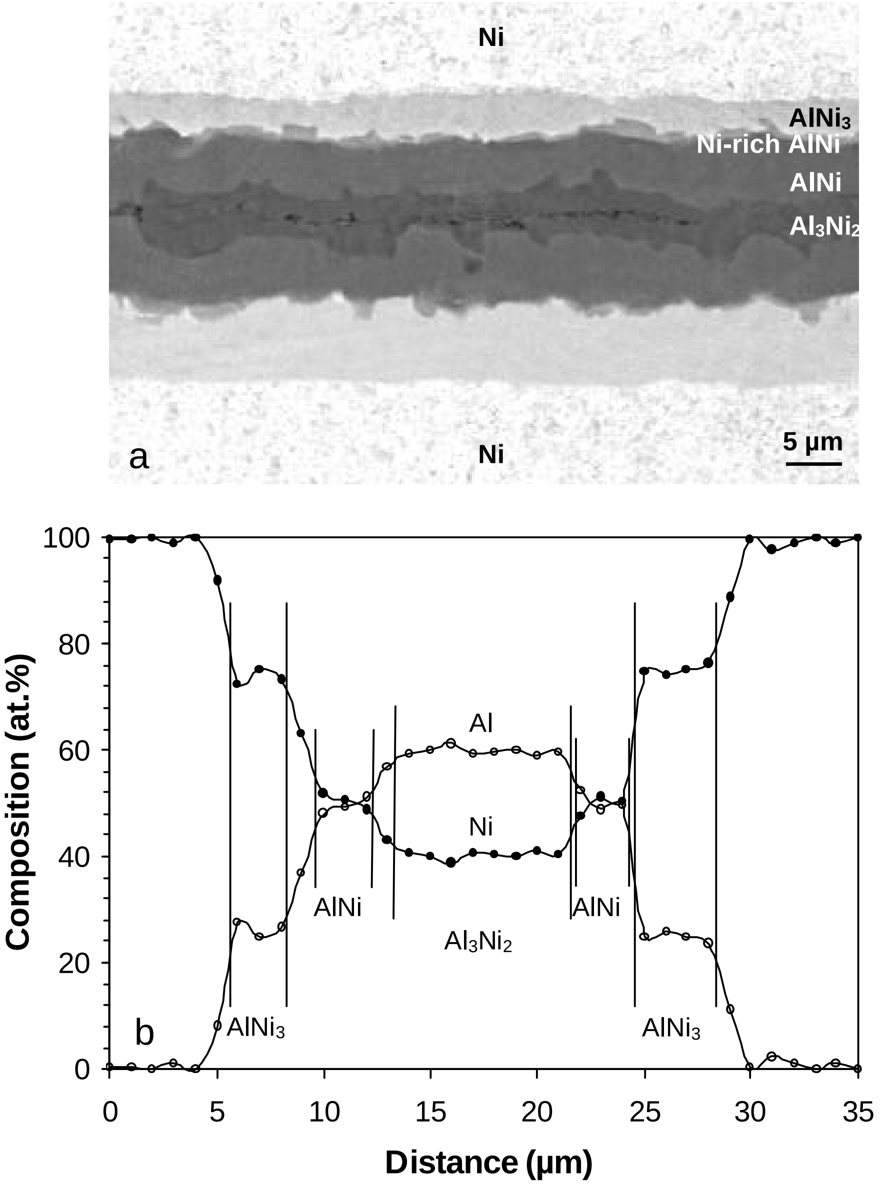

Fig. 6.5. SEM micrograph of the cross-sectional view of a Ni/Al/Ni interconnection after 20 min of reaction time at 720°C (a) and corresponding EDX line-scans for Ni and Al (b).

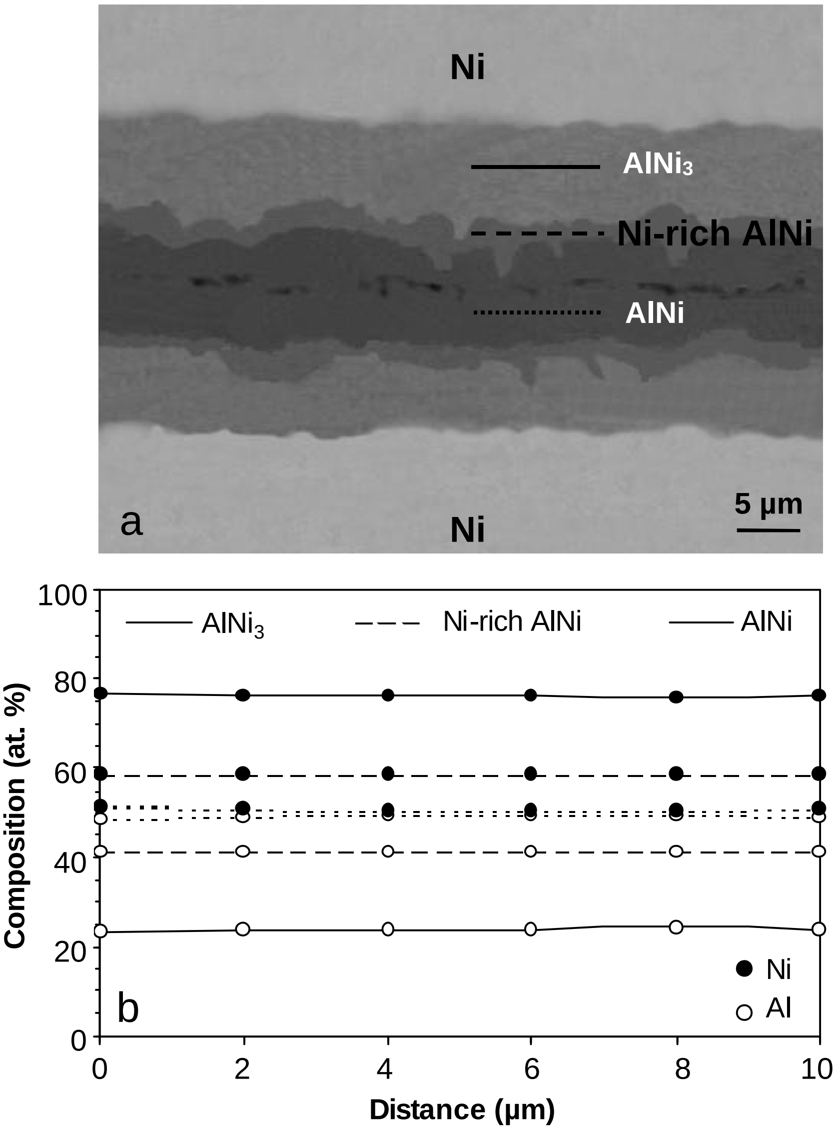

Fig. 6.6. Optical micrograph of the cross-sectional view of a Ni/Al/Ni interconnection after 3 h of reaction time at 720°C (a) and corresponding EPMA line-scans along the stoichiometric AlNi , Ni-rich AlNi and AlNi$_3$ phases (b).

The Ni/Al/Ni situation is even more complicated by the fact that when appeared (see Fig. 6.4 and Fig. 6.5), NiAl is an intermediate layer between the Al$_3$Ni$_2$ and AlNi$_3$ phases. The formation and growth of NiAl requires supply of Ni atoms from the Ni substrate through the AlNi$_3$ layer in which the self-diffusivity of Al-substitute is lower than that of Ni [64]. It is suggested that the peculiarity of the diffusion process in the NiAl compound itself and the complexity of the diffusion in the $AlNi_3$ phase could be responsible for the formation of two distinct zones of NiAl in the Ni/Al/Ni interconnection zone.

Further annealing at 720°C leads to the growth of the Ni-rich AlNi compound at the expense of the stoichiometric AlNi. After 10 h of annealing the zone occupied by the stoichiometric AlNi is no longer visible and the joint comprises only the Ni-rich AlNi and $AlNi_3$ phases (Fig. 7a) with chemical compositions corresponding to the chemical formula (EPMA data: Fig. 7b). After 30 h of reaction time at 720°C all the Ni-rich AlNi has been entirely converted into $AlNi_3$ according to:

$$\text{Ni-rich NiAl}(Al_2Ni_3) + 3\ Ni \rightarrow 2\ AlNi_3 \qquad (6.3)$$

XRD analysis conducted on the fracture surface of a joint after 10 h at 720°C indicated the occurrence and $AlNi_3$. Peaks corresponding to the AlNi phase were also identified and they can be attributed to the so called Ni-rich AlNi but supplementary investigation must be performed to prove this hypothesis.

A joint composed of only the $AlNi_3$ phase advantageous for practical application; the melting temperature of this phase is 1360°C, which is almost twice higher than the fabrication temperature and indicates a great potential of the diffusion soldering process for the fabrication of joints with a good thermal stability. All the reaction stages of phase formation are summarized in the following sequence:

$$\text{Al (liquid)} \rightarrow Al_3Ni \rightarrow Al_3Ni_2 \rightarrow \text{stoichiometric AlNi} \rightarrow \text{Ni-rich AlNi} \rightarrow AlNi_3 \qquad (6.4)$$

Additional experiments showed that the thickness of the Al foil (6-50 µm) does not have effects in the morphology and order of appearance of the intermetallic phases during the diffusion soldering. Only the total time required to complete the reaction sequence decreases significantly for the thinner Al foil. For example, the Al_3Ni_2 phase was completely consumed after 20 min of reaction for an Al foil thickness of 6 µm whereas for the same time using an Al foil 15 µm thick this phase was still present in the central zone of the joint (Fig. 6.5).

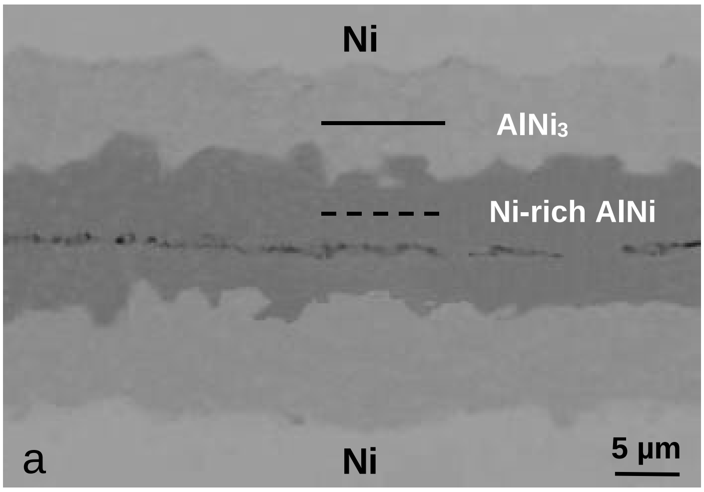

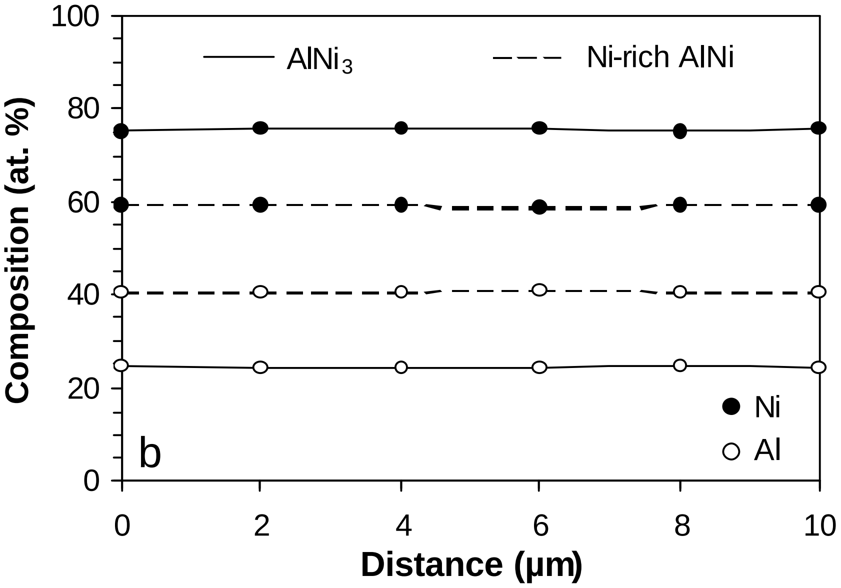

Fig. 6.7. Optical micrograph of the cross-sectional view of a Ni/Al/Ni interconnection after 10 h of reaction time at 720°C (a) and corresponding EPMA line-scans along the Ni-rich AlNi and $AlNi_3$ phases (b).

Porosity in the central zone can be observed (see Fig. 6.4-Fig. 6.7). This may be attributed to the oxygen trapping while placing the Al foil between the Ni substrates. Indeed, the EDX inspection performed revealed some small amount of oxygen.

6.4 Conclusions

- The formation of Ni/Al/Ni joints starts with the reaction of liquid Al with solid Ni, leading to the formation of the Al_3Ni intermetallic phase.
- Next, interdiffusion in the solid state leads to the formation of the following phases sequentially: Al_3Ni_2, stoichiometric AlNi, Ni-rich AlNi, and $AlNi_3$. At intermediate stages of annealing two to four phases can exist simultaneously.
- Two variants of the NiAl phase, namely, a Ni-rich one (58.5 at.% Ni) and the stoichiometric AlNi, are present in the joints.
- The joining process after 30 h of reaction at 720°C leads to a joint composed of solely $AlNi_3$.
- The high melting point of $AlNi_3$ (1360^{o}C) suggests a good potential for the diffusion soldering for joining of heat dissipating devices used in electronics and electrotechnics.

7 Appendix B: Kinetic behaviour of diffusion-soldered Ni/Al/Ni interconnections

G.A. López, S. Sommadossi, P. Zieba, W. Gust, E.J. Mittemeijer*

*Institute of Metallurgy and Materials Science, Polish Academy of Sciences, Cracow, Poland

The layer growth of intermetallic phases occurring in Ni/Al/Ni interconnections formed by the process of diffusion soldering was studied. The layer thicknesses as a function of the treatment time at 720 °C and the Ni concentration profiles in the interconnection zone were measured for the stoichiometric AlNi, Ni-rich AlNi, and $AlNi_3$ compounds. The growth rate constants were calculated, considering the incubation and transition periods preceding the steady-state growth of the intermetallic phases. The fastest growth occurs for stoichiometric AlNi and the slowest growth occurs for Ni-rich AlNi. The values of the integral interdiffusion coefficients for the stoichiometric AlNi, Ni-rich AlNi, and $AlNi_3$ were determined; the results fall within the range of values presented in previous work dedicated to Ni/Al diffusion couples.

7.1 Introduction

Diffusion soldering appears to be a promising technology for realizing joining of components in electronic and electric devices. The process is based on an isothermal solidification reaction between a thin layer of a molten material and solid substrates. Thereby, one or more intermetallic phases develop, which posses melting temperatures much higher than the temperature used for the fabrication of the joint.

Recently, for the first time, diffusion soldering has been successfully applied to make a stable high-temperature Ni/Al/Ni interconnection (see [65] or Section 6). The phases appearing at subsequent stages of the process were identified and characterized. The formation of a Ni/Al/Ni joint starts with the reaction of liquid Al with solid Ni (substrate) to form the Al_3Ni intermetallic phase. Further, solid-solid reactions occur by interdiffusion of Ni and Al, which lead to the successive formation of Al_3Ni_2, stoichiometric AlNi, Ni-rich AlNi, and $AlNi_3$ phases. The joining process eventually, after 30 h of reaction at 720°C, leads to the sole presence of $AlNi_3$ in the Ni/Al/Ni interconnection. The high melting temperature of the $AlNi_3$ phase (1360°C) makes Ni/Al/Ni joining very attractive for interconnections between resistive heaters and electric leads, e.g., hot plates.

For quantitative modelling of the process of joint formation the determination of parameters that control the growth rate of the intermetallic phases is a prerequisite. In the existing literature such results pertain mostly to the high-temperature variant of diffusion soldering, named diffusion brazing or transient liquid-phase bonding. However, in this process intermetallic phases do not occur (see, for example, [66],[67]). For the description of the reaction occurring in the interconnection zone of diffusion-soldered components one may rather look at the treatment of interdiffusion in multiphase diffusion couples experiments with markers; see Refs. [68],[70]. However, in the diffusion couples changes of the concentration occur over distances (hundreds of microns) much larger than those occurring diffusion-soldered couples, where the reaction zone has a limited extent of 20 to 1 μm. Further, more research work on diffusion-soldered couples revealed a faster rate of diffusion than observed in the earlier experiments [7].

Against this background, research appears essential for a better understanding of the diffusion processes involved during the formation and growth of intermetallic phases in diffusion-soldered components. The present work was carried out to obtain quantitative data about the kinetics of growth of the intermetallic phases in Ni/Al/Ni interconnections. The increase in thickness of the intermetallic layers was determined as function of reaction time. From these results the interdiffusion coefficients for the stoichiometric AlNi, Ni-rich AlNi, and $AlNi_3$ phases were calculated.

7.2 Experimental

A commercial Al foil (15 µm thick) was sandwiched between two Ni substrates (99. 999 wt.% purity) The assembly was heated up rapidly (200-300 °C/s) to 720 °C and annealed at this temperature for times up to 30 h to induce the isothermal reaction of liquid Al and solid Ni to form the intermetallics. The joint was fabricated under a slight mechanical pressure (≈ 0.5 MPa) in a specially prepared thermal load press kept under vacuum (rest pressure of 10 Pa) in an Ar box to avoid the oxidation of the sample. The subsequent steps of assembly preparation and joint fabrication have been described in more detail in Ref. [65] or Section 6. Cross-sections of the joints were prepared for the metallographic analysis by embedding in epoxy, grinding and polishing, using 1 µm diamond paste as last step.

Measurements of the chemical composition in the interconnection zone across the joint were carried out using an electron probe microanalyser (EPMA) Cameca SX100 equipped with 5 wave-length dispersive spectrometers or using a Link ISIS energy-dispersive X-ray (EDX) spectrometer attached to the scanning electron microscope Philips XL 30. For details, see Ref. [65] or Section 6.

The thickness of the intermetallic layers was measured from the screen of a video system connected to a Zeiss-Axiophot-type light microscope (LM) at a total magnification of 5000:1. Because some of the intermetallic layers were not fully planar during growth, the thickness was determined as the average from the measurements of the growth distance at 20-30 randomly chosen positions. The resolution was ±0.2 µm and the standard deviation for the thickness values was in the range 0.1 - 0.25 µm.

7.3 Results and discussion

7.3.1 Growth rate of intermetallic phases

The formation of the intermetallic phases in the reaction zone of Ni/Al/Ni interconnections occurs that fast that the initially formed Al_3Ni, by liquid-solid reaction, is rapidly consumed by the Al_3Ni_2 phase, formed subsequently by solid-solid reaction, in a first stage of the process. No liquid Al is present after 5 min of the reaction at 720^oC, and at this stage the thickness of the Al_3Ni_2 layer starts to decrease because of the formation of subsequent phases (AlNi, Ni-rich AlNi and $AlNi_3$) at the cost of Al_3Ni_2 and Ni. Consequently, kinetic data on the growth of Al_3Ni_2 could not be obtained. Therefore, the kinetic analysis was restricted to the formation of the stoichiometric AlNi, Ni-rich AlNi, and $AlNi_3$ intermetallics.

A typical optical micrograph, showing the AlNi layers and the $AlNi_3$ layers in the Ni/Al/Ni joint after 10 min of reaction time, is presented in Fig. 7.1. Table 7.1contains the measured thickness values of the intermetallic layers for various reaction times. The growth of an intermetallic phase can be generally expressed by the following equation:

$$Dx = k \times t^n \quad \text{or} \quad \log Dx = \log k + n \log t \qquad (7.1)$$

where Dx is the thickness of the reaction layer, k is the rate constant, t is the time of reaction, and n is the time exponent. In the present case, from the log Dx - log t diagrams, the values of n were found to be 0.5±0.1 for the involved phases. Hence, the growth of the layers obeys a parabolic law, which is compatible with volume diffusion control of the layer growth (see cf. [31],[71]).

As discussed in Ref. [31] there are several causes that could lead to a deviation from rate control by a pure volume diffusion process. For example, in many diffusion experiments the layer growth is faster in the beginning of the process because of the presence of small grains at the start, which leads to a distinct contribution by the relatively fast grain-boundary diffusion process. After this initial transition period, the process becomes rate controlled by volume diffusion and a parabolic growth is observed.

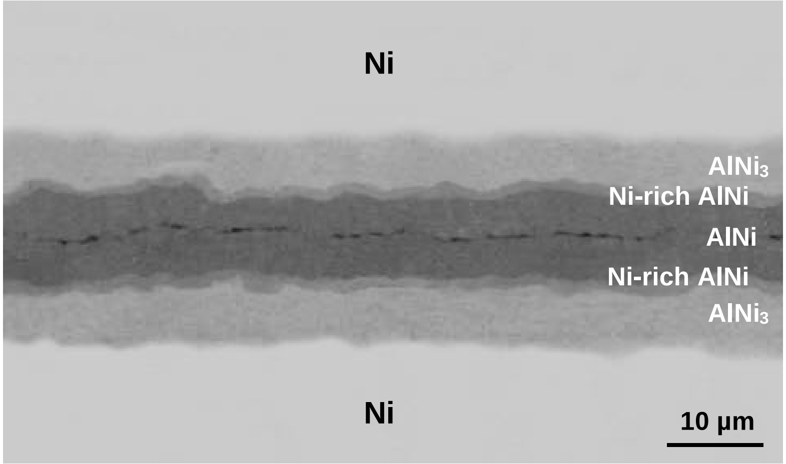

Fig. 7.1. Light optical micrograph of the cross-section of a Ni/Al/Ni interconnection after 3 h of reaction time at 720°C.

Table 7.1. Thickness of the layers of the intermetallic phases formed in Ni/Al/Ni interconnections produced at 720°C.

Reaction time	Layer thickness *Dx* (µm)		
(h)	Stoichiometric AlNi	Ni-rich AlNi	$AlNi_3$
0.083	0.8	-	1.2
0.167	1.2	-	3.3
0.333	2	-	3.6
0.5	2.4	0.5	3.8
1	3.9	0.8	4.0
3	-	1.6	5.2
10	-	2.4	7.8
20	-	-	11.2
30	-	-	13.6
k [m^2/s]	2.22×10^{-15}	7.78×10^{-17}	8.17×10^{-16}

The growth of the intermetallic phases studied in this work (see above) is presented in Fig. 7.2. The appearance of stoichiometric AlNi requires a certain incubation time as clearly follows from a plot of Dx^2 versus t (Fig. 7.2a). The rate constant k can straightforwardly be determined from the slope of the straight line fitted to data points in the plot. Similarly, it is concluded that the growth of Ni-rich AlNi requires no incubation time (Fig. 7.2b). For the growth of the $AlNi_3$ phase a Dx vs. $t^{1/2}$ plot was applied because such a plot exhibits more clearly than a Dx^2 vs. t plot that a transition period preceding the parabolic growth stage occurs (Fig. 7.2c) [72]. Eliminating the data points corresponding to the transition period, Fig. 7.2d shows a Dx^2 vs. t plot for the remaining data and the rate constant for the parabolic growth of the $AlNi_3$ phase has been derived from the slope of the straight line fitted through the data points in this plot. The parabolic growth constants, k, determined from the slopes of the straight lines fitted to the data pertaining to parabolic growth in Fig. 7.2 have also been listed in Table 7.1.

A parabolic growth for the phases concerned was also observed upon analysing the reaction diffusion in Ni-Ni_2Al_3 laminated structures [73], and the corresponding parabolic growth constants are of the same order of magnitude as those presented in this work.

Clearly stoichiometric AlNi exhibits the fastest growth rate, which, recognizing a small value for the concentration gradient (practically stoichiometric compound), can be attributed to a relatively high value of the interdiffusion coefficient. The two variants of AlNi have been treated as two separate phases, because the growth of the stoichiometric AlNi started before the Ni-rich AlNi phase had been formed. The existence of Ni-rich AlNi was first detected after 20 min of reaction at 720°C; at this stage the stoichiometric AlNi and $AlNi_3$ layers had thicknesses of 2 and 3.6 µm, respectively.

According to the accepted phase diagram (Fig. 7.3) [74] only an AlNi phase with a relatively large composition range (47.7 at.% Ni – 60.7 at.% Ni, at 720°C) could occur. The present observation, which parallels data presented in Ref. [73], can be interpreted such that either the phase diagram has to be modified or that kinetic reasons are responsible for the occurrence of two modifications of the AlNi phase.

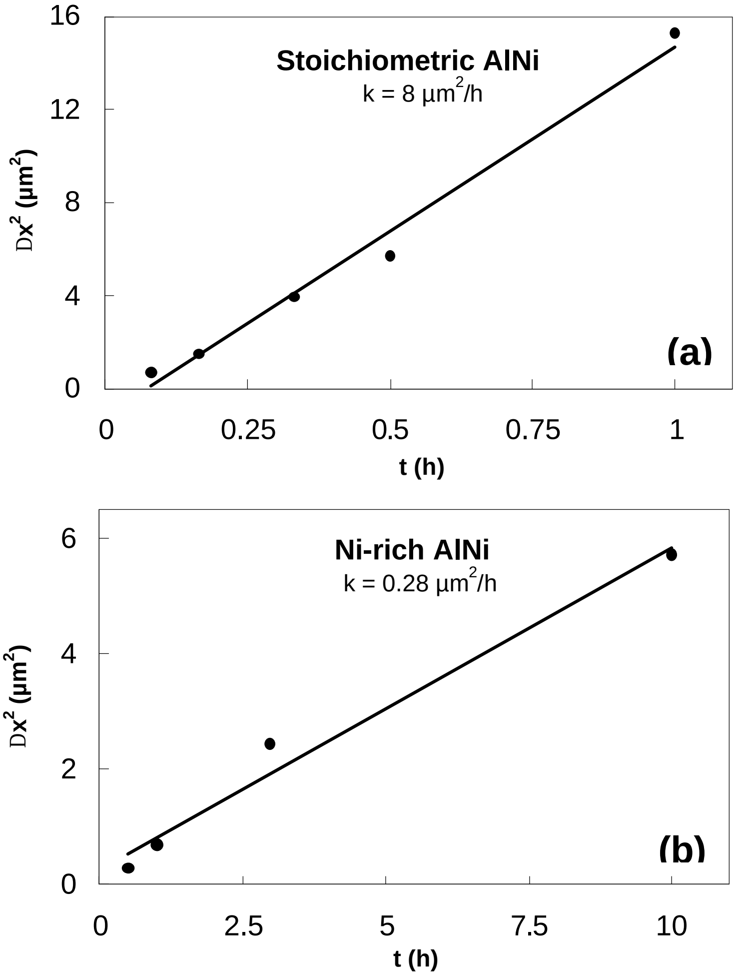

Fig. 7.2. Time dependence of the layer width for stoichiometric NiAl (a), Ni-rich NiAl (b), and $AlNi_3$ (c and d) in Ni/Al/Ni interconnections upon reaction at 720°C.

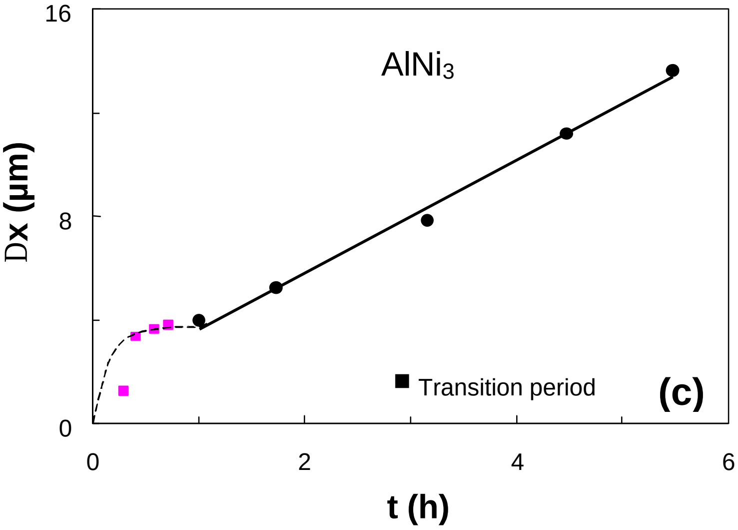

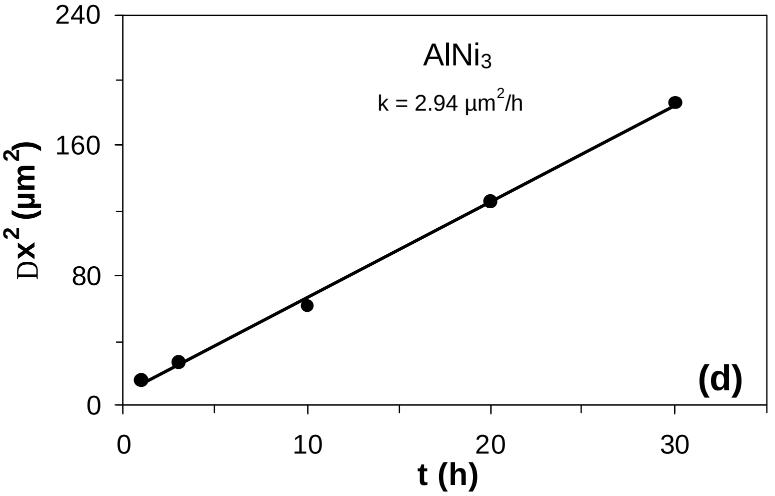

Fig. 7.2. Continued. Time dependence of the layer width for stoichiometric NiAl (a), Ni-rich NiAl (b), and $AlNi_3$ (c and d) in Ni/Al/Ni interconnections upon reaction at 720°C.

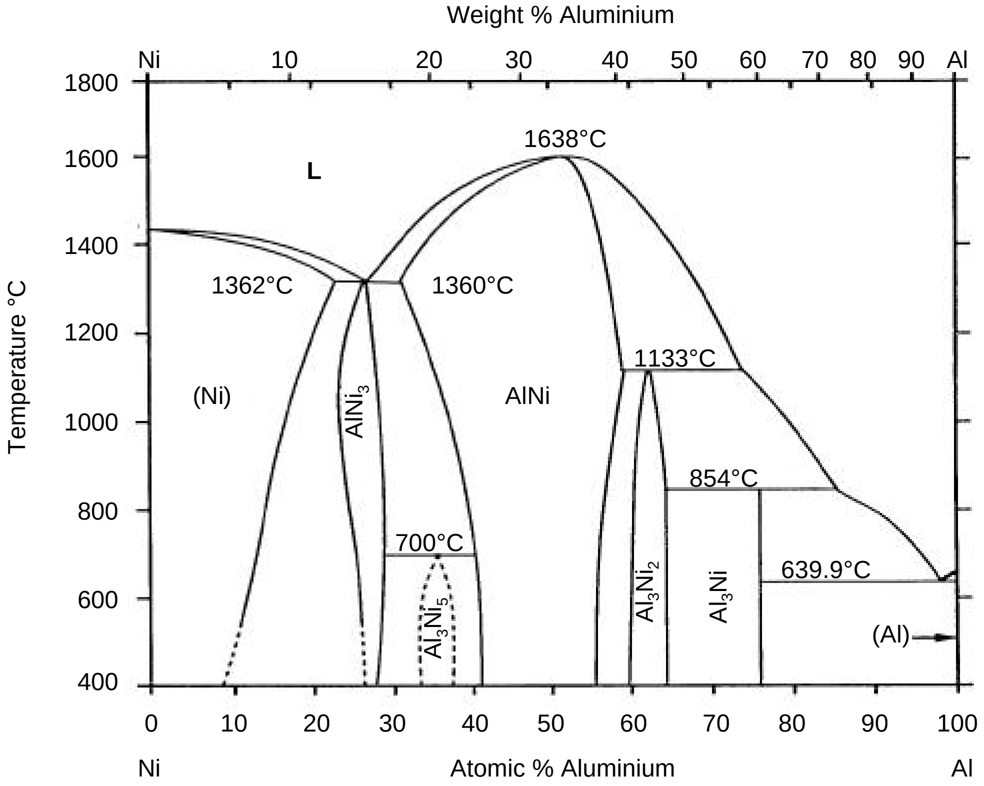

Fig. 7.3. The Ni-Al phase diagram [74].

7.3.2 *Integral interdiffusion coefficient*

The determination of the intrinsic diffusion coefficients of Al and Ni requires the use of inert markers. In this paper, no makers were employed, but so-called interdiffusion coefficients $\tilde{D}$ could be determined for the involved intermetallic phases. Treatments of single-phase and multiphase diffusion in binary systems were presented by Kidson [12] and later by Wagner [13]. By modifying the Sauer-Freise generalization [19] of the Boltzmann-Matano analysis (see cf. [20],[21]), Wagner developed a relationship between the interdiffusion coefficient, the parabolic growth rate constant, and the concentration at the interfaces, thought to be constant and equal to their equilibrium values. This approach is convenient because the concentration profile determined for each of the intermetallic layers formed in the reaction zone Ni/Al/Ni is practically a horizontal line (for details, see Ref. [65] or Section 6). Then, if the Boltzmann-Matano analysis would be applied to determine the interdiffusion coefficient, $\tilde{D}$, as function of the concentration, it will be associated with a very large error since the concentration gradient approaches zero and thus ∂x/∂C goes to infinity (*x*-distance coordinate, *C*-concentration). To avoid this problem, an integral diffusion coefficient, $\tilde{D}_{int}$, is introduced [13] by integrating $\tilde{D}$ in phase *i* over the distance coordinate and, thereby, avoiding the determination of the concentration gradient. Thus, in the case where formation of phase *i* occurs, from phases (*i*-1) and (*i*+1) coexisting with phase *i*, the following expression holds:

$$\tilde{D}_{\text{int}} = \Delta N^i\, \tilde{D}^i_{av} = \frac{\left(N^i - N^{(i-1)''}\right)\left(N^{(i+1)'} - N^i\right)}{N^{(i+1)'} - N^{(i-1)''}} k^i \qquad (7.2)$$

$$k^i = \frac{\left(\Delta x^i\right)^2}{2t} \qquad (7.3)$$

Here, *i* is the serial number of a phase *i* corresponding to the integral interdiffusion coefficient $\tilde{\mathrm{D}}^i_{\text{int}}$, N^i is the average mole fraction of component B in phase *i*, $N^{i-1''}$ and $N^{i+1'}$ are the mole fractions of component B in phases *i*-1and *i*+1 coexisting with phase *i*, and $\Delta N^i = N^{i'} - N^{i''}$ is the difference in B component composition of the phase *i* at the interfaces between the phases (*i*-1) and *i* and between the phases *i* and (*i*+1).

Equation (7.2) was obtained under the following conditions:

- The interface concentrations do not change with time.
- The layer shows parabolic growth.
- The differences in molar volumes amongst the various phases are negligible.

Wagner’s equation was successfully applied for the determination of the integral interdiffusion coefficient in single-phase NiAl couples [70], and in the AlNi and Ni_3Al phases using a vapour-solid technique [69]. The example below shows how to use Eq. (7.2) in order to calculate the integral interdiffusion coefficient of $AlNi_3$ from the rate constant extracted from the growth of the $AlNi_3$ layer:

$$\tilde{D}_{\text{int}} = \Delta N \ \tilde{D}_{av}^{AlNi_3} = \frac{\left(N^{AlNi_3} - N^{Ni-rich\,AlNi\,"}\right)\left(N^{Ni\,'} - N^{AlNi_3}\right)}{N^{Ni\,'} - N^{Ni-rich\,AlNi\,"}} k^{AlNi_3} \tag{7.4}$$

where *DN* is the difference in Ni concentration of $AlNi_3$ at the interfaces between Ni-rich AlNi and $AlNi_3$ and between $AlNi_3$ and (Ni) solid solution ($N^{AlNi_3\,'}$ - $N^{AlNi_3\,''}$); $N^{AlNi_3\,'}$ and $N^{AlNi_3\,"}$ are the Ni concentrations of $AlNi_3$ at the interfaces between Ni-rich AlNi and $AlNi_3$ and between $AlNi_3$ and (Ni) solution, respectively. Data for $N^{Ni-rich\,AlNi\,"}$, the Ni concentration of Ni-rich AlNi at the interface between Ni-rich and $AlNi_3$, and for $N^{Ni'}$, the Ni concentration of (Ni) at the interface between $AlNi_3$ and (Ni), were taken from the published equilibrium phase diagram [74]. The value for $N_{Ni}^{AlNi_3}$ was taken equal to the average composition for this phase as determined by EPMA (see Ref. [65] or Section 6).

The equilibrium values of the concentration range of the stoichiometric and Ni-rich AlNi phases are unknown [74]. Here, it is assumed that the two phases exist in the homogeneity range of AlNi reported in the literature as two different compounds. At the high-Ni content side, the Ni-rich AlNi phase was considered to be in equilibrium with $AlNi_3$ and the equilibrium concentration of AlNi taken from the phase diagram was assumed to be the equilibrium concentration for Ni-rich AlNi. Then, as a zeroth order approximation, a symmetrical composition range around the average composition as obtained by EPMA (see Ref. [65] or Section 6) was assumed for this phase. An analogous approach was adopted for stoichiometric AlNi; in this case the phase was considered to be in equilibrium with Al_3Ni_2 at the low-Ni content side of the phase diagram. The data required for the calculation and the resultant values of the integral interdiffusion coefficients are listed inTable 7.2 and Table 7.3, respectively. The corresponding diffusivities determined in other studies (see cf. [68]-[70],[12]) for the same temperature have been given as well in Table 7.3. In Refs. [68] and [71], where values for AlNi were reported for the "AlNi" phase, no distinction between stoichiometric AlNi and Ni-rich AlNi was made, which makes a direct comparison with the present data difficult. In fact all data from the cited literature can only be taken as an indication of the order of magnitude for the diffusion coefficients because they were obtained using various approaches.

Table 7.2. Compositions of the intermetallic phases in Ni/Al/Ni interconnections.

Phase	Composition range as per phase diagram (at.%)	Average composition of the interconnection (at.%)
Al_3Ni_2	36.8 – 40.8	-
Stoichiometric AlNi	47.7 – 53.1*	48.9
Ni-rich AlNi	57.7 – 60.7*	59.2
$AlNi_3$	72.2 – 77.5	75.6
(Ni)	87.5 – 100	-

*This composition range was adopted for the calculation of the diffusivities (see text).

Table 7.3. Integral interdiffusion coefficients $\tilde{D}_{\text{int}}$ [m^2/s] in Ni/Al/Ni interconnections. Note that values presented in Refs. [68] and [71] pertain to the “AlNi” phase taken as the combination of stoichiometric and Ni-rich AlNi phases.

Phase	This study	Ref. [68]	Ref. [69]	Ref. [70]	Ref. [71]
AlNi	1.1×10^{-16}	8.0×10^{-16}	2.4×10^{-14}	1.1×10^{-18}	2.2×10^{-17}
Ni-rich AlNi	3.23×10^{-18}		3.2×10^{-21}	4.2×10^{-16}	
$AlNi_3$	5.4×10^{-17}	4.0×10^{-16}	1.0×10^{-15}	-	4.9×10^{-18}

In any case it can be concluded that the results presented in this work are in good agreement with the tendency that the diffusion in stoichiometric AlNi is the fastest and in Ni-rich AlNi is the slowest (e.g. compare with the results in Ref. [71]). It should be noted that differences as large as three orders of magnitude occur between the $\tilde{D}_{int}$ values obtained by the different authors. The value determined here for $AlNi_3$ falls between the extreme values reported in [68] and [71].

7.4 Conclusions

- The calculated growth rate constants for the intermetallic phases present in Ni/Al/Ni interconnections clearly indicate the fastest growth for stoichiometric AlNi and the slowest growth for the Ni-rich AlNi.
- The values of the integral interdiffusion coefficients determined for the stoichiometric and Ni-rich AlNi and $AlNi_3$ phases are between the extremes of the widely scattering data of earlier work.

8 References

[1] B. Richards, Mater. World, **Jan**. (2001) 19-21.

[2] G. Humpston and D. Jacobson, ‘Principles of soldering and brazing’, Materials Park, OH, ASM International (1993).

[3] M. Abtew and G. Selvaduray, Mater. Sci. Eng. **27**, (2000) 95-141.

[4] C.R. Kao, Mater. Sci. Eng. A **238** (1997) 196-201.

[5] I. Manna, S. Bader, W. Gust, and B. Predel, Phys. Stat. Sol. (a) **119a** (1990) K9-K13.

[6] D.M. Jacobson and G. Humpston, Soldering Surf. Mount Technol. **10** (2) (1992) 27-32.

[7] S. Baber, W. Gust, and H. Hieber, Acta Metall. Mater. **43** (1995) 329-337.

[8] A. Strecker, U. Salzberger, and J. Mayer, Prakt. Metallogr. **30** (1993) 482-495.

[9] M. Gigla, “Carinev-Electron Diffraction Solutions”, University of Silesia, Katowice (1996).

[10] P. Villars and L.D. Calvert, “Pearson’s handbook of crystallographic data”, Materials Park, OH, ASM International (1991) 2873-2874.

[11] T. B. Massalski (Editor-in-Chief), “Binary Alloy Diagrams”, Materials Park, OH, ASM International (1990) 1424-1425.

[12] G. V. Kidson, J. Nucl. Mater. **3** (1961) 21-29.

[13] C. Wagner, Acta Metall. **17** (1969) 99-107.

[14] G.J. Harvey and D.I. Cameron, J. Austral. Inst. Met. **4** (1969) 255-261.

[15] V.I. Dyvkov: J. Mater. Sci. **21** (1986) 3078-3085.

[16] C.-P. Chen and Y.A. Chang, ‘Diffusion in ordered alloys’, (ed. B. Fultz, R.W. Cahn, and D. Gupta), Warrendale, PA, The Minerals, Metals & Materials Society (1993) 169-184.

[17] T.P. Rajasekharan and K. Schubert, Z. Metallkd. **72** (1981) 275-279.

[18] V.I. Dybkov, ‘Growth kinetics of chemical compound layers’, Great Abington,

Cambridge, Cambridge International Science Publishing (1998).

[19] F. Sauer and V. Freise, Z. Elektrochem. **66** (1962) 353.

[20] L. Boltzmann, Wiedemanns Ann. Physik **53** (1894) 959.

[21] C. Matano, Jpn. J. Phys. **8** (1933) 109-113.

[22] K. Suganuma, Current Opinions in Solid State and Mater. Sci. **5** (2001) 55-64.

[23] J. Glazer, Int. Mater. Rev. 40, **2** (1995) 65-93.

[24] Z. Mei, J.W. Morris Jr., J. Electron. Mater. **21** (1992) 401-407.

[25] J. Seyyedi, Soldering Surf. Mount. Technol. **13** (1993) 26-32.

[26] J.L. Freer, J.W. Morris Jr., J. Electron. Mater. **21** (1992) 547-652.

[27] A.D. Romig Jr., F.G. Yost, P.F. Hlava, "Proc. Conf. on Microbeam Analisis-1984", A.D. Romig Jr., J.I. Goldstein (Eds.), San Francisco Press, San Francisco, CA, (1984) 87-94.

[28] D.M. Jacobson, S.P.S. Sangha, Soldering Surf. Mount. Technol. **8**, 2 (1996) 12-15.

[29] W. Köster, T. Gödecke, D. Heine, Z. Metallkd. **72** (1972) 802-807.

[30] J.S. Kirkaldy, D.J. Young, "Diffusion in the condensed state", The Institute of Metals, London (1987) 361-400.

[31] F.J.J. van Loo, Prog. Solid St. Chem. **20** (1990) 47-99.

[32] D. Gur, M. Bamberger, Acta Mater. **46** (1998) 4917-4923.

[33] V.I. Dybkov, "Growth kinetics of chemical compound layers", Cambridge Int. Sci. Publ., Cambridge (1998).

[34] H. Schmalzried, "Chemical kinetics of solids", VCH, Weinheim (1995).

[35] J.W. Christian, "The theory of transformation in metals and alloys", Pergamon Press, Oxford (1975).

[36] D.A. Porter, K.E. Easterling, "Phase transformations in metals and alloys", Van Nostrand Reinhold Co. Ltd., Oxford (1981).

[37] N.K. Tu, R.D. Thompson, Acta Metall. **30** (1982) 947-952.

[38] R.N. Chopra, M.N. Ohring, R.S. Oswald, Thin Solid Films **94** (1982) 279-288.

[39] D.S. Dunn, T.F. Marinis, W.M. Sherry, C.J. Williams, Mater. Res. Soc. Symp.

Proc. **40** (1985) 129-138.

[40] Shohji, S. Fujiwara, S. Kiyono, K.F. Kobayashi, Scripta Mater. **40** (1999) 818-820.

[41] F.G. Yost, F.P. Ganyard, M.M. Karnowsky, Metall. Trans. A **7** (1976) 1141-1148.

[42] J.K. Brandon, W.B. Pearson, D.J.N. Tozer, Acta Cryst. B **31** (1975) 774-779.

[43] Frear D.R., Jones W.R., Kinsman K.R., "Solder mechanics - a state of the art assessment", The Minerals, Metals & Materials Society, Warrendale, PA (1991).

[44] Frear D.R., Vianco P.T.: Metall. Mater. Trans. A **25** (1994) 1509.

[45] Bartels F., Morris J.W., Jr., Dalke G., Gust W.: J. Electr. Mater. **23** (1994) 787.

[46] Khanna P.K., Dalke G., Gust W., Z. Metallkd. **90** (1999) 722.

[47] Kuhmann J.F., Preuss A., Adolphi B., Maly K., Wirth T., Oesterle W., Pittroff W., Weyer G., Fanciulli M.: IEEE Electr. Comp. Technol. Conf. (1997) 120.

[48] van den Meerakker J.E.A.M., Baarslag P.C., Walrave W., Vink T.J., Daams J.L.C., Thin Solid Films **266** (1995) 152.

[49] Kunert M, Baretzky B, Baker SP, Mittemeijer EJ, Metall. & Mater. Trans. A **32A** (2001) 1201-1209.

[50] Baker S.P., Thin Solid Films **308-309** (1997) 289-296.

[51] Berkovich E.S.: Indust. Diamond Rev. **11** (1951) 129-132.

[52] Dieter G.E. in: Mechanical Metallurgy, McGraw-Hill, New York (1976).

[53] Cam G., Kocak M.: Inter. Mater. Rev. **43** (1998) 1.

[54] H. Okamoto, J. Phase Equilibria **14**, (1993) 257.

[55] M. Durand-Charre, "The Microstructure of Superalloys", Gordon and Breach Science Publishers, Amsterdam, (1997) 29.

[56] J.H. Wood, E.H. Goldman, "Superalloys II", edited by C.T Sims, N.S. Stoloff, and W.C. Hagel, John Wiley, New York, (1987) 359.

[57] S. Schankar, L.L. Seigle, Metall. Trans. A **9** (1978) 1467.

[58] C.-L. Tsao, S.-W. Chen, J. Mater. Sci. **30** (1995) 5215.

[59] K. Bouche, F. Barbier, A. Coulet, Z. Metallkd. **88** (1997) 446.

[60] P.K. Khanna, S. Sommadossi, G. Lopez, E. Bielanska, P. Zieba, L.S. Chang, W.

Gust, E.J. Mittemeijer, in Microstructural Investigation and Analysis **Vol. 4**, edited by B. Jouffrey and J. Svejcar, , DGM and Wiley-VCH, Weinheim (2000) 219.

[61] J.L. Puchou, E. Pichoir, La Res. Aerospatiale **3** (1984) 13.

[62] P. Villars, “Pearson's handbook-desk Edition. Crystallographic data for intermetallic phases” **Vol. 1**, ASM International, Materials Park, OH (1997) 444.

[63] S. Kim, Y. A. Chang, Metall. Mater. Trans. A **31** (2000) 1519.

[64] S.V. Divinski, ST. Frank, U. Södervall, Chr. Herzig, Acta mater. **46** (1998) 4369.

[65] G.A. López, S. Sommadossi, P. Zieba, W. Gust, E.J. Mittemeijer, Interface **9** (2001) 371.

[66] Y. Zhou, W.F. Gale, T.H. North, Int. Mater. Rev. **40** (1995) 181

[67] W.D. MacDonald, T.W. Eagar, “The metal science of joining”, M.J. Cieslak, J.H. Perepezko, S. Kang, M.E. Glicksman (Eds.), The Minerals, Met. and Mater. Soc., Warrendale, PA (1992) 93.

[68] M.M.P. Janssen, G.D. Rieck, Trans. AIME **239** (1967) 1372.

[69] S. Shankar, L.L. Seigle, Metall. Trans. A **9** (1978) 1467.

[70] S. Kim, Y.A. Chang, Metall. Mater. Trans. A **31** (2000) 1519.

[71] S.P. Garg, G.B. Kale, R.V. Patil, T. Kundu, Intermetallics **7** (1999) 901.

[72] B. Pieraggi, Oxid. Met. **27** (1987) 177.

[73] L. Farber, I. Gotman, E.Y. Gutmanas, Defect Diff. Forum **643** (1997) 142.

[74] P. Nash, M.F. Singleton, J.L. Murray, “Phase diagrams of binary nickel alloys”, P. Nash (Ed.), Materials Park, OH (1991) 3.

[75] J. Philibert, “Atom movements – Diffusion and mass transport in solids”. Les editions de Physique, Courtaboeuf (1991).

9 Acknowledgements

I would like to thank specially to the Ministry of Education and Culture of Argentina to have financed more than the two thirds of my Ph.D. study and to Prof. E.J. Mittemeijer for the remaining economic support. He also gave me the opportunity to carry out my Ph.D. work at the Max Planck Institute for Metals Research. I want also to thank to Prof. E.J. Mittemeijer for the critical readings and corrections made on several drafts of this work.

I desire to express my gratefulness towards Prof. W. Gust, my direct supervisor, for his invaluable contribution during all the instances of my work. For the fruitful discussions, for the advised methodology of work, for the large amount of corrections of reports and papers, and for his permanent intention to transmit his vast and rich experience of investigator I express my gratefulness and respect to him. I would like also to express my gratefulness towards Prof. J. A. Vivas Hohl for encouraging me to start with my Ph.D. project and to establish the contact with Prof. Gust.

Special mention deserves the contribution made by Dr. S.K. Bhatnagar, Dr. P.K. Khanna and Dr. P. Zieba, who have collaborated in the accomplishment of this investigation. To all of them I express my gratitude. The works made by G. López and J. Huici during their master thesis, in the frame of my Ph.D., have contributed in great extent to the content of Chapters 4, 6 and 7. Therefore, I desire to make explicit my gratitude to them.

Finally, I want to mention the invaluable spiritual support received from Kurt, my life companion. Without his words of encouragement and the advices given at the difficult moments, my work would not have arrived at its good end. The support of my relatives and friends has also played an important role in this work.

I feel the necessity to include tens of names in this section of gratefulness but it is not possible. Nevertheless, I always will remember all those unnamed people who have helped me in the accomplishment of this work, as well as teaching me about the German society and its cultural aspects.

10 Curriculum Vitae

Silvana Andrea SOMMADOSSI

born on 02.12.1973 in Neuquén, Argentina

School

1979-1986	school, “Escuela Rural N° 124”, Centenario, Prov. Neuquén
1987-1991	secondary school, “C.P.E.M. N° 1”, Centenario, Prov. Neuquén

Higher education

1992-1998	university, “Universidad Nacional del Comahue”, Neuquén Degree dissertation: “Characterization of the Ag-Pb-Sn system for application in microelectronics” Degree: Chemical Engineer
1999-2002	Ph.D. at Max Planck Institute for Metals Research and at Institute of Physical Metallurgy, Stuttgart University, Stuttgart